2
2008

This is to certify that the
dissertation entitled

KINETIC/SPECTROSCOPIC INVESTIGATION OF TauD
INTERACTIONS WITH INHIBITORS AND
ISOLATION/CHARACTERIZATION OF THE PUTATIVE
Fe^{II}/α-KETOGLUTARATE DEPENDENT DIOXYGENASE
AND FLAVIN-DEPENDENT DEHYDROGENASE CsiD
AND YgaF.

presented by

Efthalia Kalliri

has been accepted towards fulfillment
of the requirements for the

___Ph.D.___ degree in ___Chemistry___

_____
Major Professor's Signature

___12/18/07___

Date

PLACE IN RETURN BOX to remove this checkout from your record.
TO AVOID FINES return on or before date due.
MAY BE RECALLED with earlier due date if requested.

DATE DUE	DATE DUE	DATE DUE

KINETIC/SPECTROSCOPIC INVESTIGATION OF TauD INTERACTIONS WITH INHIBITORS AND ISOLATION/CHARACTERIZATION OF THE PUTATIVE Fe^{II}/α-KETOGLUTARATE DEPENDENT DIOXYGENASE AND FLAVIN-DEPENDENT DEHYDROGENASE CsiD AND YgaF.

By

Efthalia Kalliri

A DISSERTATION

Submitted to
Michigan State University
In partial fulfillment of the requirements
For the degree of

DOCTOR OF PHILOSOPHY

Department of Chemistry

2008

ABSTRACT

KINETIC/SPECTROSCOPIC INVESTIGATION OF TauD INTERACTIONS WITH INHIBITORS AND ISOLATION/CHARACTERIZATIONS OF THE PUTATIVE Fe^{II}/α-KETOGLUTARIC DEPENDENT DIOXYGENASE AND FLAVIN-DEPENDENT DEHYDROGENASE CsiD AND YgF.

By

Efthalia Kalliri

TauD, an *Escherichia coli* Fe^{II}/α-ketoglutarate (αKG)-dependent dioxygenase, catalyzes the hydroxylation of aminoethanesulfonate (taurine) to produce an intermediate that decomposes to provide sulfite as a cellular sulfur source. Complexes of TauD with Co^{II}, Ni^{II}, and *N*-oxalylglycine (NOG) (known inhibitors of this class of enzymes) were kinetically and spectroscopically investigated. The metal ions were shown to be slow-binding competitive (with Fe^{II}) inhibitors of the enzyme, and substitution of Co^{II} for Fe^{II} was found to produce a chromophore that can serve as a diagnostic marker for αKG-dependent dioxygenases. Kinetic studies revealed that NOG is a weak competitive (with αKG) inhibitor of TauD. Despite the close structural similarity of NOG to αKG, the TauD-Fe^{II}-NOG complex was incapable of activating oxygen or catalyzing NOG decarboxylation.

CsiD is encoded by a gene (*csiD*) located upstream of the γ-aminobutyric acid (GABA) operon (*gabDTP-csiR*) in *E. coli* and is induced by carbon starvation. The crystal structure of CsiD revealed it to be a putative Fe^{II}/αKG-dependent dioxygenase. Spectroscopic studies of purified CsiD were used to prove that Fe^{II} and αKG bind as a

chelate at its active site. An uncoupled reaction was observed in which αKG and oxygen were consumed and succinate was produced in the absence of any primary substrate. Comparisons between the *E. coli* wild type and a *csiD*-knockout strain were undertaken in order to examine the function of CsiD. Numerous compounds were tested as potential substrates of the putative dioxygenase by monitoring oxygen consumption with an oxygen electrode assay, but the function of this protein remains unknown.

The *ygaF* gene of *E. coli* is located immediately downstream of *csiD*, with which it is coregulated, and just upstream of the *gabDTP-csiR* operon. On the basis of sequence comparisons, YgaF had been proposed to be a putative FAD-dependent oxidoreductase with an unknown function. Cloning and overexpression of *ygaF* was used to produce the YgaF protein for characterization. YgaF was shown to possess non-covalently bound FMN, which undergoes a single-step, two-electron redox process ($E°$ ~20 mV) during photoreduction or titration with dithionite. Rapid reoxidation of reduced YgaF by oxygen and formation of a characteristic flavin-sulfite complex provided evidence that it is an oxidase. The function of YgaF was investigated via metabolic studies of *E. coli* wild-type and *ygaF*-knockout cells together with examination of various compounds as substrates of YgaF. The results identified YgaF as an L-2-hydroxyglutarate oxidase.

To my dearest father, mother, sister

&

Beloved fiancé Kostas

ACKNOWLEDGMENTS

Finally, I would like to thank my family. My father, mother, and sister for their love, support and understanding, and my fiancé Kostas with whom we did this journey together.

TABLE OF CONTENTS

LIST OF TABLES

LIST OF FIGURES

x

Images in this dissertation are presented in color.

LIST OF SCHEMES

ABBREVIATIONS

αKG	α-Ketoglutarate
αKG-Ds	αKG-dependent dioxygenases
CarC	Carbapenem synthase
CAS	Clavaminate synthase
DAOCS	Deacetoxycephalosporin C synthase
DEA/NO	Diethylammonium (Z)-1-(*N*,*N*-diethylamino)diazen-1-ium -1,2-diolate
DTT	Dithiothreitol
EDTA	Ethylenediamine tetraacetic acid
EPR	Electron paramagnetic resonance
EXAFS	Extended X-ray Absorption Fine Structure
FAD	Flavin adenine dinucleotide
FMN	Flavin mononucleotide
HEPES	N-(2-Hydroxyethyl)piperazine-N'-(2-ethanesulfonic acid)
HPPD	4-Hydroxyphenylpyruvate dioxygenase
KO	Knock-out
LMCT	Ligand-to-metal charge-transfer
MLCT	Metal-to-ligand charge-transfer
NADH	Nicotinamide adenine dinucleotide
NADPH	Nicotinamide adenine dinucleotide phosphate
NIR MCD	Near-infrared magnetic circular dichroism
NMR	Nuclear magnetic resonance

NO	Nitric acid
NOG	*N*-oxalylglycine
OPDA	*o*-Phenylenediamine
PCD	Protocatechuic 3,4-dioxygenase
PCA	Protocatechuic acid
P3H	Proline 3-hydroxylase
P4H	Prolyl 4-hydroxylases
RR	Resonance Raman
SDS-PAGE	Sodium dodecyl sulfate-polyacrylamide gel electrophoresis
TauD	Taurine/αKG dioxygenase
TfdA	2,4-D dioxygenase

CHAPTER 1

INTRODUCTION

α-ketoglutarate dependent dioxygenases

Dioxygen (O_2) is one of the major air components (20.95%), and it is necessary for aerobic respiration in animals. The reduction of oxygen is very strictly controlled by nature. Despite the fact that the reactions of oxygen with organic molecules are thermodynamically favored (exothermic), these reactions are relatively slow. The kinetic barrier has its origin in the fact that oxygen's ground state has a triplet spin, while organic biological molecules have singlet ground states, and consequently interactions between them are spin forbidden.[1] Nature overcomes this barrier by using molecules capable of one-electron chemistry that can reduce dioxygen by exciting it to one of its singlet states. Enzymes that use O_2 to oxidize their substrates utilize specific cofactors that promote the spin inversion. Such cofactors include organic molecules that can stabilize a radical (e.g., the isoalloxazine ring of a flavin), metal ions that are redox active (e.g. iron), and combinations of the two (e.g., the porphyrin ring of a heme). Non-heme iron dioxygenases including α-ketoglutarate (αKG)-dioxygenases are included in the hybrid cofactor class because they employ a combination of a metal ion (Fe(II)) and an organic molecule (αKG) to perform the O_2 spin inversion.

Reactions of αKG-dependent dioxygenases and related enzymes

αKG-dependent dioxygenases (αKG-Ds) consist of an enzyme family covering a wide range of reactions of biological significance. All αKG-Ds have an iron atom at their active sites and usually they require three substrates: αKG, molecular oxygen and a primary substrate, which varies depending on the role of the particular enzyme. The general reaction catalyzed by these enzymes is the hydroxylation of their primary

2

substrate (shown in Figure 1). Enzymes in this family are called dioxygenases because both oxygen atoms of molecular dioxygen are inserted into the substrates; one into the cosubtrate αKG leading to carbon dioxide (CO_2) and succinate, and the other into the primary substrate.

αKG-Ds carry out a large number of chemical reactions including hydroxylation (aliphatic and aromatic), hydroxylation-elimination, carboxyl formation (from aldehyde or ketone), epoxidation, desaturation, ring expansion/closure, epimerization, and halogenation (that was discovered very recently).[2,3] The proteins of this family have highly diverse biological roles too, including protein side-chain modifications, repair of alkylated DNA/RNA, biosynthesis of antibiotics and plant products, lipid metabolism, and biodegradation of a wide variety of small molecules (reviewed by Hausinger).[3] A brief introduction of the reactions catalyzed by several important representatives of the αKG-Ds is given below, followed by a discussion of the general catalytic cycle.

$$RH + HOOC\text{-}CO\text{-}CH_2\text{-}CH_2\text{-}COOH + O_2 \xrightarrow{\alpha KG\text{-}D} R(O)H + HOOC\text{-}CH_2\text{-}CH_2\text{-}COOH + CO_2$$
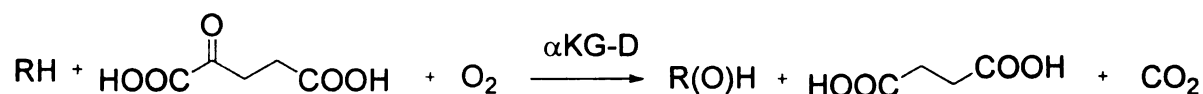
Figure 1. General reaction of the α-ketoglutarate-dependent dioxygenases (αKG-Ds).

Prolyl 4-hydroxylase

Prolyl 4-hydroxylase (P4H) is included in the side-chain modification subgroup, and it is historically significant because it was the first identified αKG-D in 1966.[4] The reaction catalyzed by P4H is the hydroxylation of the proline residue, as shown in Figure 2. P4H activity has been found in mammals (where it plays a key step in collagen

3

biosynthesis and serves a critical role in hypoxic signalling) and in plants (where it modifies proline-rich glycoproteins that are components of the cell wall.[5,6]
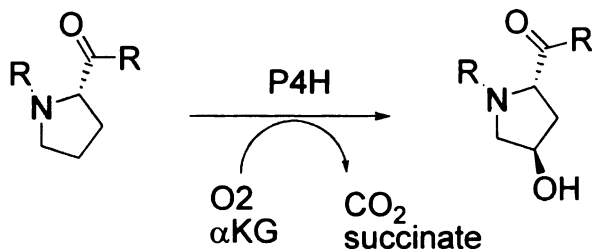
Figure 2. Prolyl 4-hydroxylase (P4H) reaction.

AlkB

Alkylating agents can produce lethal mutagenic lesions by methylating DNA. AlkB is an *Escherichia coli* demethylase that repairs 1-methyladenine and 3-methylcytosine lesions in DNA and RNA. Its activity remained unknown for more than 20 years from the time *alkB* was first identified as a gene involved in repair of alkylation damage.[7] Finally, in 2002 the enzyme was shown to hydroxylate the methyl group by αKG-D chemistry, resulting in a spontaneous departure of formaldehyde and recovery of adenine and cytosine, respectively (Figure 3).[8,9,10]

Clavaminate synthase

Clavaminate synthase (CAS) is involved in the biosynthesis of the antibiotic clavulanic acid. CAS catalyzes three steps in the biosynthesis.[11] The first step is the hydroxylation of deoxyguanidinoproclavaminic acid (β-lactam) yielding guanidinoproclavamic acid. The next step is a hydrolysis of the guanidine group catalyzed

4

by an amidinohydrolase. CAS then catalyzes two steps, cyclization of proclavaminic acid and desaturation, producing finally clavulanic acid (Figure 4).

A)

B)
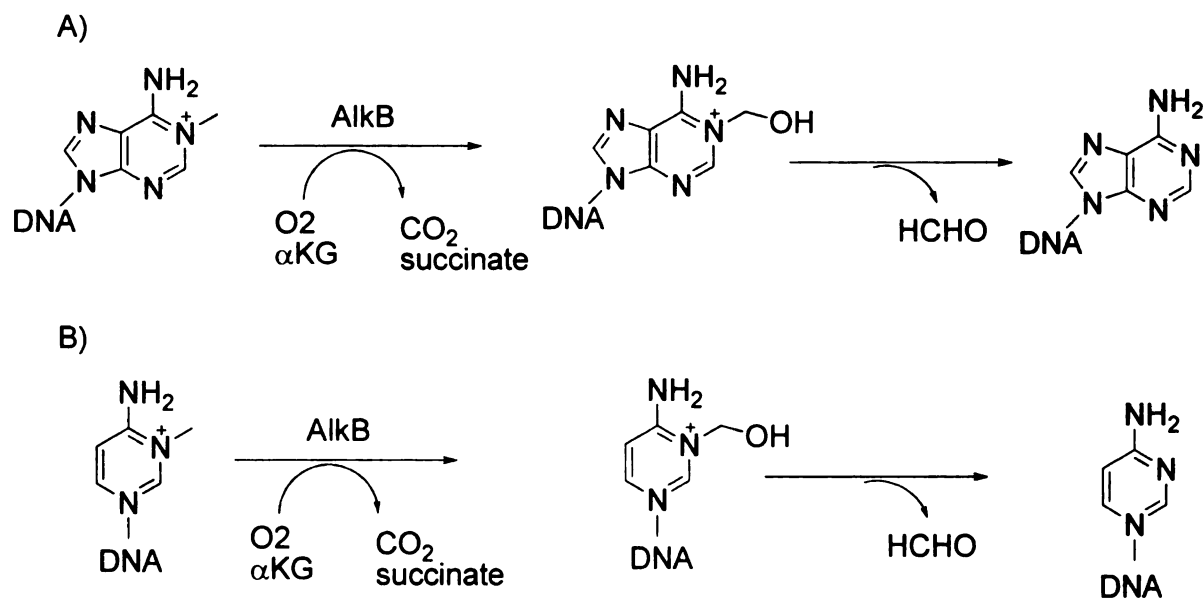
Figure 3. Reaction of AlkB having A) 1-methylated adenine and B) 3-methylated cytosine as a substrate.
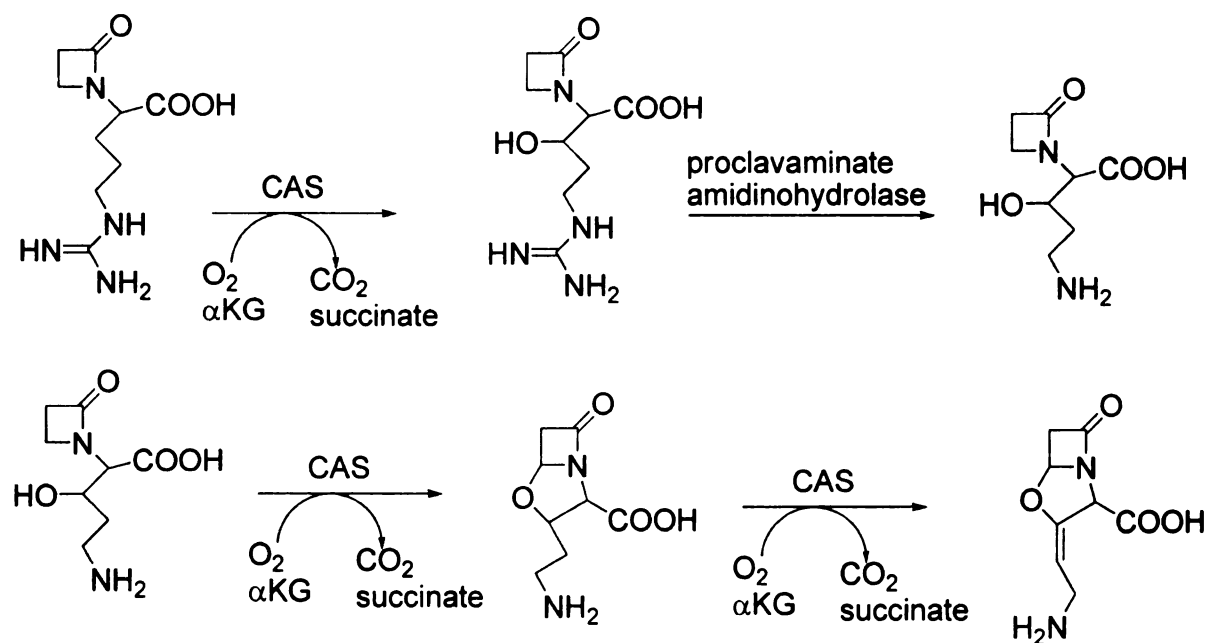
Figure 4. CAS is involved in three out of four steps of clavulanic acid biosynthesis.

Taurine dioxygenase

αKG-Ds are also involved in biodegradation of the molecules supplying with sulfur, phosphorous or carbon when the cell is undergoing starvation for the particular element. In *E. coli* under sulfur starvation, the operon *tauABCD* is activated and provides the organism with proteins that are involved in taurine (2-aminoethanesulfonate) uptake (TauA, TauB, and TauC) and degradation (TauD).[12,13] TauD is an αKG-D that hydroxylates the C-1 position of taurine, creating an unstable intermediate which decomposes to aminoacetaldehyde and sulfite, as shown in Figure 5.[14] TauD is one of the very well studied enzymes of this superfamily. Some experiments that I performed with this particular enzyme are reported in Chapter 2.
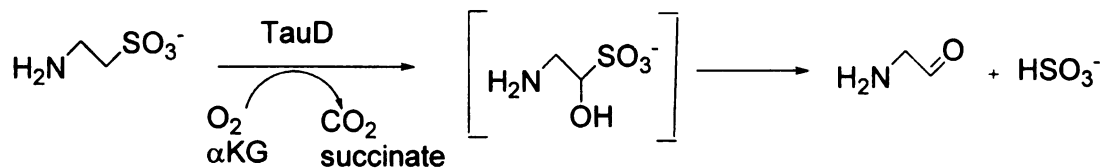
Figure 5. Reaction of TauD.

4-hydroxyphenylpyruvate dioxygenase

Several enzymes are included in the αKG-D superfamily because they exhibit similarities in sequence or catalytic mechanism even though they may not require αKG. 4-Hydroxyphenylpyruvate dioxygenase (HPPD) exhibits chemical parallels, but is not related in sequence to αKG-Ds. It catalyzes the second step of the tyrosine catabolism pathway.[15] HPPD doesn't utilize αKG as a cosubstrate, and its only substrate is an α-keto acid (4-hydroxyphenylpyruvate) which is cleaved (Figure 6).[16] Actually the mechanism

6

involves decarboxylation, acetyl group migration and oxygenation (with both oxygen atoms getting incorporated into the aromatic product) steps.
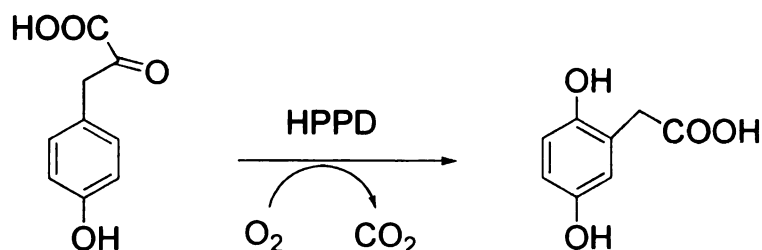
Figure 6. Reaction of HPPD.

General characteristics and mechanistic studies of the αKG-dependent dioxygenases

3D structure

Crystallization of αKG-D proteins started only about 10 years ago, and proceeded so fast that there are more than 50 entries of crystal structures in the Protein Data Bank. These enzymes have been reported to exist in various oligomeric forms. For instance, CAS is a monomer;[17] whereas DAOCS (deacetoxycephalosporin C synthase), which is involved in the cephalosporin synthesis from penicillin, has been found in both monomeric and trimeric states.[18] TauD crystallized as a dimer;[19] and AtsK (alkylsulfatase), a close relative of TauD that produces sulfate from alkylsulfates, is a tetramer.[20] The highest oligomeric form found in the αKG-D family is hexameric, reported for CarC (carbapenem synthase), an enzyme involved in carbazole degradation.[21]

The monomers of all known crystal structures of this family contain the "jelly-roll" motif. This fold consists of two four-stranded antiparallel β-sheets that are twisted clockwise (Figure 7).[22] The structure of the jelly roll motif is supported by α-helices that

7

are conserved and pack alongside the major β-sheet. HPPD, which is a relative of this enzyme family, doesn't exhibit this motif in its structure.[16]
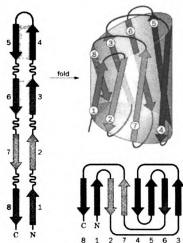
Figure 7. Structure of the jelly-roll motif.[23]

General reaction mechanism

The catalytic cycle (Figure 8) of the αKG-Ds starts with the metal ion being hexacoordinated with three amino acid residues (Asp/Glu and two His) and three water molecules in an octahedral geometry. The usual order for addition of substrates starts with binding of the cosubstrate αKG, resulting in bidentate chelation of the Fe(II), displacing two water molecules (intermediate B).[24,25] Subsequently, addition of the primary substrate leads to the removal of the last water molecule from the coordination environment of the metal ion (intermediate C), creating a place for oxygen binding. The primary substrate coordinates in the active site, in close vicinity to Fe(II), but it doesn't interact directly with it.[19] Oxygen binding to the Fe(II) site has been proposed to lead to Fe(III)-superoxo or Fe(IV)-peroxo complexes (intermediates D),[3] which finally collapse to a ferryl oxo complex (intermediate E), a species which is to date the only identified and characterized iron-oxygen intermediate.[26,27] Finally, the products, oxygenated primary substrate,

8

succinate, and carbon dioxide, are released and three water molecules bind to the Fe(II), returning the enzyme to its starting state, ready for a new cycle. Each step of the catalytic cycle is analyzed below.
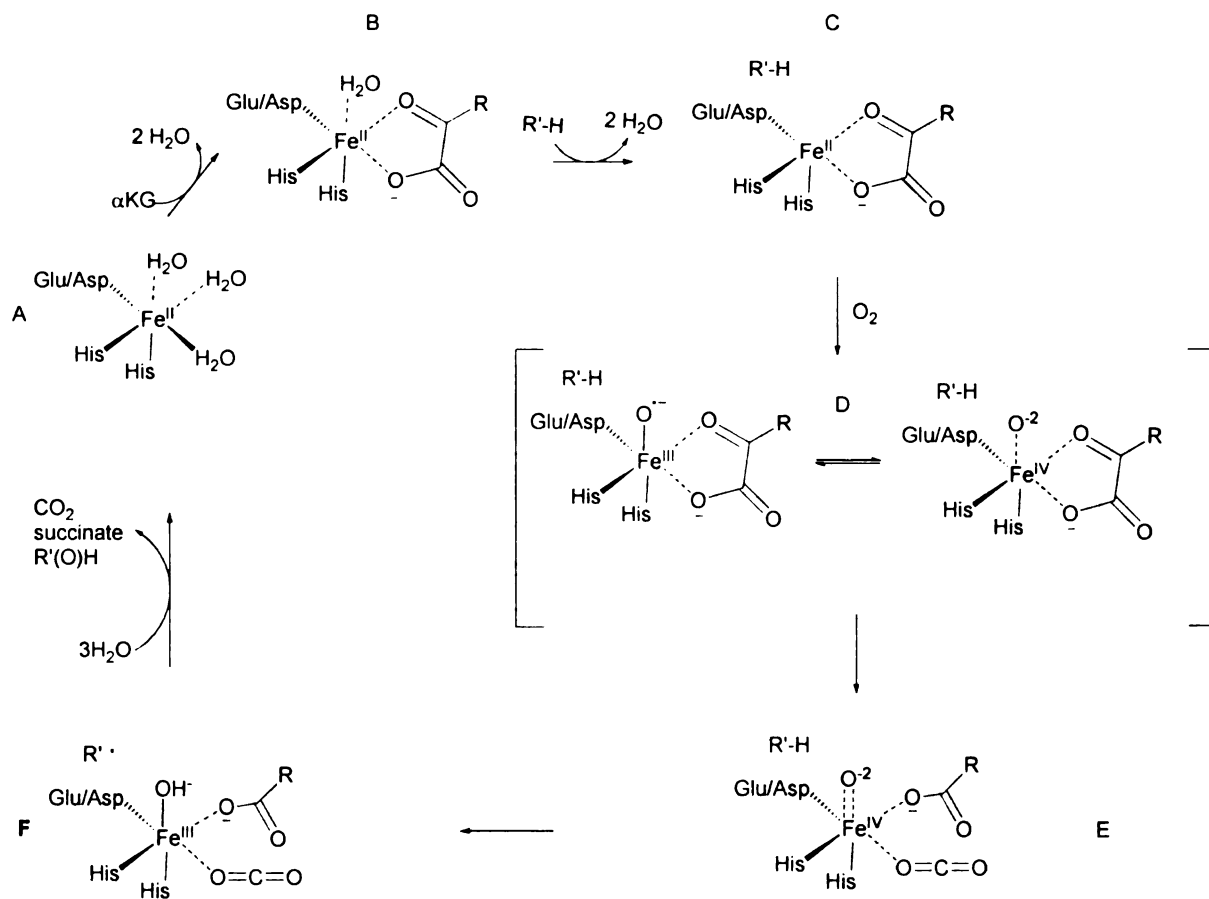
Figure 8. General mechanism of αKG-dependent dioxygenases. Description of the steps is reported in the text.

Resting state

The metal ion is involved only in the mechanism of the enzyme, and has nothing to do with the structure of the proteins, since apoenzymes of several αKG-Ds have been crystallized and showed that they adopt similar overall conformations with the

holoenzymes.[2] The Fe(II) in the holoenzyme in the absence of any substrate (resting state) appears in an octahedral geometry with three water molecules and three amino acid residues as ligands. The three amino acid residues that bind Fe(II) in the active site constitute "the facial triad", which includes two histidines and one carboxylic acid (Asp or Glu) found in a HXD/EX$_n$H motif.[28] Examples of amino acids constituting the facial triad in different enzymes are given in Table 1. HPPD shows deviations from this behavior, having two histidines (His161 and His240) and a glutamic acid (Glu322) binding the Fe(II) in a HX$_{\sim65}$HX$_{\sim50}$E motif that rather resembles an extradiol dioxygenase.[29]

The crystal structures of the resting state of P3H (proline 3-hydroxylase) and DAOCS have been solved.[30,31] The near-infrared magnetic circular dichroism (NIR MCD) spectrum of CAS in the resting state exhibited two d-d transitions at 917 and 1085 nm associated with to the distorted octahedral center.[32]

Protein	Organism	Metal coordinating residues
TauD	*Escherichia coli*	His99, Asp101, His255
CAS	*Streptomyces clavuligerus*	His144, Glu146, His279
DAOCS	*Streptomyces clavuligerus*	His183, Asp185, His243
CarC	*Erwinia carotovora*	His101, Asp103, His251
AtsK	*Pseudomonas putida*	His108, Asp110, His264

Table 1. List of the facial triad of several αKG-Ds.[19,17,31,21,20]

αKG binding to the active site

Displacement of two water molecules permits binding of αKG in a bidentate fashion to the ferrous active-site ion via the C1 carboxylate and the C2 keto group as

shown in Figure 8. This complex structure was first proposed based on spectroscopic experiments on CAS,[32] and later proven from various αKG-Ds crystal structures (e.g. CAS and AtsK).[17,20] All proteins of this family in the presence of αKG and in the absence of oxygen, exhibit a characteristic chromophore at around 500 nm with slight variations of the maxima and intensities (e.g., 530 nm for TauD, 500 nm for CAS).[24,33] This absorption was assigned by Solomon and coworkers to metal-to-ligand charge-transfer (MLCT) transitions due to excitation of electrons from the d (yz, x^2-y^2, z^2) orbitals of the iron atom to the π* orbitals of αKG.[33] Resonance Raman (RR) spectroscopy of TauD yielded vibrations at 460 cm^{-1} and 1700 cm^{-1}, which were assigned to metal-to-ligand stretching and C = O vibrations respectively.[34] The αKG cosubstrate can bind to the Fe(II) in two different ways, "in line" and "off line", depending on the coordination position of the C1 carboxylate group of αKG. When the C1 carboxylate group of αKG is *trans* to the proximal His, this is called "in-line" coordination and oxygen can bind and directly attack the substrate. Examples of enzymes that belong in this category are CAS and TauD.[17,19] On the other hand, in the "off-line" coordination, the C1 carboxylate group of αKG is *trans* to the distal histidine residue and the active site must undergo reorganization for bound O_2 to react with the substrate. Representatives of this category are the enzymes CarC and DAOCS.[21,35]

Binding of the primary substrate

The primary substrate binds in close proximity to, but not in direct contact with, the metal ion, forcing the last water molecule ligand to leave. The departure of the solvent results in a change from six-coordinate octahedral geometry to five-coordinate square

pyramidal geometry of the iron complex. Several X-ray structures of enzymes with both substrates bound (under anaerobic conditions) have been published.[3] The change in the iron coordination can be monitored spectroscopically. For example, the addition of taurine to TauD alters the characteristic MLCT chromophore so that it is blue shifted from 530 nm to 520 nm.[24] RR spectra of TauD also demonstrate a shift, from features at 460 and 1700 cm^{-1} to features at 470 and 1688 cm^{-1}, upon taurine binding to the active site with a consequent change in the iron complex geometry.[34]

Oxidation

Dioxygen binding to the iron complex is a critical step in the oxidation of the cosubstrate and primary substrate of all the αKG-Ds. Delocalization of electron density from the cosubstrate to the iron ion facilitates the single-electron reduction of the molecular oxygen that is necessary for its spin inversion. O_2 takes the place of a water molecule in the primary coordination sphere of the ferrous ion. Observation of the accumulation of three spectroscopically distinct oxygen intermediates in HPPD proves the existence of multiple oxygen complexes during a single turnover.[36] Nevertheless, the only proven iron-oxygen intermediate is the ferryl-oxo ($Fe(IV)=O^{-2}$) complex (intermediate E in Figure 8), which has been observed in TauD and P4H catalytic cycle.[26,37,38] The particular intermediate of TauD was observed by stopped-flow UV-visible spectrophotometry to absorb at 318 nm.[37] Rapid freeze-quench techniques combined with Mössbauer spectroscopy (on a TauD sample) were used to trap and characterize the TauD intermediate as being paramagnetic with an integer-spin ground-state S≥2. Subsequent cryoreduction of the complex formed a high-spin Fe(III) species, confirming the Fe(IV)

oxidation state of the reported intermediate.[37] The existence of the ferryl-oxo species was also confirmed by Proshlykov *et al.* using RR and cryogenic continuous flow methods.[26] The Fe(IV)=O^{-2} was directly identified by the isotope-sensitive vibration $\nu_{Fe=O}$ in the 800 cm^{-1} region, which shifted from 821 cm^{-1} for ^{16}O to 787 cm^{-1} for ^{18}O. Moreover, EXAFS spectroscopy was used to determine that the distance between the iron and the oxygen of the TauD oxo-intermediate was 1.62 Å, similar to the corresponding distance of model complexes.[39] This intermediate abstracts a hydrogen atom from substrate to form a carbon centered radical and Fe(III)-OH, followed by hydroxyl radical rebound to generate the product.

HPPD reacts with molecular oxygen 3,600 times faster in the presence of its primary substrate and such reactivities with O$_2$ are similarly enhanced in other αKG-Ds;[40] nevertheless, it has been shown *in vitro* that the absence of primary substrate leads to uncoupled reactions and results in enzyme inactivation and self-modification.[41,42,43] In the general uncoupled reaction one atom of dioxygen incorporates into the cosubstrate as the metal site oxidizes and the inactive enzyme is reactivated by ascorbate. An alternative type of uncoupled reaction is found in TauD which generates a 550 nm chromophore; in this case an αKG-dependent process leads to hydroxylation of a side chain, which by RR spectroscopy was identified as an Fe(III)-catecholate species. The self-hydroxylated Tyr73 residue, or dihydroxyphenylalanine, forms a complex with the oxidized, active-site iron ion to generate the distinctive ligand-to-metal charge-transfer feature.[41] A similar example was reported for the dichlorophenoxyacetate/α-ketoglutarate dioxygenase (TfdA) which formed a hydroxylated Trp in the absence of its primary substrate.[42] The blue ferric complex that is formed under these conditions is catalytically inactive. Reductants like

ascorbate can return the iron to its ferrous state, but it cannot reverse the side chain modifications; in some cases this treatment restores a portion of the catalytic activity of the dioxygenase.[44]

Products formation and release

Formation of the oxygenated primary substrate (R(O)H) accompanies the oxidative decarboxylation of αKG, and release of the products is one of the last steps of the catalytic cycle. An interesting experiment was performed by Yu *et al.* in order to observe the generation of the products of AlkB.[45] Anaerobic crystals of holo-AlkB complexed with αKG and 1-methyl adenine nucleotide (dT-(1-me-dA)-dT) were exposed to molecular oxygen. As a result, αKG converted to succinate and demethylation of the nucleotide was observed. Concerning product release, there is debate whether CO_2 and succinate dissociate during or after the turnover is complete.[2] In any case, CO_2 is the first product to dissociate, followed by succinate.

Flavoenzymes

Structures of flavins

More than a century ago, Blyth reported the existence of a yellow pigment in the content of whey, which he named lactochrome.[46] Over the years many other yellow pigments were observed in nature, including hepatoflavin and verdoflavin that were named on the basis of their biological sources or their physical properties. Subsequently, these compounds were all shown to be riboflavins. Richard Kuhn and Paul Karren independently determined the structure of flavin and proved it by chemical synthesis, as reviewed by Vincent Massey.[58] The structure of riboflavin and its natural variants are shown in Figure 9. Riboflavin got its name from its structural components 7,8-dimethylisoalloxazine (which was named flavin from the latin "flavous" that means yellow) and the reduced form of D-ribose. Lumichrome and lumiflavin are riboflavin derivatives after photolysis at pH < 7 and pH > 9 respectively. The riboflavin moiety in some cases is attached to adenosine diphosphate forming FAD (flavin adenine dinucleotide), and in other circumstances is bound to phosphate forming FMN (flavin mononucleotide).

Diversity of flavoenzymes

The biologically active forms of riboflavin, FMN and FAD, have been found to be cofactors for many enzymes. It has been estimated that genes encoding flavin-containing proteins comprise of 1-3 % of the prokaryotic and eukaryotic DNA.[47] The high abundance of flavoproteins in cells, together with the importance of their biological roles, has led to extensive studies of these enzymes. They are involved in an amazingly wide range of

15

reactions.[48,49,50] It has been shown that flavoenzymes are involved in typical dehydrogenation reactions[51] (using a large variety of metabolites as substrates), electron transfer from and to redox centers,[50] light emission,[52] activation of dioxygen, photochemistry[53] signal transduction related to programmed cell death[54] and DNA damage[55] and repair.[53] Their substrates can be alcohols, aldehydes, ketones, acids, amino acids, amines, dithiols, hydroxy acids, and other compounds.[56]
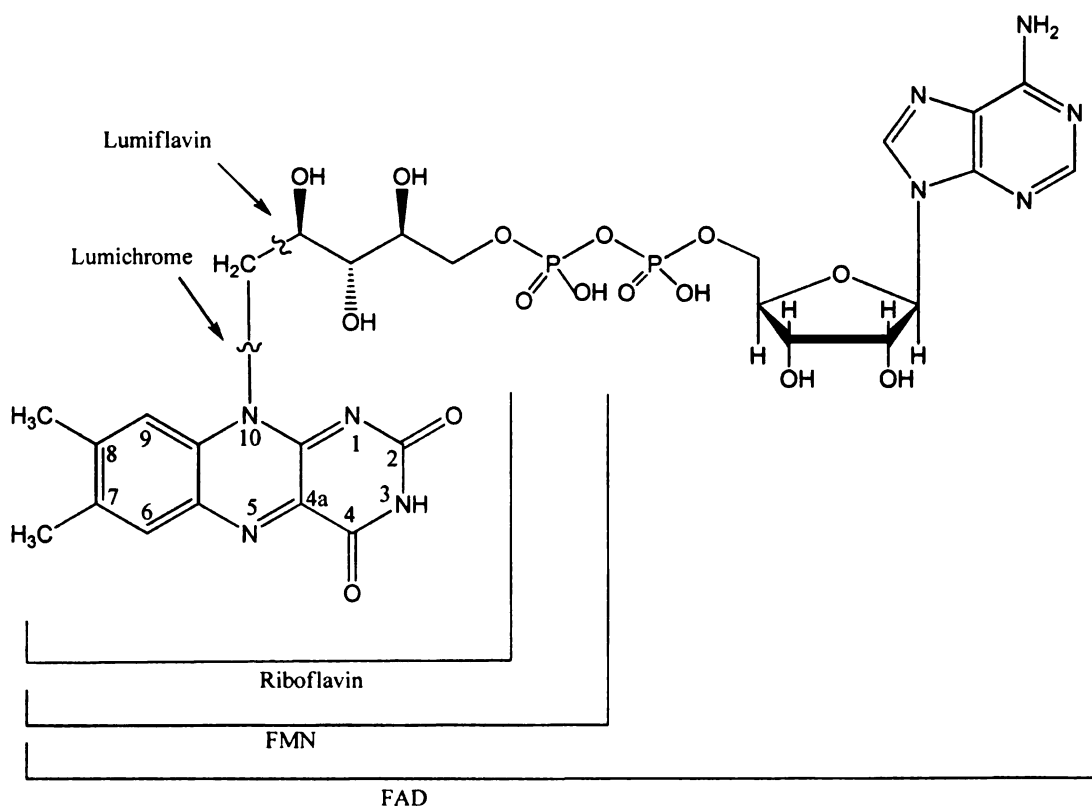
Figure 9. The structures of flavins.

16

Flavin redox chemistry

Redox states of flavin.

Flavoenzymes are involved in a plethora of reactions because of the chemical versality of the alloxazine ring. The isoalloxazine moiety is the redox active part of the flavin molecule, whereas the side-chain, including the adenine moiety, functions mainly to anchor the coenzyme to the active site. Flavins can exist in the oxidized, one-electron-reduced (semiquinone) and two-electron (fully) reduced state, as shown in Figure 10. Every state can occur in cataionic, neutral, or anionic forms.[57] Based on the pK_a, six out of the nine forms are observed under physiological conditions.
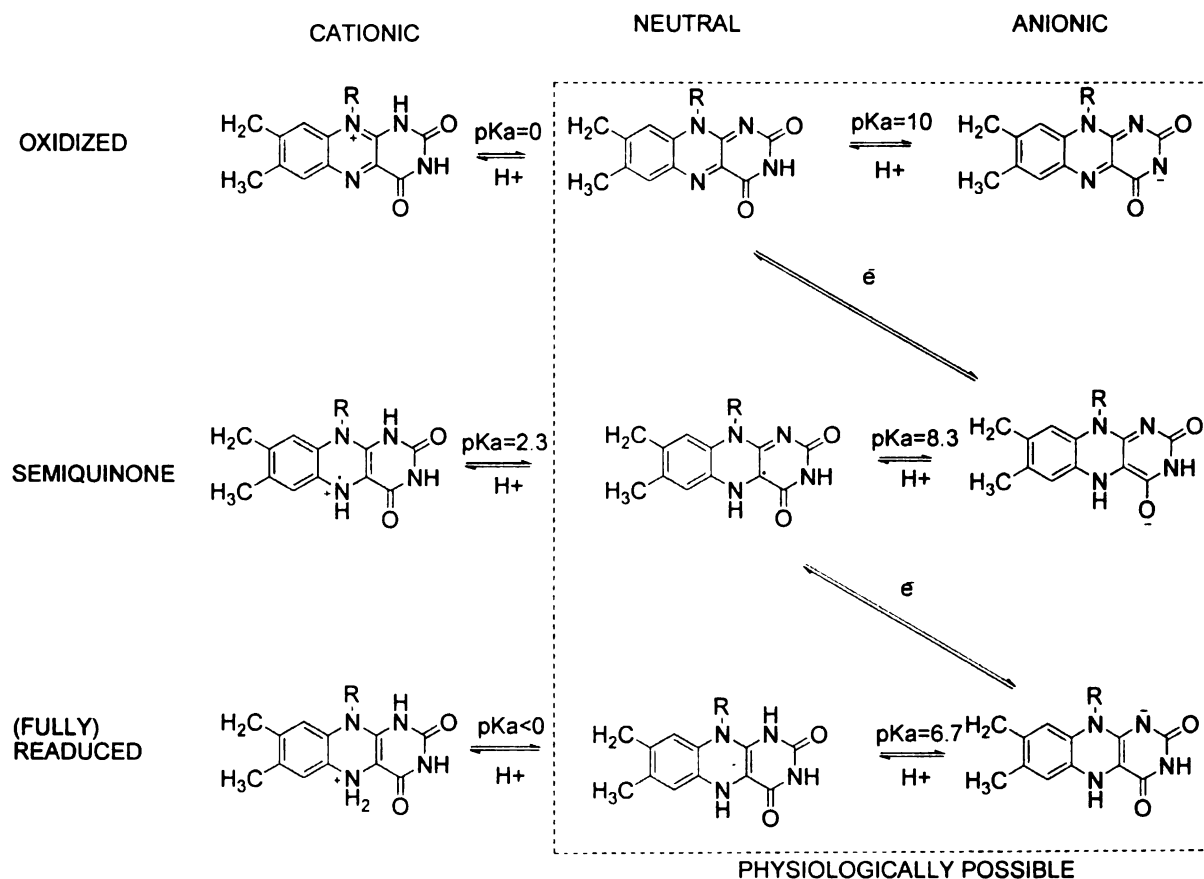
Figure 10. Redox states of flavin.

17

An advantage of studying flavoenzymes is that the investigator can monitor the redox-dependent reactions they catalyze using a spectrophotometer. An example is shown in Figure 11.[58] The oxidized form of the flavin has yellow color and a distinct spectrum with dual maxima at ~380 nm and ~450 nm (the wavelength varies slightly in each protein). For an anionic semiquinone the intensity of the 380 nm feature increases, while the 450 nm peak decreases. The neutral anionic form of the cofactor has an absorbance transition around 600 nm. The fully reduced form of flavin is colorless.
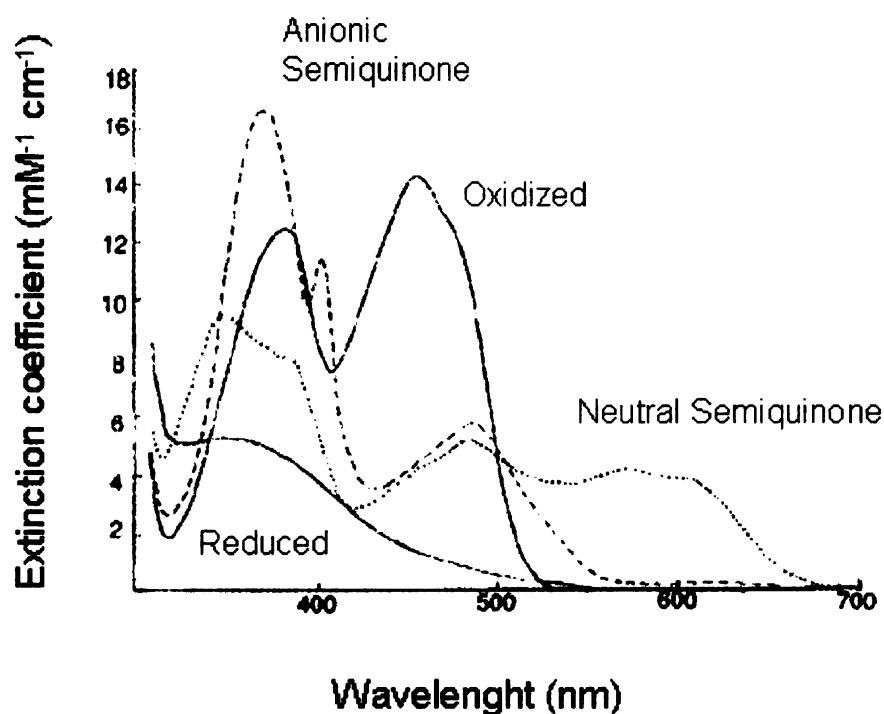
Figure 11. Absorption spectra of the redox states of glucose oxidase.[58]

Many flavoenzymes catalyze reactions through a single two-electron flavin-reduction step and do not form any semiquinone intermediate. On the other hand, other

18

flavin-containing enzymes catalyze mechanisms involving two, one-electron steps for flavin reduction with the intermediacy of a semiquinone. The reduced proteins are reoxidized by reactions that again utilize either one, two-electron step, or two, one-electron steps (only the overall processes are depicted in Figure 12.
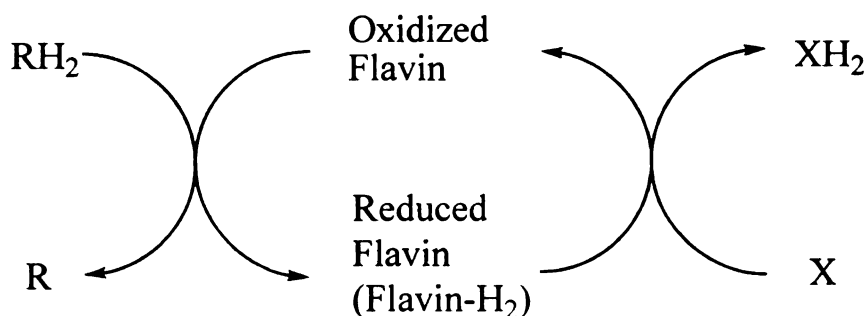
Figure 12. Reductive and oxidative half reactions of flavoproteins.

In solution, a mixture of oxidized and reduced free flavin is observed in equilibrium, where an amount of flavin semiquinone is formed, as shown in Scheme 1. At physiological pH (pH 7) the radical species accounts for only 5% of the total, in a mixture containing equal amounts of oxidized and reduced states.[58] When flavin is bound in the active site of a protein, this equilibrium can be altered dramatically resulting in a broad range of stabilization of the semiquinone species.

$$Fl_{ox} + Fl_{red} \rightleftharpoons 2\,FlH\cdot$$
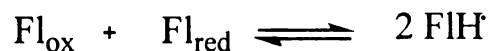
Scheme 1. Equilibrium of different reduction states of flavin.

Redox potential of flavoproteins.

Free flavin has a redox potential of −210 mV at pH 7;[48] however, when interacting

with residues at the active center of flavoenzymes, this value can change dramatically. The

lowest flavoprotein redox potential ever reported is -495 mV for the semiquinone/reduced

couple of the flavodoxin from *Azotobacter vinelandii*,[59] and the highest potential recorded

is +80 mV for the semiquinone/reduced couple of thiamin dehydrogenase.[60] The wide

range of potentials reflects the strong modulation exerted by the protein environment on

the cofactor redox properties. Strongly positive charges in the proximity of the flavin

cause an increase in the observed redox potential,[49] as confirmed by crystallographic

studies.[61] By contrast, negative charges near the coenzyme lead to decreases of the redox

potential.

Hydrogen bonds between the flavin and protein residues can tune the redox

potential as well. The N1-C2=O portion of the isoalloxazine (shown in Figure 9) has been

shown to be in contact with positive charges associated with Lys or Arg side chains, as

well as with the α helix N-terminus.[49] This interaction is responsible for the stabilization

of the reduced form of the flavin; therefore it increases the redox potential. Another

important locus for hydrogen bonds is the N5 of the isoalloxazine. The N5 position

becomes protonated upon oxidation of a substrate; therefore the particular hydrogen bond

disfavors the reaction from occurring. Higher redox potentials have been found for

enzymes which lack such a hydrogen bond with the N5 of the flavin (e.g. Fl_{ox}/Fl_{red}: +55

mV for vanilly-alcohol oxidase, Fl_{ox}/Fl_{semiq}: -33 mV and Fl_{semiq}/Fl_{red}: -17 mV for glycolate

oxidase).[49, 62]

The flavin molecule typically is strongly, but non-covalently, bound to flavoenzymes. In addition, some enzymes bind the coenzyme using a covalent bond, as shown in Figure 13.[63] The covalent bond between the enzyme and the cofactor reduces the oxidative power of the flavin, as proven by mutagenesis experiments where the covalent bond was elimimated.[64]
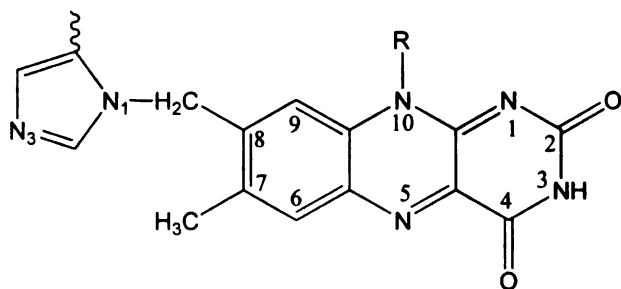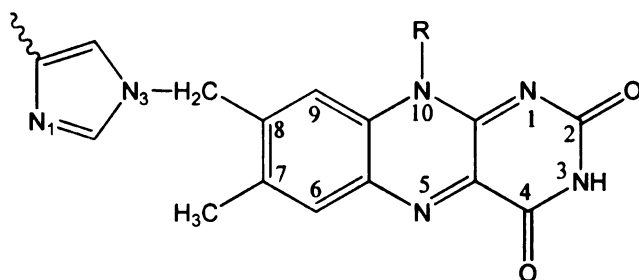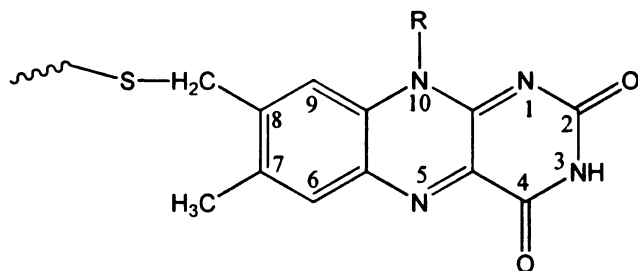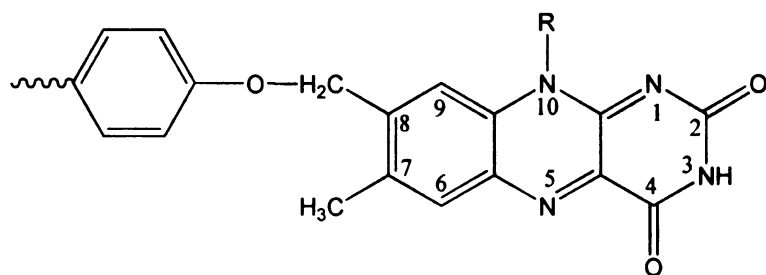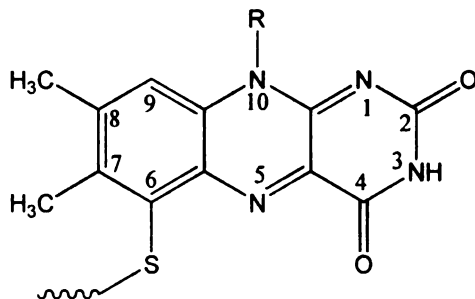
Figure 13. Covalent protein-flavin bonds observed in flavoenzymes.

Photoreduction.

Photoreduction is another common property of flavins. The flavin takes two electrons from a variety of electron donors to form its fully reduced state.[46] As for chemical reductants, reduction can occur either in a single, two-electron step or with the intermediacy of a partially reduced species (semiquinone). Photoreduction of flavoenzymes often is more difficult than for the free coenzyme; however, Vincent Massey and co-workers demonstrated that photoreduction of several flavoenzymes is facilitated by having free flavin as a catalyst in the reaction solution.[65] It was envisioned that catalytic amounts of free flavin can trigger the light-mediated reduction of flavoenzymes, as is shown in Scheme 2. EDTA (ethylenediamine tetraacetic acid) is the most common photoreductant in such studies, and is added to the mixture of flavoenzyme and free flavin. Free flavin (Fl) is photoreduced by light irradiation (reaction 1), then reacts with the flavoenzyme (E-Fl). This reduction can go through one two-electron step (no intermediates generated) or via two one-electron reactions (semiquinone intermediate is formed; reactions 3a and 3b). The most effective, and therefore the most commonly utilized, free flavin used in this experiment is 5-deazaflavin, which possesses a nitrogen atom at the position typically occupied by C5.[66]

As expected, the photoreduction of a flavoenzyme can be monitored spectroscopically. The absorption at ~450 nm of the oxidized protein decreases as the reduction proceeds. There are many examples where semiquinones (indicated by the increase in absorbance at ~370 nm for the anionic species) can be observed, such as the one shown in Figure 14.[67] In other cases, neutral semiquinones are formed or direct reduction to the fully reduced flavin is observed.

23

$$\text{Fl}_{ox} \xrightarrow[\text{hv}]{\text{EDTA}} \text{Fl}_{red}\text{H}_2 \qquad \text{reaction 1}$$

a) no intermediate formed

$$\text{Fl}_{red}\text{H}_2 + \text{E-Fl}_{ox} \longrightarrow \text{Fl}_{ox} + \text{E-Fl}_{red}\text{H}_2 \qquad \text{reaction 2}$$

b) intermediate formed

$$\text{Fl}_{red}\text{H}_2 + \text{E-Fl}_{ox} \longrightarrow \text{FlH}^{\cdot} + \text{E-Fl}_{red}\text{H}^{\cdot} \qquad \text{reaction 3a}$$

$$\text{Fl}_{red}\text{H}_2 + \text{E-Fl}_{red}\overset{\cdot}{\text{H}} \longrightarrow \text{FlH}^{\cdot} + \text{E-Fl}_{red}\text{H}_2 \qquad \text{reaction 3b}$$

$$2\,\text{FlH}^{\cdot} \rightleftharpoons \text{Fl}_{ox} + \text{Fl}_{red}\text{H}_2 \qquad \text{reaction 3c}$$
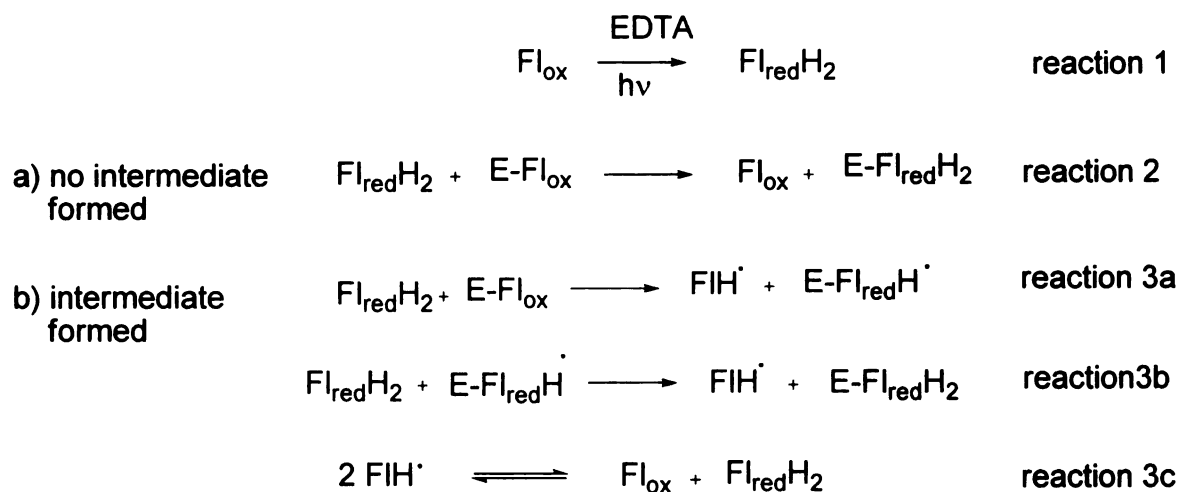
Scheme 2. Mechanism of flavoprotein photoreduction with free flavin as catalyst.
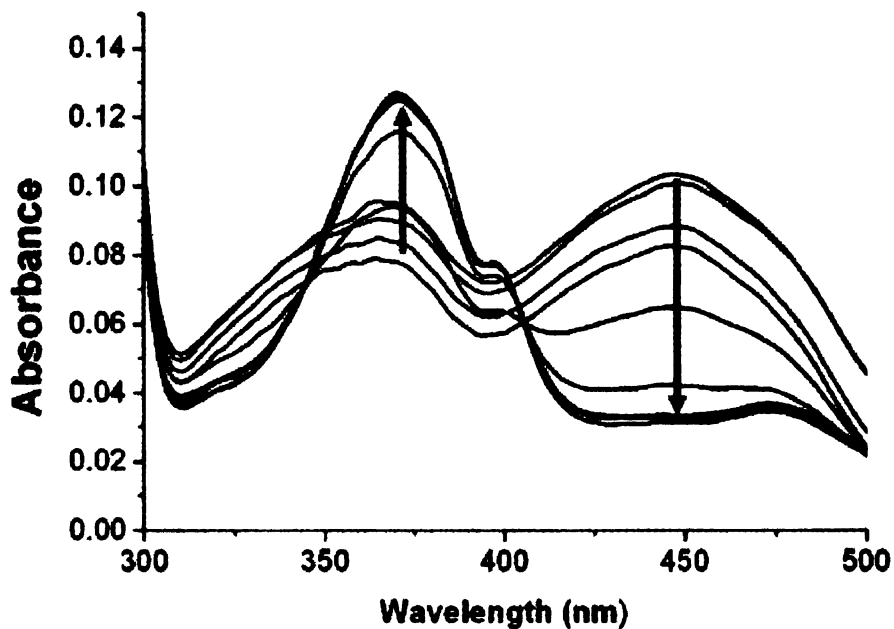
Figure 14. Photoreduction of AidB.[67]

24

Classification of flavoenzymes

The abundance of flavoenzymes in nature and their participation in a wide variety of roles is reflected in their classification, which is based on the substrates recognized and the reactions catalyzed. The classic categorization has separated these enzymes into three groups: oxidases, monooxygenases, and dehydrogenases. The large number of dehydrogenases identified with diverse properties has forced the scientific society to split that category into subclasses. Therefore, by taking into account the type of reactions catalyzed, the reactivity with oxygen and the nature of additional redox centers in the protein, flavoenzymes are now constituted into five groups oxidases, monooxygenases, electron transferases, flavoproteins with auxiliary redox centers, and enzymes with unknown function.[50]

Oxidases.

Oxidases are flavoproteins which, when in their fully reduced form, react very rapidly with molecular oxygen to yield the oxidized form of the enzyme and hydrogen peroxide (Scheme 3).

$$Fl_{red}H_2 \quad + \quad O_2 \longrightarrow Fl_{ox} \quad + \quad H_2O_2$$
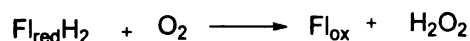
Scheme 3. Oxidation of the two-electron reduced flavin by molecular oxygen.

The high redox potential of the O_2/H_2O_2 couple (+270 mV at pH 7) drives the reaction of Scheme 3 to the products, but this is a hindered process because it is spin forbidden.[68] Oxygen is in the triplet state and the reduced-form flavin is in the singlet

state. In order to proceed, an electron transfer from the flavin to the oxygen takes place, yielding a caged radical pair.[69] The rate of the reaction of molecular oxygen with flavoenzymes varies widely, depending on the accessibility and environment of the flavin. In particular, some oxidases react rapidly with oxygen (e.g., 1.5×10^6 M^{-1} s^{-1} and 8.5×10^4 are the rate constant of glucose oxidase and glycolate oxidase respectively).[70,71] For free flavins the step after the formation of the caged radical pair is the appearance of a flavin hydroperoxide intermediate, which is heterolytically cleaved to H_2O_2 and oxidized flavin (Flavin 7). For the oxidases, there is no detectable flavin hydroperoxide intermediate. This can mean: 1) the intermediate is formed and decays really fast, or 2) instead of the generation of that intermediate, a second electron is transferred from the flavin radical to the caged superoxide to directly form H_2O_2 (Figure 15).
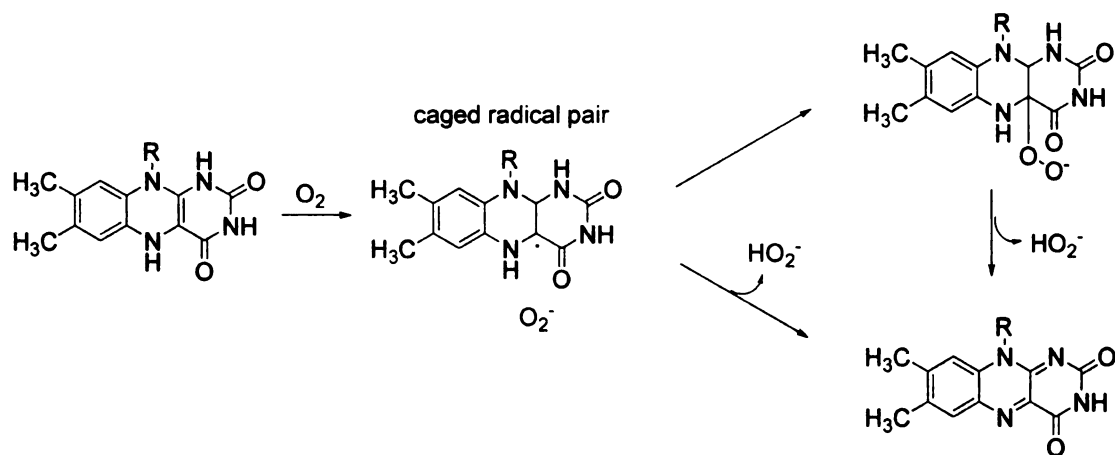
Figure 15. Possible pathways of reaction of oxygen with reduced flavin.

Another reaction characteristic of this group of enzymes is the formation of a stable flavin N(5) adduct with sulfite (Figure 16).[72] This complex doesn't absorb in the visible range, therefore titration of sulfite in an oxidase solution exhibits a gradual

decrease of the flavin absorbance. An example is shown in Figure 17. The dissociation constant K_d of the flavin-sulfite complex for oxidases is in the micromolar range. It has been found that the K_d of sulfite can be correlated with the oxidation reduction potential of the flavoprotein.[73]
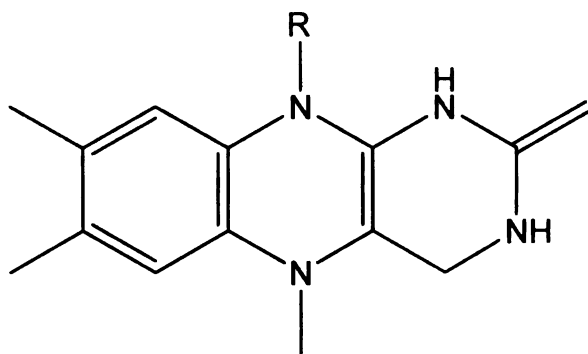
Figure 16. The flavin-sulfite complex is a covalent N(5) adduct.
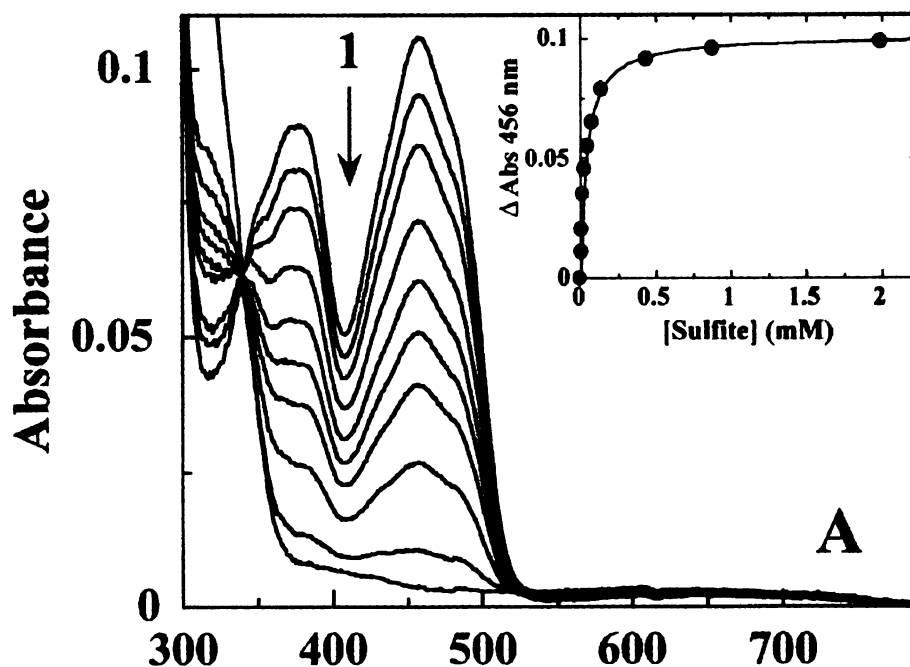
Figure 17. Binding of sulfite to glycine oxidase from *Bacillus subtilis*.[74]

A question that still needs to be answered is whether there are any structural rules that can give hints about the reactivity of flavoenzymes with oxygen. In other words: can we predict if a flavoprotein is an oxidase by looking its 3D structure? According to Mattevi, the answer to this question is no.[75] Two proteins that are very similar structurally are glycolate oxidase and flavocytochrome b_2 (Figure 18). Despite their highly conserved active centers, they exhibit very different oxygen reactivities. Flavocytochrome b_2 has a rate constant for reactions with oxygen of close to zero, whereas glycolate oxidase reacts with a second-order rate constant of 8.5 x 10^4 M^{-1} s^{-1}. The only differences are a replacement of a Trp to Leu and an orientation change of a peptide (Ala198) in the flavocytochrome b_2 that are in contact with the N4-C4a locus of the flavin. From the above observation it can be concluded that changes in the steric constraints and polarity of the area around N4-C4a can greatly modulate oxygen activity.
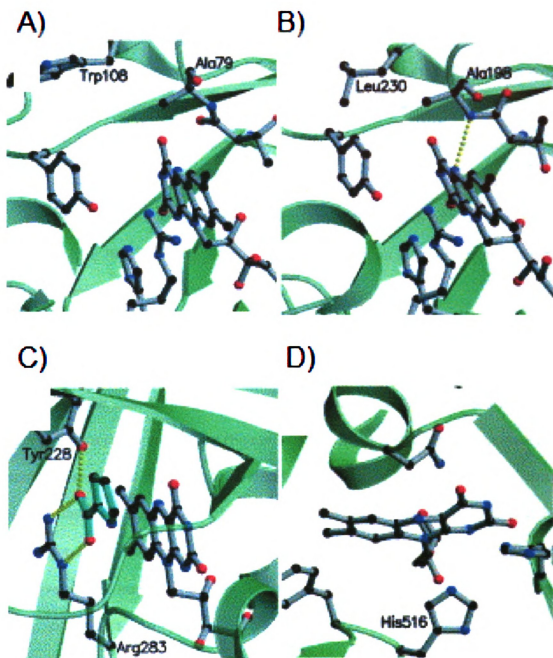
Figure 18. Structure of the active site of several flavoproteins. A) glycolate oxidase, B) flavocytochrome b_2, C) D-amino acid oxidase, and D) glucose oxidase.[75]

Another factor that has been examined is the ability of oxygen to reach the flavin in the active site of a protein. Although it had been thought that the flavins of the oxidases

might be more accessible than those in other flavoenzymes, flavocytochrome b_2 and selected other proteins have accessible flavin which doesn't react with oxygen, and D-amino acid oxidase and other representatives react with oxygen even though they have a shielded coenzyme (Figure 18). Thus, flavin accessibility is not an obvious determining factor for defining the protein reactivity with oxygen. Similarly, whether the flavin is planar or distorted does not determine the reactivity of oxidases. For example, the flavin of D-amino acid oxidase has a planar conformation, whereas that of glucose oxidase is distorted (Figure 18). Therefore, there is no clear connection between the structure of a flavoprotein and its reactivity with oxygen.

Flavoprotein monooxygenases.

As for the case in oxidases, the reduced state of monooxygenases reacts with oxygen to form a caged radical pair (Figure 19). The difference between an oxidase and a monooxygenase is that the first uses molecular oxygen as an electron acceptor, whereas the second inserts an oxygen atom into the substrate.[50] Such enzymes that use NADH or NADPH for their reductive step are called external flavoprotein monooxygenases.[76] Alternatively, the internal flavoprotein monooxygenases utilize a non-nicotinamide primary substrate to reduce the flavin. An example of this group is the lactate monooxygenases, where lactate is oxidized to pyruvate by reducing the flavin of the enzyme. The reduced enzyme then reacts with oxygen, and the C4a-hydroperoxy intermediate reacts with pyruvate to form acetate and carbon dioxide. The resulting C4a-hydroxyflavin completes a catalytic cycle by returning to its oxidized form by dehydration. In the absence of substrate the hydroperoxy intermediate decays to the

oxidized form of protein and hydrogen peroxide, giving the same product as if it were an oxidase. The reactions that are catalyzed by flavin monooxygenases are very diverse, as shown in Figure 20.[76]

These enzymes stabilize neither the cationic nor the neutral semiquinone intermediate. Also, in contrast to oxidases, they don't react with sulfite to form the flavin N(5)-sulfite adduct.[68] Depending on the type of oxygenation, the intermediate C(4a)-hydroperoxyflavin acts as nucleophile (e.g., in Baeyer-Villiger oxidation) or electrophile (e.g., hydroxylation).[68]
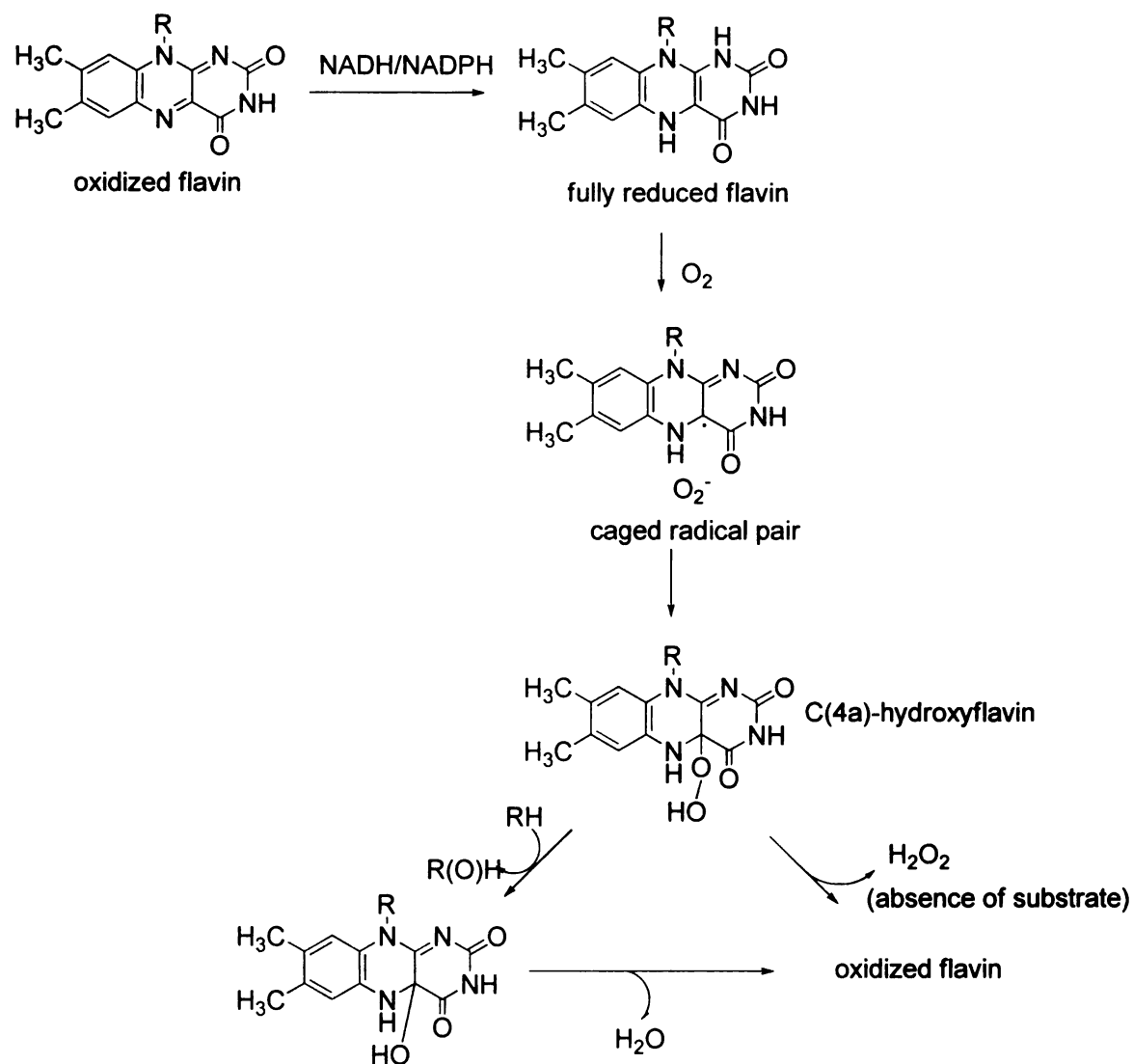
Figure 19. Mechanism of external flavoprotein monooxygenases.
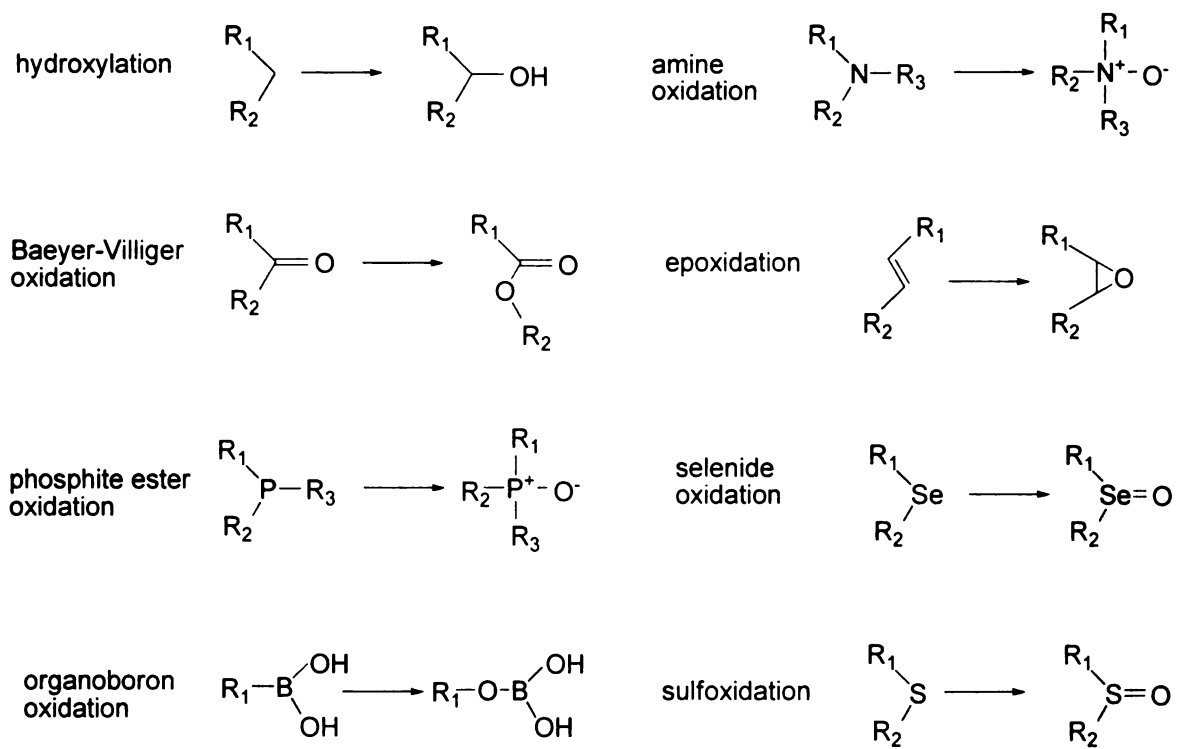
Figure 20. Reactions catalyzed by flavin monooxygenases.

Electron transferases.

Flavoproteins that react with one-electron acceptors or donors and produce O_2^- on reaction with molecular oxygen are called electron transferases. In contrast to oxidases and monooxygenases, the transfereses react sluggishly with oxygen. Also, they don't form the flavin N(5)-sulfite adduct that is characteristic of the oxidase reaction. These proteins stabilize the blue neutral semiquinone intermediate. Another characteristic of these proteins is that most of the flavin molecule is buried in the active site, and only the dimethyl benzene ring is freely accessible to solvent.

There are two groups of electron transferases.[50] The first includes proteins such as flavodoxin and ferredoxin-NADP reductase. This group catalyses electron transfer

between two redox proteins as part of photosynthetic, nitrogen- or sulfate-reducing, hydrogen-evolving, or other electron systems.

Acyl-coenzyme A (CoA) dehydrogenases, which constitute the second group of transferases, catalyze electron transfer reactions that feed electrons into the respiratory chain. Acyl-CoA dehydrogenases are reduced by two electrons as they convert substrate to trans-enoyl-CoA, containing a carbon-carbon double bond.[77] The reduced acyl-CoA dehydrogenase transfers the 2 e⁻, one by one, to another flavoprotein, the electron-transferring flavoprotein.[78] An unusual characteristic of the enzyme is that in the absence of the enoyl-CoA product, the blue neutral semiquinone is stabilized, whereas the red cationic semiquinone is stabilized in the presence of the product.[50]

Flavoproteins with auxiliary redox centers.

The flavoprotein disulfide oxidoreductase has a disulfide as the additional redox center in close juxtaposition to the FAD.[50] NADH or NADPH interacts with the flavin and transfers two electrons that reduce a redox active disulfide. The reduced cysteines then interact with the second substrate which is usually a dithiol, such as glutathione in glutathione reductase, thioredoxin in thioredoxin reductase, or trypanothione in trypanothione reductase. In some cases, the second substrate is not a disulfide; e.g., mercuric ion reductase, NADH peroxidase, NADH oxidase, and 2-ketopropyl-coenzyme M carboxylase/oxidoreductase catalyze reduction of Hg^{2+}, hydrogen peroxide, and molecular oxygen, and the reductive carboxylation of 2-ketopropyl-coenzyme M, respectively.

34

A second subcategory of flavoenzymes with auxiliary redox centers includes the flavocytochromes, which are heme-containing flavoproteins.[50] A very well known example of this class is yeast lactate dehydrogenase, which oxidizes lactate to pyruvate while the flavin (FMN) is reduced by two electrons. The $FMNH_2$ transfers the reducing equivalents one by one to the cytochrome b, which is reoxidized by its external electron acceptor.[79]

The third subset is the non-cytochrome metal-containing group. A representative example is xanthine oxidase, which contains a molybdopterin cofactor and an iron-sulfur cluster ([Fe_2S_2]) in addition to the FAD coenzyme. As Mo is reduced (Mo^{+6} goes to Mo^{+4}), the substrate xanthine is oxidized to urate.[80] The molybdenum cofactor is then re-oxidized by sequential one-electron transfer steps to the FAD through the iron-sulfur clusters. Finally, the $FADH_2$ reduces NAD^+ in order to complete the catalytic cycle.

Flavoenzymes of unknown function.

A very interesting case of a flavoenzyme with unknown function is the old yellow enzyme (OYE), which surprisingly was the first flavoprotein discovered (1932).[81] It was characterized "old" because in 1938 a second "new" yellow protein was isolated.[82] This enzyme together with many other uncharacterized enzymes that have sequence similarity with it comprise a separate family because of their distinct physicochemical characteristics together with uncertainty about their physiological role.

OYE is rapidly reduced by NADPH and can be reoxidized by oxygen.[83] It is believed that NADPH is the physiological reductant; however, the reoxidation with molecular oxygen is slow, and is lower than that obtained with substrates such as

quinones.[82] This enzyme has a variety of substrates, all of them phenolic compounds. Additionally, a very unique behavior of OYE is the development of an intense long absorption spectrum upon binding of the phenolic substrate (Figure 21).[83]
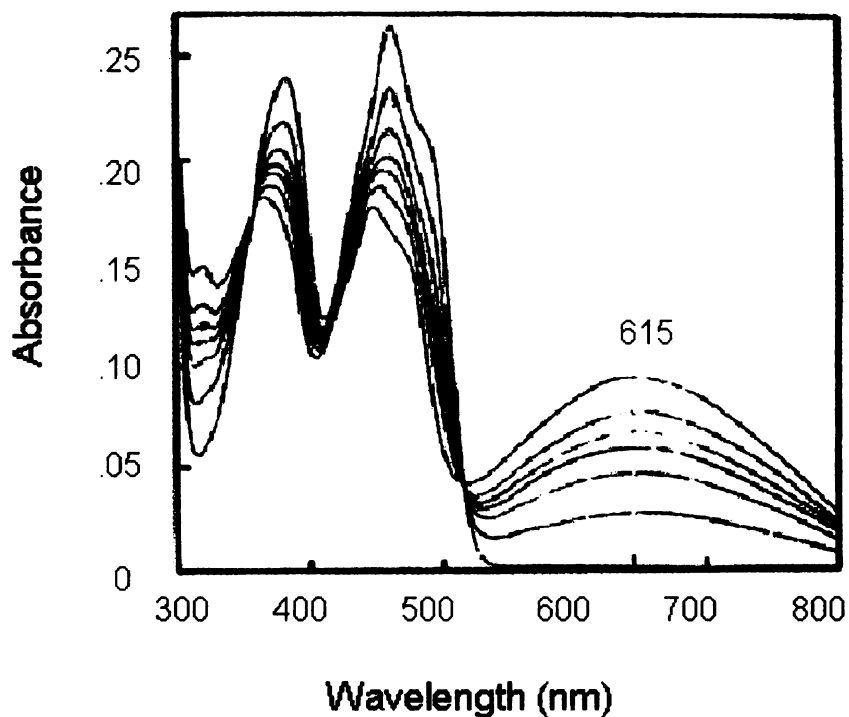
Figure 21. Titration of OYE with p-chlorophenol.[83]

Thesis outline

The following chapters describe three projects that I carried out in the Hausinger laboratory, and do not include additional studies performed while in the laboratory of Joan Broderick.

Chapter 2 details my kinetic and spectroscopic investigation of TauD interactions with Co(II), Ni(II) and N-oxalylglycine (NOG) inhibitors. These metal ions were shown to

cause slow-binding, competitive inhibition of the enzyme. When Fe(II) was replaced by Ni(II), no observable chromophore was produced. On the other hand, when Co(II) was used, a chromophore was obtained, which could be used as a diagnostic marker for αKG-dependent dioxygenases. Kinetic studies on NOG revealed that, despite its close structural similarity to αKG, it is a weak competitive inhibitor of TauD. The NOG-bound state of the enzyme was shown to be incapable of oxygen catalyzed oxidative decarboxylation.

Chapter 3 describes my efforts toward purification and characterization of an *Escherichia coli* αKG-dependent dioxygenase, CsiD, of unknown function. This protein, encoded by the *csiD* gene and activated by carbon starvation, has been crystallized; however, its ability to bind and utilize αKG had not been shown. Anaerobic absorption and EPR spectra of the holoenzyme in the presence of the cosubstrate proved that αKG binds in a bidentate manner to Fe(II) at the active site. Furthermore, the uncoupled reaction of CsiD was probed, using various methods. Finally, the function of the dioxygenase was investigated with a direct method (oxygen consumtion), together with metabolic studies that compared the *Escherichia coli* wild type with the CsiD knock out strains utilizing several probes.

The final chapter describes my examination of YgaF, which is encoded by a gene that is adjacent to *csiD*. YgaF had been proposed to be an FAD-oxidoreductase, but its role was unknown. Here, the first cloning and overexpression of the enzyme is reported. General characterization of YgaF includes photoreduction, titration with sulfite, gradual reduction with dithionite, determination of its redox potential and demonstration that its flavin is non-covalently bound. Oxygen was shown to reoxidize the flavin rapidly, demonstrating that the protein is an oxidase. Various compounds were tested as substrates

of YgaF and studies that compared the metabolism of *E. coli* wild type and YgaF knock out cells were undertaken as well. The only significant activity of YgaF was observed with L-2-hydroxyglutarate.

REFERENCES

[1] Feig, A. L., and Lippard, S. J. (1994) Reactions of non-heme iron(II) centers with dioxygen in biology and chemistry. *Chem. Rev. 94*, 759-805.

[2] Purpero, V., and Moran, G. (2007) The diverse and pervasive chemistries of the α-keto acid dependent enzymes. *J. Biol. Inorg. Chem. 12*, 587-601.

[3] Hausinger, R. P. (2004) Fe(II)-α-ketoglutarate-dependent hydroxylases and related enzymes. *Crit. Rev. Biol. Mol. Biol. 39*, 21-68.

[4] Hutton, J. J., Jr., Trappel, A. L., and Udenfriend, S. (1966) Requirement for α-ketoglutarate, ferrous ion and ascorbate for collagen proline hydroxylase. *Biochem. Biophys. Res. Commun. 24*, 179–184.

[5] Kivirikko, K.I., and Pihlajaniemi, T. (1998) Collagen hydroxylases and the protein disulfide isomerase subunit of prolyl 4-hydroxylase. *Adv. Enzymol. Rel. Areas Mol. Biol. 72*, 325–398.

[6] Hieta, R., and Myllyharju, J. (2002) Cloning and characterization of a low molecular weight prolyl 4-hydroxylase from *Arabidopsis thaliana*. Effective hydroxylation of proline-rich, collagen-like, and hypoxia-inducible transcription factor α-like peptides. *J. Biol. Chem. 277*, 23965–23971.

[7] Kataoka, H., Yamamoto,Y., and Sekiguchi, M. (1983) A new gene (*alkB*) of *Escherichia coli* that controls sensitivity to methyl methane sulfonate. *J. Bacteriol. 153*, 1301–1307.

[8] Chen, B. J., Carroll, P., and Samson, L. (1994) The *Escherichia coli* AlkB protein protects human cells against alkylation-induced toxicity. *J. Bacteriol. 176*, 6255–6261.

[9] Dinglay, S., Trewick, S. C., Lindahl, T., and Sedgwick, B. (2000) Defective processing of methylated single-stranded DNA by *E. coli alkB* mutants. *Genes Develop. 14*, 2097–2105.

[10] Aas, P. A., Otterlei, M., Falnes, P. O., Vagbe, C. B., Skorpen, F., Akbari, M., Sundheim, O., Bjoras, M., Slupphaug, G., Seeberg, E., and Kurkan, U. E. (2003) Human and bacterial oxidative demethylases repair alkylation damage in both RNA and DNA. *Nature 421, 859–863*.

[11] Lloyd, M. D., Merrit, K. D., Lee, V., Sewell, T. J., Wha-Son, B., Baldwin, J. E., Schofield, C. J., Elson, S. W., Baggaley, K. H., and Nicholson, N. H. (1999) Product-

substrate engineering by bacteria: studies on clavaminate synthase, a trifunctional dioxygenase. *Tetrahedron 55*, 10201-10220.

[12] Van Der Ploeg, J. R., Weiss, M. A., Saller, E., Nashimoto, H., Saito, N., Kertesz, M. A., and Leisinger, T. (1996) Identification of sulfate starvation-regulated genes in *Escherichia coli*: a gene cluster involved in the utilization of taurine as a sulfur source. *J. Bacteriol. 178*, 5438-5446.

[13] Fukumori, F., and Hausinger, R. P. (1993) *Alcaligenes eutrophus* JMP134 "2,4-dichlorophenoxyacetate monooxygenase" is an a-ketoglutarate-dependent dioxygenase. *J. Bacteriol. 175*, 2083-2086.

[14] Eichhorn, E., van der Ploeg, J. R., Kertesz, M. A., and Leisinger, T. (1997) Characterization of a-ketoglutarate-dependent taurine dioxygenase from *Escherichia coli*. *J. Biol. Chem. 272*, 23031-23036.

[15] Gissen, P., Preece, M. A., Willshaw, H. A., and McKiernan, P. J. (2003) Ophthalmic follow-up of patients with tyrosinaemia type I on NTBC. *J. Inherit. Metab. Dis. 26*, 13-6.

[16] Moran, G. R. (2005) 4-Hydroxyphenylpyruvate dioxygenase. *Arch. Biochem. Biophys. 433*, 117-128.

[17] Zhang, Z., Ren, J., Stammers, D. K., Baldwin, J. E., Harlos, K., and Schofield, C. J. (2000) Structural origins of the selectivity of the trifunctional oxygenase clavaminic acid synthase. *Nat. Struct. Biol. 7*, 127-133.

[18] Lloyd, M. D., Lee, H.-J., Harlos, K., Zhang, Z.-H., Baldwin, J. E., Schofield, C. J., Charnock, J. M., Garner, C. D., Hara, T., Terwisscha Van Scheltinga, A. C., Valegard, K., Viklund, J. A. C., Hajdu, J., Andersson, I., Danielsson, A., and Bhikhabhai, R. (1999) Studies on the active site of deacetoxycephalosporin C synthase. *J. Mol. Biol. 287*, 943-960.

[19] Elkins, J. M., Ryle, M. J., Clifton, I. J., Dunning Hotopp, J. C., Lloyd, J. S., Burzlaff, N. I., Baldwin, J. E., Hausinger, R. P., and Roach, P. L. (2002) X-ray crystal structure of *Escherichia coli* taurine/a-ketoglutarate dioxygenase complexed to ferrous iron and substrates. *Biochemistry 41*, 5185-5192.

[20] Müller, I., Kahnert, A., Pape, T., Sheldrick, G. M., Meyer-Klaucke, W., Dierks, T., Kertesz, M., and Usòn, I. (2004) Crystal structure of the alkylsulfatase AtsK: insights into the catalytic mechanism of the Fe(II) a-ketoglutarate-dependent dioxygenase superfamily. *Biochemistry 43*, 3075-3088.

[21] Clifton, I. J., Doan, L. X., Sleeman, M. C., Topf, M., Suzuki, H., Wilmouth, R. C., and Schofield, C. J. (2003) Crystal structure of carbapenem synthase (CarC). *J. Biol. Chem.* *278*, 20843-20850.

[22] Stirk, H. J., Woolfson, D. N., Hutchinson, E. G., and Thornton, J. M. (1992) Depicting topology and handedness in jellyroll structures. *FEBS Lett. 308*, 1-3.

[23] Picture taken from: http://courses.cm.utexas.edu/jrobertus/ch339k/overheads-1/JellyRollBarrel.jpg

[24] Ryle, M. J., Padmakumar, R., and Hausinger, R. P. (1999) Stopped-flow kinetic analysis of *Escherichia coli* taurine/a-ketoglutarate dioxygenase: interactions with a-ketoglutarate, taurine, and oxygen. *Biochemistry 38*, 15278-15286.

[25] Hegg, E. L., Whiting, A. K., Saari, R. E., McCracken, J., Hausinger, R. P., and Que, L., Jr. (1999) Herbicide-degrading a-keto acid-dependent enzyme TfdA: metal coordination environment and mechanistic insights. *Biochemistry 38*, 16714-16726.

[26] Proshlyakov, D. A., Henshaw, T. F., Monterosso, G. R., Ryle, M. J., and Hausinger, R. P. (2004) Direct detection of oxygen intermediates in the non-heme Fe enzyme taurine/a-ketoglutarate dioxygenase. *J. Am. Chem. Soc. 126*, 1022-1023.

[27] Riggs-Gelasco, P. J., Price, J. C., Guyer, R. B., Brehm, J. H., Barr, E. W., Bollinger, J. M., Jr., and Krebs, C. (2004) EXAFS spectroscopic evidence for an Fe=O unit in the Fe(IV) intermediate observed during oxygen activation by taurine:alpha-ketoglutarate dioxygenase. *J. Am. Chem. Soc. 126*, 8108-9.

[28] Clifton, I. J., McDonough, M. A., Ehrismann, D., Kershaw, N. J., Granatino, N., and Schofield, C. J. (2006) Structural studies on 2-oxoglutarate oxygenases and related double-stranded β-helix fold protein. *J. Inorg. Biochem. 100*, 644-669.

[29] Serre, L., Sailland, A., Sy, D., Boudec, P., Rolland, A., Pebay-Peyroula, E., and Cohen-Addad, C. (1999) Crystal structure of *Pseudomonas fluorescens* 4-hydroxyphenylpyruvate dioxygenase: an enzyme involved in the tyrosine degradation pathway. *Structure 7*, 977-988.

[30] Clifton, I. J., Hsueh, L.-C., Baldwin, J. E., Harlos, K., and Schofield, C. J. (2001) Structure of proline 3-hydroxylase. Evolution of the family of 2-oxoglutarate dependent dioxygenases. *Eur. J. Biochem. 268*, 6625-6636.

41

[31] Valegard, K., Terwisscha van Scheltinga, A. C., Lloyd, M. D., Hara, T., Ramaswamy, S., Perrakis, A., Thompson, A., Lee, H. J., Baldwin, J. E., Schofield, C. J., Hajdu, J., and Andersson, I. (1998) Structure of a cephalosporin synthase. *Nature 394*, 805-809.

[32] Pavel, E. G., Zhou, J., Busby, R. W., Gunsior, M., Townsend, C. A., and Solomon, E. I. (1998) Circular dichroism and magnetic circular dichroism spectroscopic studies of the non-heme ferrous active site in clavaminate synthase and its interaction with α-ketoglutarate cosubstrate. *J. Am. Chem. Soc. 120*, 743-753.

[33] Pavel, E. G., Zhou, J., Busby, R. W., Gunsior, M., Townsend, C. A., and Solomon, E. I. (1998) Circular dichroism and magnetic circular dichroism spectroscopic studies of the non-heme ferrous active site in clavaminate synthase and its interaction with α-ketoglutarate cosubstrate. *J Am. Chem. Soc. 120*, 743-753.

[34] Ho, R. Y. N., Mehn, M. P., Hegg, E. L., Liu, A., Ryle, M. A., Hausinger, R. P., and Que, L., Jr. (2001) Resonance Raman studies of the iron(II)-α-keto acid chromophore in model and enzyme complexes. *J. Am. Chem. Soc. 123*, 5022-5029.

[35] Lee, H. J., Lloyde, M. D., Clifton, I. J., Baldwin, J. E., and Schofield, C. J. (2001) Kinetic and crystallographic studies on deacetoxycephalosporin C synthase (DAOCS). *J. Mol. Biol. 308*, 937-948.

[36] Winters, K. J., Purpero, V. M., Kavana, M., and Moran, G. R. (2005) Accumulation of multiple intermediates in the catalytic cycle of (4-hydroxyphenyl)pyruvate dioxygenase from *Streptomyces avermitilis*. *Biochemistry 44*, 7189-7199.

[37] Price, J. C., Barr, E. W., Tirupati, B., Bollinger, J. M., Jr., and Krebs, C. (2003) The first direct characterization of a high-valent iron intermediate in the reaction of an α-ketoglutarate-dependent dioxygenase: a high-spin Fe(IV) complex in taurine/α-ketoglutarate dioxygenase (TauD) from *Escherichia coli*. *Biochemistry 42*, 7497-7508.

[38] Hoffart, L. M., Barr, E. W., Guyer, R. B., Bollinger, J. M., Jr., and Krebs, C. (2006) Direct spectroscopic detection of a C-H-cleaving high-spin Fe(IV) complex in a prolyl-4-hydroxylase. *Proc. Natl. Acad. Sci. USA 103*, 14738-14743.

[39] Riggs-Gelasco, P. J., Price, J. C., Guyer, R. B., Brehm, J. H., Barr, E. W., Bollinger, J. M., Jr., and Krebs, C. (2004) EXAFS spectroscopic evidence for an Fe=O unit in the Fe(IV) intermediate observed during oxygen activation by taurine:alpha-ketoglutarate dioxygenase. *J. Am. Chem. Soc. 126*, 8108-8109.

[40] Winters, K. J., Purpero, V. M., Kavana, M., Nelson, T., and Moran, G. R. (2003) (4-Hydroxyphenyl)pyruvate dioxygenase from *Streptomyces avermitilis:* the basis for ordered substrate addition. *Biochemistry 42*, 2072-2080.

[41] Koehntop, K. D., Marimanikkuppam, S., Ryle, M. J., Hausinger, R. P., and Que, L. (2006) Self-hydroxylation of taurine/α-ketoglutarate dioxygenase: evidence for more than one oxygen activation mechanism. *J. Biol. Inorg. Chem. 11*, 63-72.

[42] Liu, A., Ho, R. Y. N., Que, L., Jr., Ryle, M. J., Phinney, B. S., and Hausinger, R. P. (2001) Alternative reactivity of an α-ketoglutarate-dependent iron(II) oxygenase: enzyme self-hydroxylation. *J. Am. Chem. Soc. 123*, 5126-5127.

[43] Bradley, F. C., Lindstedt, S., Lipscomb, J. D., Que, L., Jr., Roe, A. L., and Rundgren, M. (1986) 4-Hydroxyphenylpyruvate dioxygenase is an iron-tyrosinate protein. *J. Biol. Chem. 261*, 11693-11696.

[44] Myllylä, R., Majamaa, K., Günzler, V., Hanauske-Abel, H. M., and Kivirikko, K. I. (1984) Ascorbate is consumed stoichiometrically in the uncoupled reactions catalyzed by propyl 4-hydroxylase and lysyl hydroxylase. *J. Biol. Chem. 259*, 5403-5405.

[45] Yu, B., Edstrom, W. C., Hamuro, Y., Weber, P. C., Gibney, B. R., and Hunt, J. F. (2006) Crystal structures of catalytic complexes of the oxidative DNA/RNA repair enzyme AlkB. *Nature 439*, 879-884.

[46] Chemistry and Biochemistry of Flavoenzymes. Volume I. by Franz Müller (1991) published by CRC Inc. Florida.

[47] De Colibus, L., and Mattevi, A. (2006) New frontiers in structural flavoenzymology. *Curr. Opin. Struct. Biol. 16*, 722-728.

[48] Ghishla, and S., and Massey, V. (1989) Mechanisms of flavoprotein-catalyzed reactions. *Eur. J. Biochem. 181*, 1-17.

[49] Fraaije, M., and Mattevi, A. (2000) Flavoenzymes: diverse catalysts with recurrent features. *Trends Biochem.Sci. 25*, 126-132.

[50] Massey V. (1995) Introduction: Flavoprotein structure and mechanism. *FASEB J. 9*, 473-475.

[51] Fitzpatrick, P. F. (2001) Substrate dehydrogenation by flavoproteins. *Acc. Chem. Res. 34*, 299-307.

[52] Becvar, J. E., and Hastings, J. W. (1975) Bacterial luciferase requires one reduced flavin for light emission. *Proc. Natl. Acad. Sci. USA 72*, 3374-3376.

[53] Komori, H., Masui, R., Kuramitsu, S., Yokoyama, S., Shibata, T., Inoue, Y., and Miki, K. (2001) Crystal structure of thermostable DNA photolyase: pyrimidine-dimer recognition chemistry. *Proc. Natl. Acad. Sci. USA 98*, 13560-13565.

[54] Susin, S. A., Lorenzo, H. K., Zamzani, N., Marzo, I., Snow, B. E., Brothers, G. M., Mangion, J., Jacotot, E., Constantini, P., and Loeffler, M. (1999) Molecular characterization of mitochondrial apoptosis-inducing factor. *Nature 397*, 441-445.

[55] Woodmansee, A. N., and Imlay, J. A. (2002) Reduced flavin promotes oxidative DNA damage in non-respiring *Escherichia coli* by delivering electrons to intracellular free iron. *J. Biol. Chem. 277*, 34055-34066.

[56] Walsh, C. (1980) Flavin coenzymes: at the crossroads of biological redox chemistry. *Acc. Chem. Res. 13*, 148-155.

[57] Miura, R. (2001) Versatility and specificity in flavoenzymes: control mechanisms of flavin reactivity. *Chem. Rec. 1*, 183-194.

[58] Massey, V. (2000) The chemical and biological versatility of riboflavin. *Biochem. Soc. Trans. 28*, 283-296.

[59] Barman, B. G., and Tollin, G. (1972) Flavin-protein interactions in flavoenzymes. Thermodynamics and kinetics of reduction of *Azotobacter* flavodoxin. *Biochemistry 11*, 4755-4759.

[60] Gomez-Moreno, C., Choy, M., and Edmondson, D. E. (1979) Purification and properties of the bacterial flavoprotein: thiamin dehydrogenase. *J. Biol. Chem. 254*, 7630-7635.

[61] Burnett, R. M., Darling, G. D., Kendall, D. S., LeQuesne, M. S., Mayhew, S. G., Smith, W. W., and Ludwig, M., L. (1974) The structure of the oxidized form of *Clostridial flavodoxin* at 1.9-A resolution. Description of the flavin mononucleotide binding site. *J. Biol. Chem. 249*, 4383-4392.

[62] Pace, C., and Stankovich, M. (1986) Oxidation-reduction of glycolate oxidase. *Biochemistry 25*, 2516-2522.

[63] Decker, K. F. (1993) Biosynthesis and function of enzymes with covalently bound flavin. *Ann. Rev. Nutr. 13*, 17-41.

[64] Fraaije, M. W., van de Hawvel, R. H. H., van Berkel, W. J. H., and Mattevi, A. (1999) Covalent flavinylation is essential for efficient redox catalysis in vanillyl-alcohol oxidase. *J. Biol. Chem. 274*, 35514-35520.

[65] Massey, V., Stankovich, M., and Hemmerich, P. (1978) Light mediated reduction of flavoproteins with flavin as catalysts. *Biochemistry 17*, 1-8.

[66] Massey, V., and Hemmerich, P. (1978) Photoreduction of flavoproteins and other biological compounds catalyzed by deazaflavins. *Biochemistry 17*, 9-17.

[67] Rohankhedkar, M. S., Mulrooney, S. B., Wedemeyer, W. J., and Hausinger, R. P. (2006) The AidB component of the *Escherichia coli* adaptive response to alkylating agents is a flavin-containing, DNA-binding protein. *J. Bacteriol. 188*, 223-230.

[68] Massey, V. (1994) Activation of the molecular oxygen by flavins and flavoproteins. *J. Biol. Chem. 269*, 22459-22462.

[69] Kemal, C., Chan, T. W., and Bruice, T. C. (1977) Reaction of $^3O_2$ with dihydroflavins. 1. N3,5-dimethyl-1,5-dihydrolumiflavin and 1,5-dihydroisoalloxazines. *J. Amer. Chem. Soc. 99*, 7272-7286.

[70] Roth, J. P., and Klinman, J. P. (2003) Catalysis of electron transfer during activation of O_2 by the flavoprotein glucose oxidase. *Proc. Natl. Acad. Sci. U.S.A. 100*, 62-67.

[71] Macheroux, P., Massey, V., and Thiele D. J. (1991) Expression of spinach glycolate oxidase in *Saccharomyces cerevisiae*: purification and characterization. *Biochemistry 30*, 4612-4619.

[72] Massey, V., Müller, F., Feldberg, R., Schuman, M., Sullivan, P. A., Howell, L. G., Mayhew, S. G., Matthews, R. G., and Foust, G. P. (1969) The reactivity of flavoproteins with sulfite. *J. Biol. Chem. 244*, 3999-4006.

[73] Müller, F., and Massey, V. (1969) Flavin-sulfite complexes and their structures. *J. Biol. Chem. 244*, 4007-4016.

[74] Job, V., Marcone, G. L., Pilone, M. S., and Pollegioni, L. (2002) Glycine oxidase from *Bacillus subtilis*. *J. Biol. Chem. 277*, 6985-6993.

[75] Mattevi, A., (2006) To be or not to be an oxidase: challenging the oxygen reactivity of flavoenzymes. *Trends Biochem. Sci. 31*, 276-283.

[76] Van Berkel, W. J. H., Kamerbeek, N. M., and Fraaije, M. W. (2006) Flavoprotein monooxygenases, a diverse class of oxidative biocatalysts. *J. Biotechnol.* *124*, 670-689.

[77] Ghisla, S., Thorpe, C., and Massey, V. (1984) Mechanistic studies with general acyl-CoA dehydrogenase and butyryl-CoA dehydrogenase: evidence for the transfer of the β-hydrogen to the flavin N(5)-position as a hydride. *Biochemistry 23*, 3154-3161.

[78] Thorpe, C., and Kim, J. J. P. (1995) Structure and mechanism of action of the acyl-CoA dehydrogenases. *FASEB J. 9*, 718-725.

[79] Rao, K. S., and Lederer, F. (1998) About the pK_a of the active-site histidine in flavocytochromes b_2 (yeast L-lactate dehydrogenase). *Protein Sci. 7*, 1531-1537.

[80] Hille, R. (1996) The mononuclear molybdenum enzymes. *Chem. Rev. 96*, 2757-2816.

[81] Warburg, O. and Christian, W. (1932) Ein zweites sauerstoffübertragendes Ferment und sein Absorptionspektrum. *Naturwissenschaften 20*, 688.

[82] Williams, R. E., and Bruce, N. C. (2002) 'New uses of an old enzyme' – the old yellow enzyme family of flavoenzymes. *Microbiology 148*, 1607-1614.

[83] Karplus, P. A., Fox, K. M., and Massey, V. (1995) Structure-function relations for old yellow proteins. *FASEB J. 9*, 1518-1526.

CHAPTER 2

Kinetic and Spectroscopic Investigation of Co^{II}, Ni^{II}, and N-Oxalylglycine Inhibition of the Fe^{II}/α-Ketoglutarate Dioxygenase, TauD

Piotr Grzyska carried out analysis of the electronic spectra of Co^{II}-substituted forms of TauD.

ABSTRACT

Co^{II}, Ni^{II}, and *N*-oxalylglycine (NOG) are well-known inhibitors of Fe^{II}/α-ketoglutarate (αKG)-dependent hydroxylases, but few studies describe their kinetics and no spectroscopic investigations have been reported. Using taurine/αKG dioxygenase (TauD) as a paradigm for this enzyme family, time-dependent inhibition assays showed that Co^{II} and Ni^{II} follow slow-binding inhibition kinetics. Whereas Ni^{II}-substituted TauD was non-chromophoric, spectroscopic studies of the Co^{II}-substituted enzyme revealed a 6-coordinate site (protein alone or with αKG) that became 5-coordinate upon taurine addition. The Co^{II} spectrum was not perturbed by a series of anions or oxidants, suggesting the Co^{II} is inaccessible and could be used to stabilize the protein. NOG competed weakly (K_i ~290 μM) with αKG for binding to TauD, with the increased electron density of NOG yielding electronic transitions for $NOG-Fe^{II}-TauD$ and taurine-$NOG-Fe^{II}-TauD$ at 380 nm (ε_{380} 90-105 $M^{-1} \times s^{-1}$). The spectra of the NOG-bound TauD species did not change significantly upon oxygen exposure, arguing against the formation of an oxygen-bound state mimicking an early intermediate in catalysis.

INTRODUCTION

Fe^{II}/α-ketoglutarate (αKG)-dependent dioxygenases couple the oxidative decarboxylation of αKG to the oxidation of their primary substrates using a mononuclear, non-heme iron metallocenter.[1] These enzymes catalyze a wide variety of crucial chemical transformations including the repair of alkylation damage in DNA or RNA,[2,3] sensing of hypoxia,[4] modification of structural proteins,[5] synthesis of various metabolites ranging from antibiotics to plant hormones,[6,7,8] and degradation of compounds such as herbicides and phytanic acids.[9,10] The focus of this study is the archetype member of this enzyme family, *Escherichia coli* taurine/αKG dioxygenase (TauD) that metabolizes aminoethane-sulfonate (Figure 5) to produce sulfite as a cellular sulfur source.[11]

Recent crystallographic and spectroscopic studies of TauD have confirmed many aspects of the general enzyme mechanism of Fe^{II}/αKG-dependent dioxygenases (Scheme 4) that was first proposed over two decades ago.[12] Structural studies reveal that the Fe^{II} center is ligated by three amino acid side chains on the same face of the metal: His99, Asp101, and His255.[13,14] In the absence of substrate, three water molecules complete the six-coordinate environment (**A**). Two waters are displaced upon binding of αKG (shown as RCOCOO⁻), which coordinates the Fe^{II} center through its C-1 carboxylate and C-2 carbonyl moieties (**B**) producing a diagnostic metal-to-ligand charge-transfer transition with a λ_{max} at 530 nm and ε_{530} of 140-240 $M^{-1} \times cm^{-1}$.[15,16] Taurine (illustrated by R'-H) binds near the active site and promotes dissociation of the remaining water ligand to shift the λ_{max} to 520 nm with ε_{520} = 180-270 $M^{-1} \times cm^{-1}$,[15,16] leaving the Fe^{II} five-coordinate and primed to react with oxygen (**C**). Binding of oxygen produces a yet uncharacterized Fe^{III}-superoxo or Fe^{IV}-peroxo species (**D**) that attacks the αKG carbonyl group, leading to

49

decomposition of αKG and heterolytic O-O bond cleavage. The resulting Fe^{IV}-oxo species (**E**) inserts oxygen into the target C-H bond of the substrate by hydrogen atom transfer and oxygen rebound, as found in heme-type oxygenases, to restore the Fe^{II} state of the enzyme. The Fe^{IV}-oxo species has been identified on the basis of stopped-flow UV/visible spectroscopy, freeze-quench Mössbauer analyses, EPR spectroscopy of cryoreduced sample, cryogenic continuous-flow resonance Raman studies, and X-ray absorption spectroscopy.[16,17,18,19,20,21]

Here, we examine the kinetics and spectroscopy of TauD interaction with three well-known inhibitors of this class of enzyme. Co^{II} and Ni^{II} inhibit prolyl and asparaginyl hydroxylases that target the hypoxia inducible factor (HIF), involved in oxygen sensing,[22] so the metal ions lead to cellular gene expression changes mimicking those observed during hypoxia.[23,24] In addition, Co^{II} inhibits several other enzyme family members including TauD[11] and 1-aminocyclopropanecarboxylate oxidase, for which the Co-bound crystal structure is known.[25] Despite the importance of these inhibitory metal ions to the functioning of Fe^{II}/αKG-dependent dioxygenases, few kinetic characterization studies and no spectroscopic investigations have been reported. Similarly, the αKG analogue *N*-oxalylglycine (NOG) is an established inhibitor of procollagen prolyl 4-hydroxylase[26,27] as well as HIF-specific prolyl and asparaginyl hydroxylases.[28,29,30] In the asparaginyl hydroxylase known as factor inhibiting HIF (FIH), the structure of the NOG-bound enzyme was determined and NOG was found to coordinate Fe in the same manner as the αKG shown in **B** of Scheme 4.[31] Furthermore, inhibition of the iron-mediated degradation of the iron regulatory protein 2 by dimethyl-NOG (which is hydrolyzed to NOG by esterases within the cell) was cited as evidence for the participation of an Fe^{II}/αKG-

dependent dioxygenase in this pathway.[32,33] As with the inhibitory metals, few NOG-related studies address the kinetics of inhibition and none examine the spectroscopic properties of the inhibited enzyme. We've chosen to study these aspects of Co^{II}, Ni^{II}, and NOG interaction with TauD as a paradigm for related systems. In addition, we sought to obtain new insights into the structures and properties of the early intermediates in TauD catalysis.
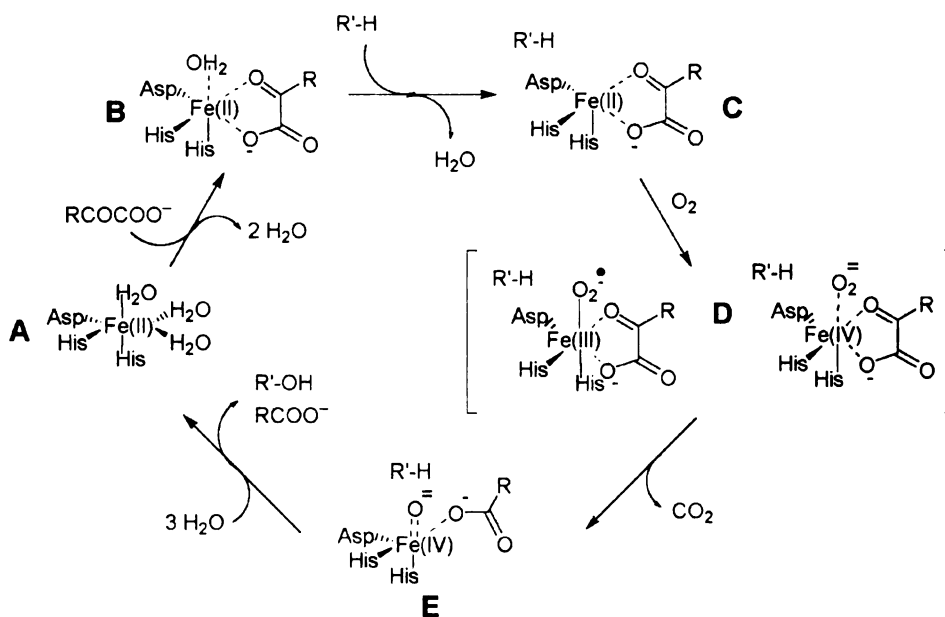
Scheme 4. Catalytic mechanism of TauD.

EXPERIMENTAL PROCEDURES

Purification of TauD apoprotein.

Cultures of *E. coli* BL21(DE3) with pME4141,[11] containing *tauD* under the control of the T7 RNA polymerase promoter, were grown in TB medium (1 L) at 37 °C with stirring at 200 rpm. When cultures reached an A_{600} of ~0.4, *tauD* expression was induced by the addition of isopropyl β-D-thiogalactopyranoside to a final concentration of 0.1 mM. Cells were harvested after ~12 h by centrifugation for 10 min at 10,000 *g* and 4 °C. The cell pellet was resuspended in 20 mL of 20 mM Tris with 1 mM EDTA (TE) buffer (pH 8.0). The sample was stored at -80 °C until disrupting the cells by using a French pressure apparatus. The lysate was clarified by centrifugation for 40 min at 150,000 *g* and applied to a DEAE-Sepharose column (5.0 cm × 30 cm, Amersham Biosciences). The column was rinsed with 2 column volumes of TE buffer (pH 8.0) and eluted by using a linear 1500 ml gradient from 70 to 230 mM NaCl in the same buffer at a flow rate of 7 ml/min. Fractions containing TauD were concentrated in an Amicon stirred cell concentrator with a 30 kDa cutoff membrane. The concentrated eluant was loaded onto a high-performance phenyl-Sepharose column (2.5 cm × 30 cm, Amersham Biosciences) equilibrated with TE buffer (pH 8.0) containing 500 mM $(NH_4)_2SO_4$. Proteins were eluted with a 1200 mL linear gradient from 500 to 0 mM $(NH_4)_2SO_4$ in the same buffer at a flow rate of 5 ml/min. The TauD-containing fractions were concentrated and extensively dialyzed against 25 mM Tris buffer (pH 8.0) at 4°C. Purified TauD apoprotein exhibited a single 32.2 kDa band when examined by denaturing polyacrylamide gel electrophoresis. Protein concentrations were estimated by using ε_{280} 46,400 $M^{-1} \times cm^{-1}$. The dialyzed apoprotein was stored frozen at -80 °C.

Enzyme assays.

TauD activity was measured by using Ellman's reagent to quantify sulfite, as previously described.[11] One unit (U) of enzyme activity is defined as the amount of enzyme that releases 1 μmol of sulfite per min at 30 °C in assay buffer containing 25 mM Tris (pH 8.0), 50 or 100 μM Fe^{II}, 50 or 100 μM ascorbate, 100 or 500 μM αKG, and 1 mM taurine. The TauD used in these studies had a specific activity ranging from 3 to 6.4 U (mg of protein)$^{-1}$.

Characterization of inhibition kinetics.

Steady-state inhibition assays were carried out during 5 min incubations using the typical assay conditions (sometimes with one component varied in concentration) and amended with the indicated concentrations of inhibitor. The assays were initiated either by adding enzyme or by adding Fe^{II} to the assay buffers. In addition, the time dependence of inhibition was assessed in some cases by removing timed aliquots to an EDTA quench solution.

Electronic spectroscopy.

Spectra were recorded at room temperature on a Shimadzu UV-2401 UV/visible spectrophotometer. All stock solutions for anaerobic binding studies were prepared inside serum vials sealed with butyl rubber stoppers and purged of oxygen by several rounds of vacuum degassing and flushing with argon using a vacuum manifold. Stock solutions of αKG (50 or 100 mM), taurine (50 or 100 mM), and NOG (kindly provided by Dr. Nicolai Burzlaff) (100 mM) were prepared in 25 mM Tris buffer (pH 8.0). Ferrous ammonium

sulfate stock solutions (25 mM) containing 5 mM ascorbate were prepared by several rounds of degassing and argon flushing of the solids, followed by addition of the desired volume of H_2O. $CoCl_2$ and $NiCl_2$ stock solutions (25 mM) were prepared by several rounds of degassing and flushing with argon inside a sealed serum vial. TauD apoprotein (0.25 or 0.5 mM subunit in 25 mM Tris buffer, pH 8.0) was placed into a 1 cm path length, 1 mL quartz cuvette fitted with a stopper and purged with argon. Other components were added by using gastight syringes (Hamilton) that had been flushed with anaerobic buffer. Selected samples were mixed with an equal volume of buffer sparged with 100 % O_2, and spectral changes were monitored over time. The effect of added H_2O_2 was examined in one sample. All spectra were corrected to account for sample dilutions.

RESULTS AND DISCUSSION

Kinetics of Inhibition of TauD by Co^{II} and Ni^{II}

The effects of Co^{II} and Ni^{II} on TauD activity were examined by using two methods to initiate the assays. First, TauD apoprotein was added to standard assay mixes containing Fe^{II} and varied concentrations of the inhibitory metal ions, incubated for 5 min, and the total sulfite product measured (Figure 22, solid lines). The data were fit to equation 1 (where [M] is the inhibitory metal ion concentration) to determine the IC_{50} (inhibitor concentration resulting in 50% inhibition, with the approximate range of this value shown in parentheses). The IC_{50} of Co^{II} was 41 μM (30-70 μM) while that of Ni^{II} was 32 μM (20-40 μM). When the TauD inhibition assays were repeated using Fe^{II} addition to initiate the reaction (Fig. 1, dashed lines), the observed IC_{50} values were 1.9 μM (1-3.5 μM) and 0.71 μM (0.60-1.0 μM) for Co^{II} and Ni^{II}, respectively. The large differences in IC_{50} values observed when using the distinct methods to initiate the reaction suggest that Fe^{II} does not readily displace the inhibitory metal ions previously bound to the protein. These differences also highlight the fact that steady-state assays that assume rapid equilibrium kinetics are inadequate for defining the true kinetic inhibition mechanism of metal ions. Despite this caveat, the IC_{50} values obtained for TauD were compared to those reported for three human HIF-specific prolyl 4-hydroxylase isozymes (38 ± 8, 100 ± 15, and 9 ± 4 μM for Co^{II}; 130 ± 76, >1000, and 120 ± 49 μM for Ni^{II}) and a collagen-specific prolyl 4-hydroxylase (14 ± 3 μM for Co^{II} and 37 ± 11 μM for Ni^{II}) along with the K_i values estimated for FIH inhibition (1.0 ± 0.4 μM for Co^{II} and 4 ± 1 μM for Ni^{II}) [22]. Curiously, Co^{II} and Ni^{II} inhibition of the HIF prolyl 4-hydroxylases was incomplete with up to 50 %

activity remaining at 0.5 mM Co^{II} and up to 55 % activity remaining at 1 mM Ni^{II}. We

attribute the incomplete inhibition of the prolyl 4-hydroxylases to their purification as

partial holoproteins, compared to TauD that was purified as the apoprotein.

% activity remaining = $100 - 100[M]/(IC_{50} + [M])$ Equation 1
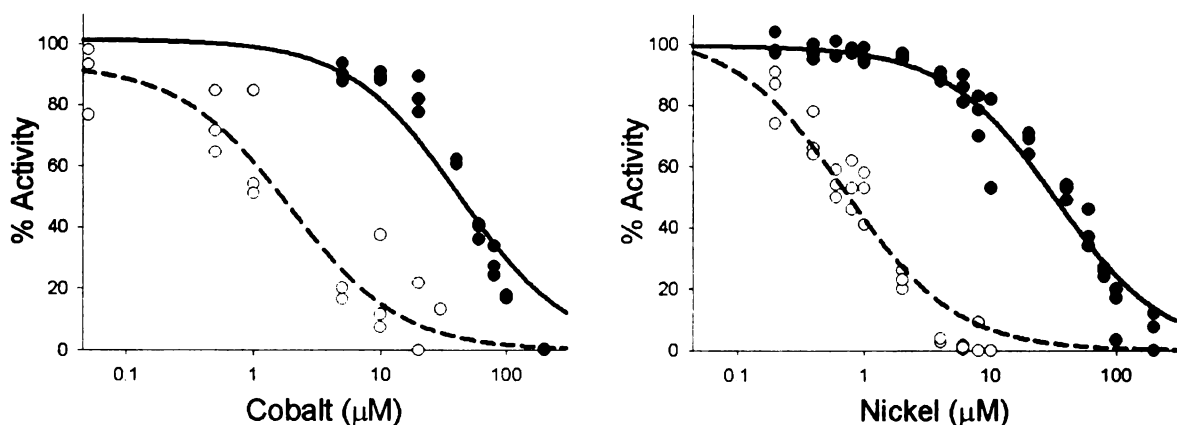
Figure 22. Inhibition of TauD by Co^{II} and Ni^{II}. The concentrations of sulfite produced
during 5 min incubations were used to assess the percent activity of TauD in standard
assay conditions containing the indicated concentrations of Co^{II} (left panel) and Ni^{II} (right
panel). The solid circles represent data associated with assays initiated with TauD
apoprotein, whereas the open circles represent data for assays initiated by Fe^{II} addition to
samples exposed to inhibitory metal ions for 2 min. The data were fit to equation 1 to
calculate IC_{50} values.

To better define the kinetic mechanism of inhibition by metal ions, the time-

dependence of Co^{II} and Ni^{II} inhibition were determined (Figure 23A and Figure 23B). In

the absence of inhibitory metal ion, sulfite production began immediately (i.e., TauD

apoprotein binds Fe^{II} rapidly) and increased steadily. When various concentrations of Co^{II}

or Ni^{II} were added at 23 sec into the assays, the rates of sulfite production were observed

to decrease over time. The apparent first-order rate constants of enzyme inactivation were

56

calculated for each assay according to equation 2 (where P_t is the amount of product at time t, v_i is the initial rate, and k_{inact} is the apparent inactivation rate constant), and the values replotted as a function of inhibitory metal ion concentrations (Figure 23C and Figure 23D). The apparent k_{inact} values were observed to saturate at high concentrations of metal ions, consistent with slow-binding inhibition kinetics (Scheme 5).[34] The initial dissociation constant K_i (k_{-1}/k_1) was estimated to be 600 ± 180 μM for Co^{II} and 166 ± 65 μM for Ni^{II}, and k_3 (equivalent to $(k_{inact})_{max}$) was estimated as 0.044 ± 0.008 s^{-1} for Co^{II} and 0.078 ± 0.0012 s^{-1} for Ni^{II}.

$$P_t = v_i\,(1\text{-exp}(-k_{inact}t))/k_{inact} \qquad\qquad \text{Equation 2}$$
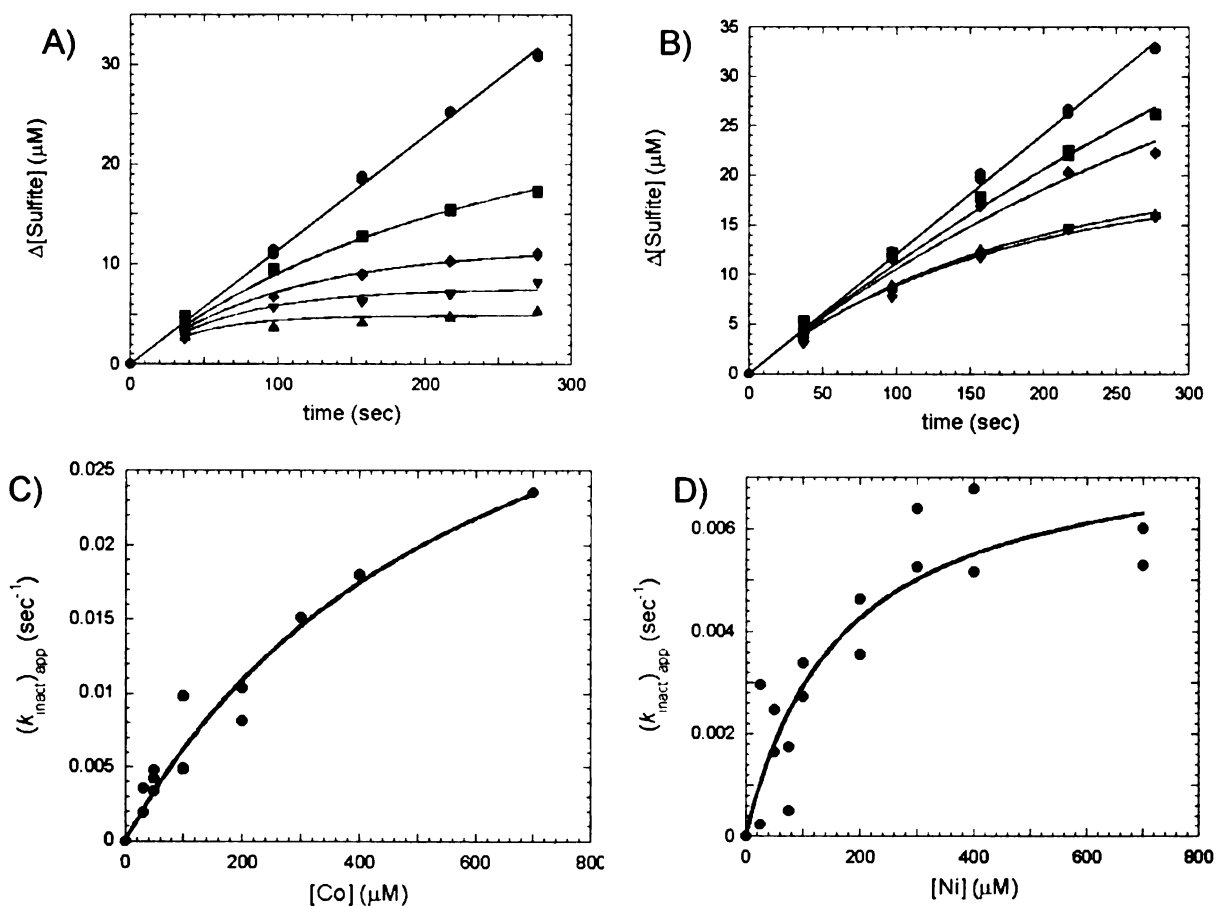
Figure 23. Time-dependent inhibition of TauD by Co^{II} and Ni^{II}. TauD apoprotein was added to standard assay conditions and varied concentrations of Co^{II} or Ni^{II} (including 0 μM, ●; 50 μM, ■, 100 μM, ◆; 300 μM, ▼, and 700 μM, ▲) were added after 23 sec (equivalent to the zero time point in the subset of studies illustrated in panels A and C). Subsequent productions of sulfite were analyzed according to equation 2 to determine the effects of inhibitory metal concentrations on k_{inact}, the apparent rates of inactivation, as illustrated in panels B and D.

Scheme 5. Slow-binding inhibition kinetics.

The addition of Co^{II} to an anaerobic sample of TauD (Figure 24A) resulted in formation of a broad peak between 450 and 600 nm, with λ_{max} at 530 nm and ϵ_{530} of 70 M^{-1} $\times$ cm^{-1} (calculated on the basis of the difference spectrum of Co^{II}-TauD minus TauD). The addition of αKG had little effect on the spectrum, whereas the further addition of taurine resulted in features at 565, 552, and 500 nm with extinction coefficients of 204, 200, and 127 M^{-1} $\times$ cm^{-1} (calculated on the basis of the difference spectrum for taurine-αKG-Co^{II}-TauD minus TauD). The magnitude of the Co^{II} extinction coefficient has been shown empirically to correlate with the coordination number in Co^{II} proteins: six-coordinate sites have extinction coefficients about 50 M^{-1} x cm^{-1}, five-coordinate sites have values between 50 and 300 M^{-1} x cm^{-1}, and four-coordinate sites possess a coefficient of more than 300 M^{-1} x cm^{-1}.[35] We conclude that the Co^{II} sites in Co^{II}-TauD and αKG-Co^{II}-TauD are six-coordinate, whereas that in taurine-αKG-Co^{II}-TauD is five-coordinate. Thus, the binding of substrate most likely leads to dissociation of a water molecule in this metal-substituted protein just as in the active, Fe^{II}-containing enzyme.

We examined the accessibility of TauD-bound Co to exogenous ligands using both taurine-αKG-Co^{II}-TauD and αKG-Co^{II}-TauD. No spectral changes were detected for either species upon addition of CN$^-$, OCN$^-$, SCN$^-$, or ClO$^-$ at 4 mM concentrations, or in the presence of 200 mM NaCl. Although the metal coordination environment of taurine-αKG-Co^{II}-TauD appears to closely resemble that of taurine-αKG-Fe^{II}-TauD, the spectrum of the Co^{II}-containing species remained unchanged when exposed to oxygen. Furthermore, despite precedence for the transformation of Co^{II} species to Co^{III}-

OOH model compounds,[36,37] no spectral perturbations were observed when H_2O_2 (up to 750 μM) was added to taurine-αKG-Co^{II}-TauD.

In contrast to the situation for Co^{II}, the addition of Ni^{II} did not affect the spectra of TauD, protein plus αKG, protein with both substrates, or for these components plus oxygen (data not shown).

A)

ε (M⁻¹ cm⁻¹)

B)

Δε (M⁻¹ cm⁻¹)

C)

Wavelength (nm)

Δε (M⁻¹ cm⁻¹)
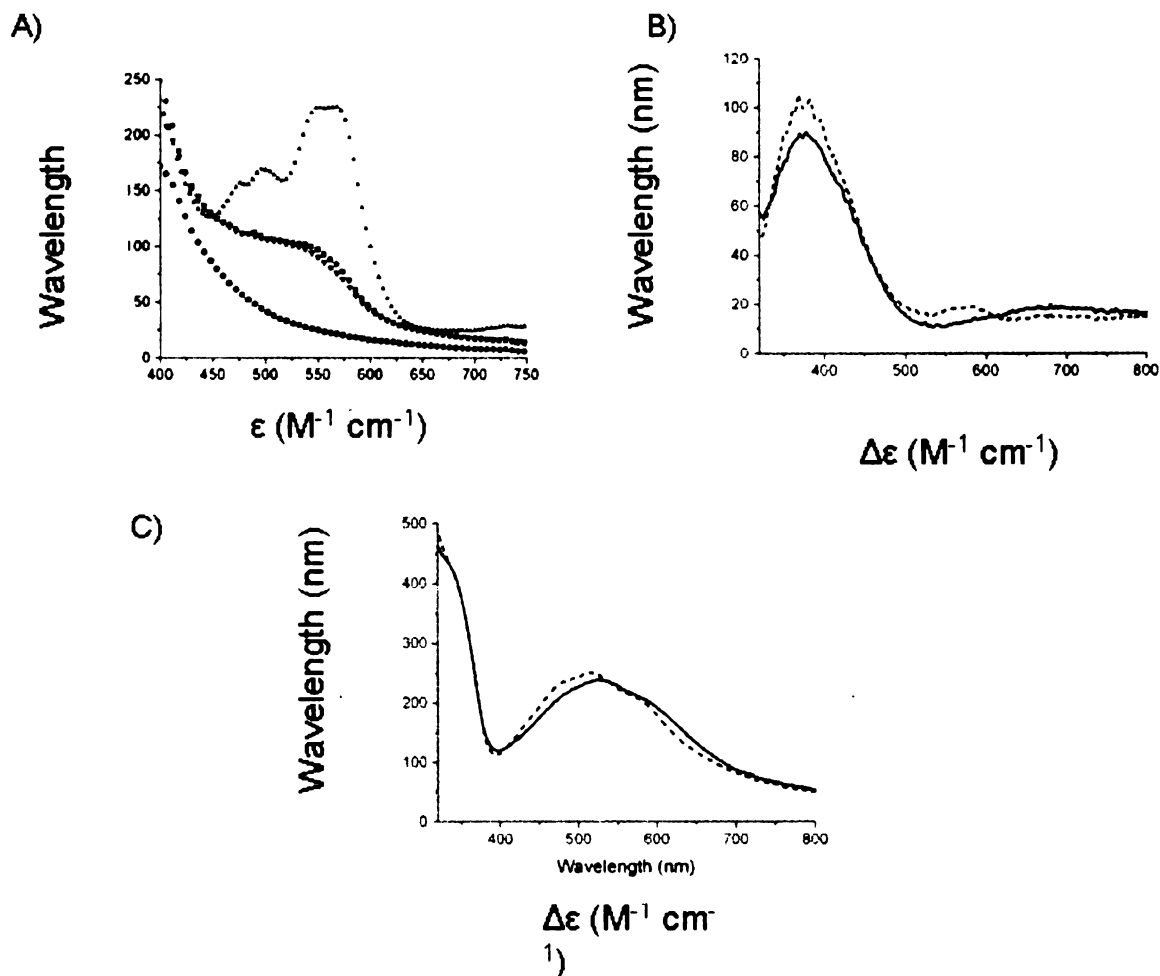
Figure 24. Electronic spectra of Co^{II}-substituted, NOG-Fe^{II}, and αKG-Fe^{II} forms of TauD. (A) An anaerobic solution of TauD apoprotein (550 μM subunit, circles) was adjusted to contain near stoichiometric amounts of Co^{II} (inverted triangles), 2 mM αKG (squares), and 2 mM taurine (triangles) in 25 mM Tris buffer, pH 8.0. (B) Analogous spectra were collected for 250 μM TauD while substituting Fe^{II} for Co^{II} and 10 mM NOG for αKG, with difference spectra shown for the taurine-NOG-Fe^{II}-TauD minus Fe^{II}-TauD (dashed line) and the NOG-Fe^{II}-TauD minus Fe^{II}-TauD samples (solid line). (C) Analogous spectra were collected using Fe^{II} and αKG, again showing difference spectra

60

for the taurine-αKG-Fe^{II}-TauD minus Fe^{II}-TauD (dashed line) and the αKG-Fe^{II}-TauD minus Fe^{II}-TauD (solid line) samples.

Kinetics of Inhibition of TauD by NOG

Steady-state kinetic inhibition studies (data not shown) were used to establish that NOG competed with αKG for binding to TauD, with a K_i of 290 ± 90 μM. *N*-oxalyglycine should be able to form all of the ionic interactions of αKG and it contains an oxamic acid moiety as a potentially better bidentate ligand for the enzyme-bound Fe^{II}, so we were surprised by the weak inhibition of TauD by this compound. For comparison, NOG was shown to be a competitive inhibitor of collagen prolyl 4-hydroxylase and FIH with markedly different K_i values of 1.9 to 7.0 μM and 1.2 ± 0.3 mM.[26,30] The reasons for this wide range of K_i values for these enzymes remain unclear, but interactions with the protein side chains probably play a role in determining this value. Studies with the structurally related compound *N*-oxalyl-D-phenylalanine provided a K_i of 83 ± 18 μM for FIH,14-fold lower than that of αKG.[30]

Spectroscopy of NOG interaction with TauD

The spectra of NOG-Fe^{II}-TauD and taurine-NOG-Fe^{II}-TauD (Figure 24B) differ significantly from the previously described spectra of αKG-Fe^{II}-TauD and taurine-αKG-Fe^{II}-TauD (shown for comparison in Figure 24C). We interpret this result in terms of the excess electron density of NOG compared to αKG (note the trianionic form of NOG versus the dianionic αKG, Scheme 6) which causes a shift of the metal-to-ligand charge-transfer transition to higher energy. While αKG-Fe^{II}-TauD is known to react with oxygen resulting in αKG decomposition, protein self hydroxylation, and the generation of a 550

nm chromophore,[38] the spectra of NOG-Fe^{II}-TauD and taurine-NOG-Fe^{II}-TauD did not change at a significant rate upon exposure to oxygen. The reduced O_2 reactivity for these species also contrasts with that observed for the product complex (succinate-Fe^{II}-TauD) that generates a 720 nm chromophore when exposed to O_2.[39] The αKG- and succinate-derived ligand-to-metal charge-transfer transitions arise from chelation of Fe^{III} by the catecholate produced by hydroxylation of Tyr73, with or without bound bicarbonate ligand.[39] We conclude that hydroxylation of Tyr73 is greatly reduced using NOG-Fe^{II}-TauD and that NOG does not undergo oxidative decarboxylation.

α-Ketoglutarate   N-oxalylglycine   deprotonated N-oxalylglycine
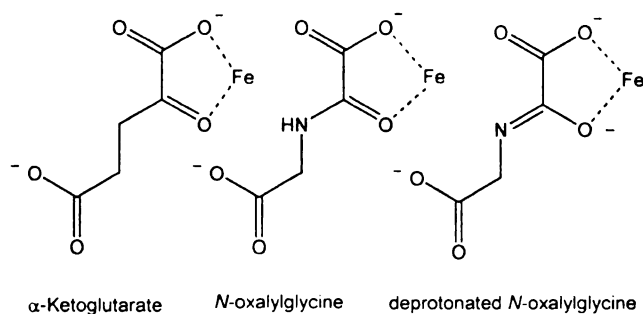
Scheme 6. Binding mode of αKG and postulated modes for binding NOG to iron metal ion.

CONCLUSIONS

Steady-state kinetic approaches are inappropriate for determining the kinetics of inhibition of $Fe^{II}/\alpha KG$-dependent hydroxylases by metal ions; rather, slow-binding kinetic inhibition methods must be utilized. The chromophore generated upon binding of both substrates to Co^{II}-substituted protein might serve as a useful diagnostic marker for this enzyme family. While the resulting Co^{II} center is most likely 5-coordinate in TauD, it does not react with added ligands including oxidants. The low reactivity of the Co^{II}- and Ni^{II}-substituted enzymes could be exploited during purification and crystallization efforts to stabilize related proteins against self-hydroxylation reactions. Despite the close structural similarity of NOG to αKG, this is a weak competitive inhibitor of TauD and the K_i ranges widely for different enzymes. The NOG-bound state of the enzyme does not react with oxygen to catalyze oxidative decarboxylation.

REFERENCES

[1] Hausinger, R. P., (2004) Fe(II)/a-ketoglutarate-dependent hydroxylases and related enzymes. *Crit. Rev. Biochem. Mol. Biol. 39*, 21-68.

[2] Trewick, S. C., Henshaw, T. F., Hausinger, R. P., Lindahl, T., and Sedgwick, B. (2002) Oxidative demethylation by *Escherichia coli* AlkB directly reverts DNA base damage. *Nature 419*, 174-178.

[3] Aas, P. A., Otterlei, M., Falnes, P. O., Vagbe, C. B., Skorpen, F., Akbari, M., Sundheim, O., Bjoras, M., Slupphaug, G., Seeberg, E., and Krokan, H. E. (2003) Human and bacterial oxidative demethylases repair alkylation damage in both RNA and DNA. *Nature 421*, 859-863.

[4] Schofield, C. J. and Ratcliffe, P. J. (2004) Oxygen sensing by hydroxylases. *Nat. Rev. Molec. Cell Biol. 5*, 343-354.

[5] Kivirikko, K. I., and Pihlajaniemi, T. (1998) Collagen hydroxylases and the protein disulfide isomerase subunit of prolyl 4-hydroxylase. *Adv. Enzymol. Rel. Areas Mol. Biol. 72*, 325-398.

[6] Baldwin, J. E., and Abraham, E. (1988) The biosynthesis of penicillins and cephalosporins. *Nat. Prod. Rep. 5*, 129-145.

[7] Dixon, R. A., and Steele, C. L. (1999) Flavonoids and isoflavonoids - a gold mine for metabolic engineering. *Trends Plant Sci. 4*, 394-400.

[8] Hedden, P. (1999) Recent advances in gibberellin biosynthesis. *J. Exper. Bot. 50*, 553-563.

[9] Fukumori, F., and Hausinger, R. P. (1993) Purification and characterization of 2,4-dichlorophenoxyacetate/α-ketoglutarate dioxygenase. *J. Biol. Chem. 268*, 24311-24317.

[10] Mukherji, M., Schofield, C. J., Wierzbicki, A. S., Jansen, G. A., Wanders, R. J. A., and Lloyd, M. D. (2003) The chemical biology of branched-chain lipid metabolism. *Prog. Lipid Res. 42*, 359-376.

[11] Eichhorn, E., van der Ploeg, J. R., Kertesz, M. A., and Leisinger, T. (1997) Characterization of α-ketoglutarate-dependent taurine dioxygenase from *Escherichia coli*. *J. Biol. Chem. 272*, 23031-23036.

[12] Hanauske-Abel, H. M., and Günzler, V. (1982) A stereochemical concept for the catalytic mechanism of prolylhydroxylase. Applicability to classification and design of inhibitors. *J. Theor. Biol. 94*, 421-455.

[13] Elkins, J. M., Ryle, M. J., Clifton, I. J., Dunning Hotopp, J. C., Lloyd, J. S., Burzlaff, N. I., Baldwin, J. E., Hausinger, R. P., and Roach, P. L. (2002) X-ray crystal structure of *Escherichia coli* taurine/α-ketoglutarate dioxygenase complexed to ferrous iron and substrates. *Biochemistry 41*, 5185-5192.

[14] O'Brien, J. R., Schuller, D. J., Yang, V. S., Dillard, B. D., and Lanzilotta, W. N. (2003) Substrate-induced conformational changes in *Escherichia coli* taurine/α-ketoglutarate dioxygenase and insight into the oligomeric structure. *Biochemistry 42*, 5547-5554.

[15] Ryle, M. J., Padmakumar, R., and Hausinger, R. P. (1999) Stopped-flow kinetic analysis of *Escherichia coli* taurine/α-ketoglutarate dioxygenase: interactions with α-ketoglutarate, taurine, and oxygen. *Biochemistry 38*, 15278-15286.

[16] Grzyska, P. K., Ryle, M. J., Monterosso, G. R., Liu, J., Ballou, D. P., and Hausinger, R. P. (2005) Steady-state and transient kinetic analyses of taurine/α-ketoglutarate dioxygenase: effects of oxygen concentration, alternative sulfonates, and active site variants on the Fe(IV) intermediate. *Biochemistry 44*, 3845-3855.

[17] Price, J. C., Barr, E. W., Glass, T. E., Krebs, C., and Bollinger, J. M., Jr. (2003) Evidence for hydrogen abstraction from C1 of taurine by the high-spin Fe(IV) intermediate detected during oxygen activation by taurine:α-ketoglutarate dioxygenase (TauD). *J. Am. Chem. Soc. 125*, 13008-13009.

[18] Price, J. C., Barr, E. W., Tirupati, B., Bollinger, J. M., Jr., and Krebs, C. (2003) The first direct characterization of a high-valent iron intermediate in the reaction of an α-ketoglutarate-dependent dioxygenase: a high-spin Fe(IV) complex in taurine/α-ketoglutarate dioxygenase (TauD) from *Escherichia coli. Biochemistry 42*, 7497-7508.

[19] Price, J. C., Barr, E. W., Hoffart, L. M., Krebs, C., and Bollinger, J. M., Jr. (2005) Kinetic dissection of the catalytic mechanism of taurine:α-ketoglutarate dioxygenase (TauD) from *Escherichia coli. Biochemistry 44*, 8138-8147.

[20] Proshlyakov, D. A., Henshaw, T. F., Monterosso, G. R., Ryle, M. J., and Hausinger, R. P. (2004) Direct detection of oxygen intermediates in the non-heme Fe enzyme taurine/α-ketoglutarate dioxygenase. *J. Am. Chem. Soc. 126*, 1022-1023.

[21] Riggs-Gelasco, P. J., Price, J. C., Guyer, R. B., Brehm, J. H., Barr, E. W., Bollinger, J. M., Jr., and Krebs, C. (2004) EXAFS spectroscopic evidence for an Fe=O unit in the

Fe(IV) intermediate observed during oxygen activation by taurine:α-ketoglutarate dioxygenase. *J. Am. Chem. Soc. 126*, 8108-8109.

[22] Hirsilä, M., Koivunen, P., Xu, L., Seeley, T., Kivirikko, K. I., and Myllyharju, J. (2005) Effect of desferrioxamine and metals on the hydroxylases in the oxygen sensing pathway. *FASEB J. 19*, 1308-1310.

[23] Goldberg, M. A., Dunning, S. P., and Bunn, H. F. (1988) Regulation of the erythropoietin gene: evidence that the oxygen sensor is a heme protein. *Science 242*, 1412-1415.

[24] Vengellur, A., Phillips, J. M., Hogenesch, J. B., and LaPres, J. J. (2005) Gene expression profiling of hypoxia signaling in human hepatocellular carcinoma cells. *Physiol. Genomics 22*, 308-318.

[25] Zhang, Z., Ren, J.-S., Clifton, I. J., and Schofield, C. J. (2004) Crystal structure and mechanistic implications of 1-aminocyclopropane-1-carboxylic acid oxidase--the ethylene-forming enzyme. *Chem. Biol. 11*, 1383-1394.

[26] Baader, E., Tschank, G., Baringhaus, K. H., Burghard, H., and Gunzler, V. (1994) Inhibition of prolyl 4-hydroxylase by oxalyl amino acid derivatives in vitro, in isolated microsomes and in embryonic chicken tissues. *Biochem. J. 300*, 525-530.

[27] Cunliffe, C. J., Franklin, T. J., Hales, N. J., and Hill, G. B. (1992) Novel inhibitors of prolyl 4-hydroxylase. 3. Inhibition by the substrate analogue N-oxaloglycine and its derivatives. *J. Med. Chem. 35*, 2652-2658.

[28] Chan, D. A., Sutphin, P. D., Denko, N. C., and Giaccia, A. J. (2002) Role of prolyl hydroxylation in oncogenically stabilized hypoxia-inducible factor-1α. *J. Biol. Chem. 277*, 40112-40117.

[29] Wojtaszek, P., Smith, C. G., and Bolwell, G. P. (1999) Ultrastructural localization and further biochemical characterization of prolyl 4-hydroxylase from Phaseolus vulgaris: comparative analysis. *Int. J. Cell Biol. 31*, 463-477.

[30] McDonough, M. A., McNeill, L. A., Tilliet, M., Papmichaël, C. A., Chen, Q.-Y., Banerji, B., Hewitson, K. S., and Schofield, C. J. (2005) Selective inhibition of factor inhibiting hypoxia-inducible factor. *J. Am. Chem. Soc. 127*, 7680-7681.

[31] Elkins, J. M., Hewitson, K. S., McNeill, L. A., Seibel, J. F., Schlemminger, I., Pugh, C. W., Ratcliffe, P. J., and Schofield, C. J. (2003) Structure of factor-inhibiting hypoxia-

inducible factor (HIF) reveals mechanism of oxidative modification of HIF-1α. *J. Biol. Chem. 278*, 1802-1806.

[32] Wang, J., Chen, G., Muckenthaler, M., Galy, B., Hentze, M. W., and Pantopoulos, K. (2004) Iron-mediated degradation of IRP2, an unexpected pathway involving a 2-oxoglutarate-dependent oxygenase activity. *Molec. Cell. Biol.* 24, 954-965.

[33] Hanson, E. S., Rawlins, M. L., and Leibold, E. A. (2003) Oxygen and iron regulation of iron regulatory protein 2. *J. Biol. Chem. 278*, 40337-40342.

[34] Morrison, J. F., and Walsh, C. T. (1988) The behavior and significance of slow-binding enzyme inhibitors. *Adv. Enzymol. Rel. Areas Mol. Biol. 61*, 201-301.

[35] Bertini, I., and Luchinat, C. High spin cobalt(II) as a probe for the investigation of metalloproteins. In *Advances in Inorganic Biochemistry*, Eichhorn, G. L.; Marzilli, L. G., Eds. Elsevier Science Publishing Company: New York, NY, 1984; Vol. 6, pp 71-111.

[36] Rajani, C., Kincaid, J. R., and Petering, D. H. (2004) Resonance Raman studies of HOO-Co(III)bleomycin and Co(III)bleomycin: identification of two important vibrational modes, nu(Co-OOH) and nu(O-OH). *J. Am. Chem. Soc. 126*, 3829-3836.

[37] Chaves, F. A., and Mascharak, P. K. (1999) Co(III)-alkylperoxo complexes: syntheses, structure-reactivity correlations, and use in the oxidation of hydrocarbons. *Acc. Chem. Res. 33*, 539-545.

[38] Ryle, M. J., Liu, A., Muthukumaran, R. B., Ho, R. Y. N., Koehntop, K. D., McCracken, J., Que, L., Jr., and Hausinger, R. P. (2003) O_2- and α-ketoglutarate-dependent tyrosyl radical formation in TauD, an α-keto acid-dependent non-heme iron dioxygenase. *Biochemistry 42*, 1854-1862.

[39] Ryle, M. J., Koehntop, K. D., Liu, A., Que, L., Jr., and Hausinger, R. P. (2003) Interconversion of two oxidized forms of TauD, a non-heme iron hydroxylase: evidence for bicarbonate binding. *Proc. Natl. Acad. Sci. USA 100*, 3790-3795.

CHAPTER 3

Isolation and characterization of CsiD

Dr. Tina Müller participated in the cloning, the Biolog plates studies, the GC-MS analysis, and testing of some molecules as CsiD substrates. Meng Li collected the EPR spectra. Dr. Jones helped in the GC-MS analysis.

ABSTRACT

CsiD, an *Escherichia coli* protein of unknown function, is a putative α-ketoglutarate (αKG)-dependent dioxygenase whose crystal structure has been reported. The *csiD* gene is located upstream of the *gabDTP-csiR* operon and regulated by carbon starvation induction, perhaps hinting at its physiological role. After cloning and overexpression of the gene, the CsiD protein was purified and shown to be a tetramer, in agreement with the literature. Binding of the αKG cosubtrate to the active site of CsiD was probed by EPR and spectrophotometric methods. The enzyme was found to catalyze an uncoupled reaction in which oxygen and αKG were consumed in the absence of primary substrate by an ascorbate-dependent process. Many compounds were tested as potential substrates of the putative dioxygenase by testing for enhanced oxygen consumption using an oxygen electrode assay, but without any positive result. Additionally, a series of comparisons between the *E. coli* wild type and *csiD*-knockout strains was undertaken, including use of Biolog plates, GC-MS metabolic studies and amino acid analysis; however, the observed differences did not reveal the role of this protein.

INTRODUCTION

The *Escherichia coli csiD* and *ygaF* genes encode proteins of unknown function and are positioned adjacent to the *gabDTP-csiR* operon (Figure 25), leading to the suggestion that CsiD may participate in the metabolic pathway for γ-aminobutyric acid (GABA) catabolism.[7] The *gab* cluster includes *gabP* encoding a transport carrier protein responsible for the uptake of GABA, *gabD* encoding a succinate semialdehyde dehydrogenase, and *gabT* encoding a GABA transaminase.[1] Succinate, the final product of the GABA catabolism, is an intermediate of the Krebs cycle. Proposed precursors to GABA include ornithine, putrescine, arginine, and agmatine (Figure 26);[2] however, a recent publication showed that GABA is not typically an intermediate in the catabolism of arginine or ornithine.[3] Rather the *astCADBE* operon is necessary for the catabolism of arginine to glutamate and AstC is involved in the catabolism of ornithine. Nevertheless, the catabolism of GABA can reasonably contribute to the metabolism of putrescine and agmatine.[3,4] The *ygaF* gene encodes a protein whose role has been investigated and is discussed in the next chapter of my thesis.

The *csiD-ygaF-gabDTP-csiR* gene cluster constitutes a complex operon which is regulated by three promoters (Figure 25).[5] The first promoter, *csiD*$_p$, is activated by CsiR (encoded downstream of the gene cluster) either upon carbon starvation or at stationary phase and affects the expression of all five genes. The σ^s factor (a subunit of RNA polymerase) is responsible for the initiation of transcription in bacteria under various stress conditions in *E. coli* (e.g. starvation, pH drop, high or low temperature). Gene activation is triggered by σ^s accumulation in cells under specific stress conditions. It was found that the *csiD* gene is induced exclusively by carbon starvation and requires a

70

cAMP-CRP activator.[6] The other two promoters, $gabD_{p1}$ and $gabD_{p2}$, are located before the *gabDTP-csiR* operon and are triggered by multiple stress induction and upon nitrogen starvation, respectively.
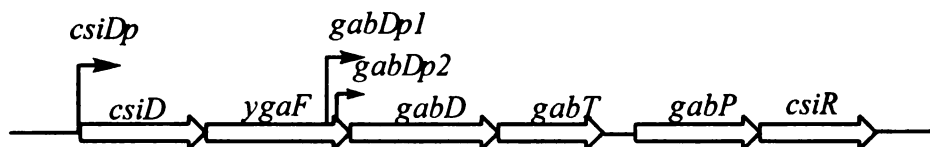
Figure 25. Location of *csiD* and *ygaF* and regulation of the *csiD-ygaF-gabDTP-csiR* gene cluster. The gene encoding YgaF is positioned downstream of and co-regulated with *csiD*. Although located immediately upstream of the *gabDTP-csiR* operon, they are not involved in GABA metabolism. The downstream gene *csiR* encodes a regulatory protein that binds at *csiD*$_p$.
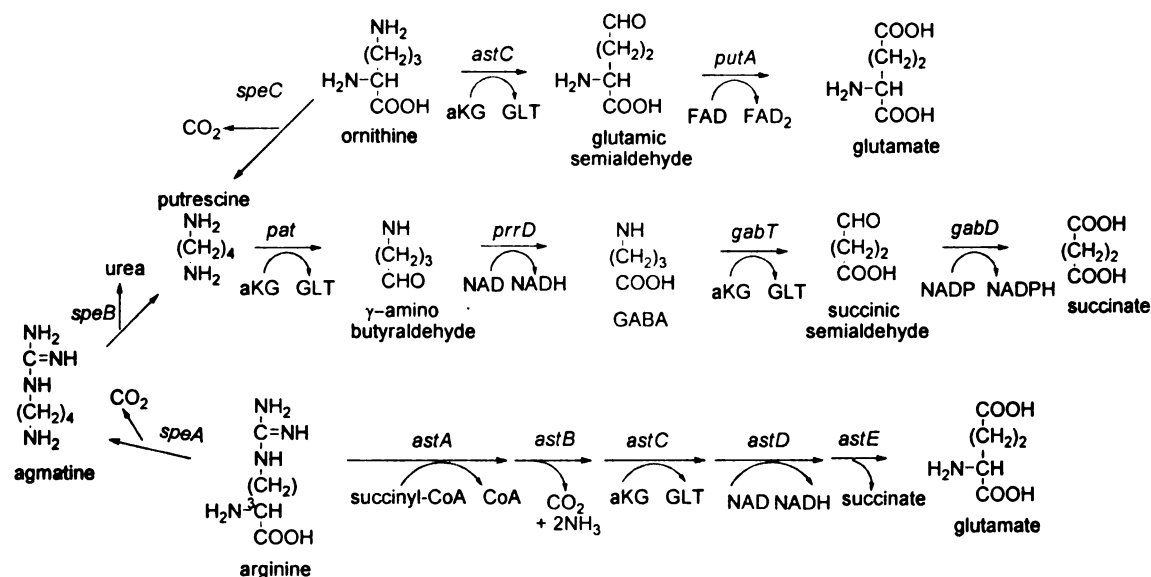
Figure 26. The metabolic pathways for catabolism of GABA, putrescine, agmatine, arginine and ornithine in *E. coli*, highlighting the intermediacy of GABA.[4]

The acronym *csi* stands for carbon starvation induced. Although CsiD is a protein of unknown function, its crystal structure was solved in 2002 and revealed it to be a member of the α-ketoglutarate (αKG)-dependent dioxygenases.[7,8] The resolved crystal structure had 2 Å resolution and behaved as a homotetramer (Figure 27). The authors used gel filtration chromatography of purified CsiD to show that it is a tetramer in the solution, confirming that the structure represents the natural state of the protein. The quaternary structure is formed through interactions of helices α1-3 from one promoter with α6-7 of the adjacent subunit via hydrophobic, hydrogen bonding, and salt interactions. Eight β sheets (β3, β5,β6,β7,β8,β14, β15 and β16) form a distorted jelly roll motif characteristic of this family of enzymes, (Figure 27B).[9] The Fe(II) in the active site is coordinated by His160, His292 and Asp162. The metal has octahedral geometry with water molecules occupying the remaining positions. Surprisingly, αKG did not bind to the active site when included it in the crystallization conditions. The authors did note some electron density at the putative active site; however, it was present at low occupancy and could not be identified.
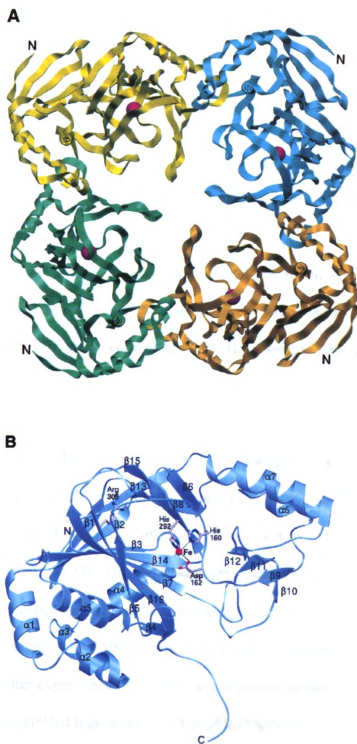
Figure 27. A) Quaternary structure of CsiD. B) A subunit of CsiD.[1]

EXPERIMENTAL PROCEDURES

Cloning and overexpression of CsiD.

One clone containing *csiD* was described previously,[7] and a second one was constructed here. The first, *csiD*₁, encoded CsiD with a His₆-tag followed by a SUMO-fusion tag at the N-terminus, with the first fifteen amino acids missing from the protein and was provided by Dr. Christopher Lima. The second construct, *csiD*₂, encoded full-length CsiD with an N-terminal His₆-tag. Expression studies with each system are described separately.

Plasmid pSMT3 (derived from pET28b plasmid) contained *csiD*₁ between the BamHI and HindIII restriction sites. The pSMT3 vector was transformed into DH5α maximum efficiency competent cells (Invitrogen), and the amplified plasmid was transformed into *E. coli* C41(DE3) cells. The transformants were plated onto Luria Broth (LB) agar containing 50 µg/ml of kanamycin. A single colony was used to inoculate 50 ml of LB medium (Difco) containing 50 µg/ml kanamycin, and cells were grown at 37 °C for 16 h. A portion (15 ml) from the overnight growth was inoculated into 1 L of Terrific Broth (Fisher Biotech) containing 50 µg/ml kanamycin at 25 °C and grown to an optical density of 0.5 at 600 nm. β–D-isopropyl-thiogalactopyranoside (IPTG) was added (0.1 mM final concentration) and the growth continued at 25 °C for 16 h. Cells were harvested by centrifugation at 7,500 x *g* for 10 min at 4 °C. These optimum expression conditions, chosen after experimentations with various growth temperatures, IPTG concentrations and cell types, yielded high levels of soluble CsiD protein.

The second construct was created by amplifying *csiD* from *E. coli* MG1655 DNA using primers 5'-CATAAGAGGATCGCTTCATATGAATGCACTGACCG-3' and 5'-

AAGCTTTTACTGATGCGTCTGGTA-3' that introduced NdeI and HindIII sites at the 5'

and 3' end of the gene, respectively. Ligation of the endonuclease treated PCR product

into identically digested pET42b (Novagen) provided in an in-frame region encoding an

N-terminal His$_6$ tag. The ligated plasmid, pET42b-csiD, was transformed into DH5α

competent cells, and the amplified plasmid was transformed into *E. coli* BL21(DE3) cells

that were plated on LB agar containing 50 μg/ml of kanamycin. A colony was used to

inoculate a culture of 50 ml LB medium containing 50 μg/ml of kanamycin and this was

grown overnight at 37 °C. An aliquot (15 ml) was used to inoculate 1 L of TB containing

50 μg/ml kanamycin, and this was grown at 37 °C until reaching an O.D.$_{600}$ of 0.2. This

culture was moved to 25 °C and shaken vigorously until reaching an O.D.$_{600}$ of 0.5 at

which point the cells were induced with 0.1 mM IPTG and the growth continued overnight

at 25 °C. The cells were harvested by centrifugation at 7,500 x g for 10 min at 4 °C. These

optimized expression conditions were chosen after experimentations with various growth

temperatures, IPTG concentrations, and transformation-competent cell types.

Purification of CsiD proteins

Both CsiD forms were purified by using the same procedure. Approximately 3 g of

harvested cells were suspended in 10 ml of lysis buffer containing 20 mM imidazole, 300

mM NaCl, 50 mM Na$_2$HPO$_4$, and 1 mM DTT, pH 8. The suspension was sonicated in a

Sonifier 450 (Branson) for 1 min at 30 W output power, and 50 % duration of the pulse

per sec. The sonication was repeated four more times with 1 min intervals in ice. The

broken cells were centrifuged at 100,000 g for 1 h at 4 °C. The soluble cell extracts (9 ml)

were loaded onto an 8 ml Ni-Sepharose 6-Fast Flow column (GE Healthcare), which had

been equilibrated with buffer A (20 mM imidazole, 300 mM NaCl, 50 mM Na_2HPO_4 pH 8). The column was washed with buffer B (100 mM imidazole, 300 mM NaCl, 50 mM Na_2HPO_4, pH 8) in order to remove any protein weakly bound to the resin. CsiD was eluted with buffer C (500 mM imidazole, 300 mM NaCl, 50 mM Na_2HPO_4, pH 8). Exchange of the buffer was performed by dialysis against 25 mM Tris, 1 mM DTT, pH 8, at 4 °C. In some cases (where specifically mentioned) the CsiD solution was incubated with 1 mM EDTA prior to dialysis against the Tris buffer.

Protein analytical methods

The protein concentration was determined as described by Bradford, with bovine serum albumin used as the standard.[10] Sodium dodecyl sulfate polyacrylamide gel electrophoresis (SDS-PAGE) (with stacking and running gels containing 5 % and 12 % acrylamide) was used for measurement of protein overexpression and assessment of protein purity.[11] The standard protein mixture used for comparison included phosphorylase b (M_r 97,400), bovine serum albumin (M_r 66,200), ovalbumin (M_r 45,000), carbonic anhydrase (M_r 31,000), trypsin inhibitor (M_r 21,500) and lysozyme (M_r 14,400) (Bio-Rad Laboratories). The native sizes of purified $CsiD_1$ and $CsiD_2$ were estimated by gel filtration chromatography using a 10 μm Protein-pak Diol(OH) column (Waters), which had been equilibrated with 100 mM Tris, 300 mM NaCl, pH 7.5, with a flow rate was 1 ml/min. The calibration protein mixture contained thyroglobulin (M_r 670,000), γ-globulin (M_r 158,000), ovalbumin (M_r 44,000), myoglobin (M_r 17,000) and vitamin B_{12} (M_r 1,350) (Bio-Rad), with added bovine serum albumin (M_r 66,200).

Binding of αKG to Fe(II)-CsiD monitored by absorption spectroscopy

Anaerobic stock solutions were prepared in sealed serum vials by alternative cycles of vacuum and argon. A stock solution of αKG (150 mM) was prepared in 25 mM Tris, pH 8.0 buffer. Mixtures of ferrous ammonium sulfate (25 mM) and ascorbic acid (5 mM) were prepared by several rounds of degassing and argon flushing of the solids, followed by addition of the desired volume of water. The procedure followed was the same as that reported for TauD.[12] CsiD$_2$ apoprotein (370 μM subunit in 25 mM Tris buffer, pH 8.0) was placed into a 1 cm path length, 300 μl quartz cuvette fitted with a stopper and was made anaerobic by 10 rounds of degassing and flushing with argon. During the whole process the protein was kept in an ice bath to avoid precipitation. Absorption spectra were taken at 25 °C on a Shimadzu UV-2401 UV/Visible spectrophotometer using the protein buffer as the baseline spectrum.

Binding of αKG to Fe(II)-CsiD monitored by electron paramagnetic resonance (EPR) analysis

A solution of Diethylammonium (Z)-1-(*N*,*N*-diethylamino)diazen-1-ium-1,2-diolate (DEA/NO) (Cayman Chemical) was added to 115 μM anaerobic protein (already containing 2 mM of αKG and/or 115 μM Fe(II)) to reach 550 μM final concentration in 300 μl quartz cuvettes fitted with rubber stoppers. Electronic spectra (300-800 nm) were recorded at 2 min intervals for ~ 40 min at 25 °C in order to demonstrate that the complex CsiD/Fe(II)/NO or CsiD/Fe(II)/αKG/NO was formed.

The anaerobic solutions were transferred to degassed EPR tubes and frozen. Continuous wave X band EPR spectra were recorded at 4 K on a Bruker ESP300E

spectrometer equipped with an Oxford liquid He cryostat by using 100 kHz modulation, 1.99 mW microwave power, and 9.99 GHz microwave frequency.

Oxygen consumption

Oxygen consumption assays were carried out using a Clark-type oxygen electrode and air-saturated buffer (50 mM imidazole pH 6.75) at 25 °C. In all cases, 2 μM YgaF was mixed with 50 μM Fe(II), 400 μM ascorbate, 1 mM αKG, and 2 mM of the potential substrates in a total volume of 5 ml.

Organic acids HPLC column

Reaction mixtures (containing enzyme and reactants in 1 ml of 25 mM imidazole buffer at pH 6.75) were incubated for various times at 30 °C, and quenched by adding 5 μl of 6 M sulfuric acid to the 300 μl aliquots. After centrifugation at 10,000 *g* for 5 min the supernatant was centrifuged in a spin column (Amicon ultrafree-MC from Millipore) at 10,000 *g* for 1 min, and 200 μl was injected onto the organic acids HPLC column, equilibrated with 13 mM sulfuric acid. The refractive index was monitored and the integrated peak intensities were compared to those of authentic standards.

Nuclear magnetic resonance (NMR) spectroscopy

NMR spectroscopy was used for identification of the product of αKG metabolism. The reaction mixture (10 ml) of 2 μM CsiD$_2$, 50 μM Fe(II), 400 μM ascorbate and 1 mM αKG in 25 mM imidazole buffer (pH 6.75) was incubated for 30 min at 30 °C. The reaction was quenched with 160 μl formic acid and the sample was centrifuged at 10,000

g for 5 min. The supernatant was centrifuged in a spin column (Amicon ultrafree-MC from Millipore) at 10,000 *g* for 1 min. The solvent was evaporated under reduced pressure (vacuum pump), the remaining solid was dissolved in deuterated water (D_2O) and the 300 MHz proton NMR spectrum was obtained. NMR spectra of control samples of αKG, succinate, and a mixture of Fe(II), ascorbate and αKG in 25 mM imidazole buffer (pH 6.75), were obtained with the same way.

Gas chromatography-mass spectrometry (GC-MS)

GC-MS was used to detect differences in the metabolites of the wild type strain (*E. coli* BW25113) and the *csiD*-deletion strain (*csiD*-KO). Colonies from BW25311 and *csiD*-KO strains were inoculated into 10 ml M9 medium (with either D-Ala as a C-source and NH_3 as the N-source, or succinate as a C-source and L-Trp as the N-source) for 24 h at 37 °C. The reason for using these sources is because the two strains had the biggest growth differences when grown in D-Ala and L-Trp as the C- and N-source, respectively. The culture of the knock out strain in addition contained kanamycin (50 µg/ml). Portions (0.5 ml) from the starter cultures were inoculated into 50 ml M9 medium (lacking kanamycin to avoid metabolite differences due to the antibiotic) and grown at 37 °C until they reached the stationary state. The cultures were mixed with equal volume of a 32.5 % MeOH in M9 salts solution (pre-chilled to –25 °C), and centrifuged for 7 min at 5800 *g*. The supernatants ($A_{BW25311}$ and $A_{csiD-KO}$) were separated from the pellets ($B_{BW25311}$ and $B_{csiD-KO}$) and frozen at –80 °C. The pellets were transferred into a pre-chilled with liquid nitrogen mortar, and homogenized with a pestle. The resulting white powder of broken cells was dissolved in 1.4 ml of methanol-chloroform-water solution in a ratio of 10:3:1.

An internal standard of ribitol (50 µl of 2 mg/ml) was added to the solutions which were incubated at 25 °C for 15 min. Water (1.4 ml) was added, and after vigorous shaking the samples were centrifugated at 2300 g for 5 min. Aliquots of 1 ml of the aqueous phase were pipetted into glass vials (Aligent) and dried in a speed vacuum overnight. The samples were derivatized by mixing a portion (80 µl) with 80 µl of 20 mg/ml methoxyamine hydrochloride dissolved in pyridine solution and incubating at 30 °C for 90 min. Then, 80 µl of N-methyl-N-(trimethylsilyl)trifluoroacetamide (MSTFA) (Aldrich) was mixed with the samples and incubated at 37 °C for 30 min. The GC-MS spectra were obtained by the MS facility at MSU.

Pull down assays to test for interactions between CsiD and YgaF

A pull down assay was performed using purified $CsiD_2$ (containing a His_6-tag) and cell extracts of untagged YgaF. Purified $CsiD_2$, as eluted from the Ni-NTA column was desalted using an Econo-pac 10 DG disposable chromatography column (BioRad) to change the buffer to 20 mM imidazole and either a) 300 mM NaCl, b) 100 mM NaCl, or c) 0 mM NaCl. $CsiD_2$ (3.2 mg in 2 ml) was incubated with cell extracts of untagged YgaF (0.2 ml) and 0.8 ml of buffer for 16 h at 4 °C. Subsequently, the mixture was loaded onto a Ni-Sepharose 6-fast flow column and the procedure for CsiD purification was followed.

Biolog plate growth assays

Four Biolog phenotype bioarray plates (Biolog) of 96 wells each with different carbon, nitrogen, phosphorous and sulfur sources were used to compare the growths of the *E. coli* BW25113 and *csiD*-KO strains. Plates denoted PM-1 and PM-2 provide various

carbon sources, PM-3 included selected nitrogen compounds and PM-4 has an array of phosphorous and sulfur sources. The two strains were streaked out on BUG+G plates (included in the kit) and incubated at 37 °C. Colonies were suspended in 40 ml inoculation fluid, and their turbidities were adjusted (by dilution or by suspension of more colonies) to match the turbidity standard as measured by the absorbance at 600 nm. Suspensions from both strains were provided succinate as the carbon source for the N, S, and P assays. Cells (100 μl) were added to each well and the plates were incubated at 37 °C for 30 h (PM-1 and PM-2) or 48 h (PM3 and PM4). The growth was monitored by the development of a purple color associated with tetrazolium dye reduction by the respiring bacteria.

Amino acid analysis

E. coli BW25113 and *csiD-KO* strains were grown in 3 ml LB that contained 50 μg/ml kanamycin for 16 h at 37 °C. The cultures (0.5 ml) inoculated into 50 ml of minimal medium (8.8 ml 5X M9 salt, 8.8 ml of 1 M $MgSO_4$, 4.4 μl of 1 M $CaCl_2$, 1 ml 50X succinate ferric citrate and 40 ml water) and incubated at 37 °C to stationary phase. Cells were harvested by centrifugation at 7,500 *g* for 10 min, re-suspended in 2 ml of 20 mM Tris-HCl, pH 8 buffer, and sonicated. Soluble cell extracts were collected by ultracentrifugation at 100,000 *g* for 1 h, and filtered using a Millipore centrifuge filters (cat. Number 4104), at 2000 g for 15 min. The filtered samples of the BW25113 and CsiD-KO strains were subjected to amino acid analysis by the Macromolecular Structure Facility of MSU. The amino acids and other compounds that can be detected by this method are listed in Table 2.

Table 2. List of amino acids and other compounds detected by amino acid analysis.

1.	Phosphoserine	24.	Leucine
2.	Taurine	25.	Tyrosine
3.	Phosphoethanolamine	26.	Cystathionine
4.	Aspartic acid	27.	Phenylalanine
5.	Methionine sulfoxide	28.	β-Alanine
6.	Threonine	29.	β-Amino-isobutyric acid
7.	Serine	30.	γ-Amino butyric acid
8.	Asparagine	31.	Homocysteine
9.	Glutamic acid	32.	Ethanolamine
10.	Glutamine	33.	Tryptophan
11.	Sarcosine	34.	Ammonia
12.	α-Aminoadipic acid	35.	δ-Hydroxylysine
13.	Glycine	36.	Aminoethylcysteine
14.	Alanine	37.	Ornithine
15.	Citrulline	38.	S-Adenosyl Homocysteine
16.	α-Amino-η-butyric acid	39.	Lysine
17.	Valine	40.	1-Methyl histidine
18.	Methionine	41.	Histidine
19.	Allo-isoleucine	42.	3-Methyl histidine
20.	Hydroxy-proline	43.	Anserine
21.	Carnosine	44.	Cysteine

22.	Arginine	45.	Isoleucine
23.	Proline		

Table 2 (continued).

Cloning of YgaF

The *ygaF* gene was amplified by PCR from *E. coli* MG1655 using Pfu polymerase and primers 5'-CAAAGGAATTGAGCATATGTATGATTTTG-3' and 5'-GCTACATCCTGTTTTCAAAAGCTTTTATTGATTAAATGCGGCGTG-3', which introduced NdeI and HindIII cutting sites into the 5' and the 3' gene ends, respectively. Ligation of the 1,269 base pair PCR product into endonuclease-treated pET42b plasmid allowed production of a non-tagged version of the YgaF protein. The pET-42b-*ygaF* plasmid was transformed into *E. coli* DH5α (maximum efficiency) competent cells, and the amplified plasmid was transformed into BL21(DE3) that was plated onto LB agar containing 50 μg/ml of kanamycin. A single colony was used to inoculate 50 ml of LB medium containing 50 μg/ml kanamycin, and the culture was grown overnight at 37 °C. A portion (15 ml) from the overnight growth was used to inoculate 1 L of TB containing 50 μg/ml kanamycin, and this culture was incubated at 25 °C for 24 h. The cells were harvested by centrifugation at 7,500 × g for 10 min, and 6 g of cells were resuspended in lysis buffer (30 mM tricine, 5 mM EDTA, 20 % glycerol, 50 μM FAD, 0.5 mM PMSF, pH 8.0). Cells were broken by sonication (Branson sonifier) and centrifuged at 27,000 × g for 1 h at 4 °C.

RESULTS

Purification of CsiD₁ and CsiD₂

The form of CsiD whose crystal structure is known,[6] here indicated as $CsiD_1$, has an N-terminal His_6-SUMO fusion tag and the first 15 amino acids of the protein sequence are missing (in order to enhance expression and solubility). The CsiD form generated by an alternate approach, the $CsiD_2$ protein, includes the complete annotated coding region (amino acids 1-325) and an N-terminal His_6 tag. Both proteins were purified to homogeneity from soluble cell extracts by Ni-NTA affinity column chromatography (Figure 28). The proteins migrated as expected from the gene sequences (49.17 kDa and 39.52 kDa, respectively). DTT (1 mM) was included in all purification steps, as well as during storage, because it enhanced protein stability. The usual yield from 1 L culture was 30-40 mg for $CsiD_1$ and 200-250 mg for $CsiD_2$.
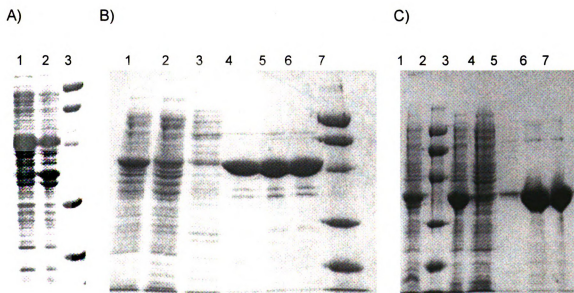
Figure 28. SDS-PAGE analysis of the expression and purification of CsiD₁ and CsiD₂.
Denatured samples were analyzed on a 12% acrylamide gel. A) Expression of $CsiD_1$: lane

1, cell extracts; lane 2, pellet; and lane 3, standard. B) Purification of CsiD$_1$: lane 1, cell extracts; lane 2, flow through of the Ni-Sepharose 6 fast flow column; lane 3, wash of the Ni resin with buffer containing 100 mM imidazole; lane 4, CsiD$_1$ elution from Ni resin with buffer containing 500 mM imidazole; lane 5, dialyzed CsiD$_1$ against 25 mM Tris, 1 mM DTT at pH 8; lane 6, concentrated CsiD$_1$; and lane 7, standard. C) Expression and purification of CsiD$_2$: lane 1, pellet; lane 2, standard; lane 3, cell extracts; lane 4, flow through of the Ni-Sepharose 6 fast flow column; lane 5, wash of the Ni resin with 100 mM imid; lane 6, CsiD$_2$ elution from Ni column with 500 mM imidazole; and lane 7, CsiD$_2$ after dialysis against 25 mM Tris, 1 mM DTT at pH 8.

Native size of CsiD.

An estimation of the native size of both purified CsiD proteins was provided by gel filtration chromatography. When compared to results derived for standard proteins (Figure 29), the elution volume of CsiD$_1$ and CsiD$_2$ (6.98 ml and 7.36 ml, respectively) indicated a tetrameric organization for both proteins (3.9-mer and 4.6-mer, respectively). These results were consistent with the X-ray analysis reported in the literature.[7]
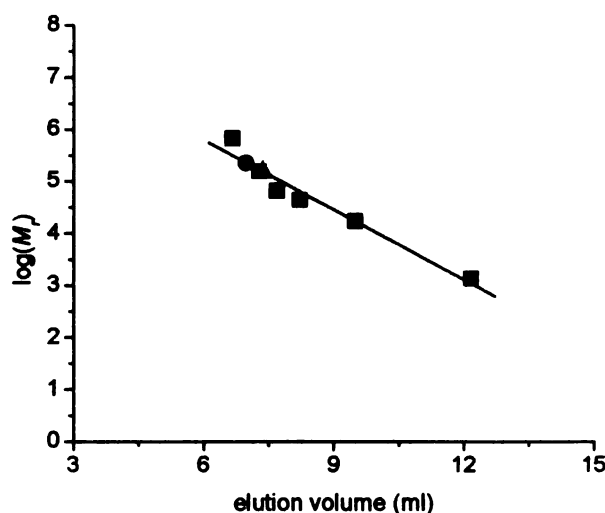
Figure 29. Determination of the native size of the CsiD$_1$ (red) and CsiD$_2$ (blue). The standard curve is shown in black.

Binding of αKG to Fe(II)-CsiD monitored by absorption and EPR spectroscopy.

A diagnostic property of the non-heme Fe(II)/αKG-dependent dioxygenase family is the formation of a chromophore observed when anaerobic apoprotein is incubated with Fe(II) and with the cosubstrate, αKG.[14] This chromophore has been attributed to metal-to-ligand charge-transfer (MLCT) transitions.[13] CsiD2 was treated with EDTA to remove any Fe(III) or Ni(II) that might be bound to the purified protein. After dialysis against EDTA-free, 25 mM Tris, 1 mM DTT buffer, the absorption spectra of anaerobic CsiD2 was obtained. An Fe(II)/ascorbate mixture was added, followed by addition of αKG to yield the spectra of Figure 30A. As shown by the difference spectrum in Figure 30B, the chromophore has λ_{max} at 510 nm with ϵ_{510} of 158 $M^{-1} \cdot cm^{-1}$. The result is similar to other proteins of this family like TauD (λ_{max} at 530 nm and ϵ_{530} in the range of 140-250 $M^{-1} \cdot cm^{-1}$),[14,15] and XanA (λ_{max} at 506 nm and ϵ_{506} of 145 $M^{-1} \cdot cm^{-1}$) (Meng Li, unpublished observations).

The EPR spectra of the CsiD/Fe(II)/NO and CsiD/Fe(II)/αKG/NO complexes were obtained in order to monitor the changes of the spectra upon αKG binding (Figure 31). NO is an oxygen analogue that converts the nonparamagnetic high spin Fe(II) (S=2) into a paramagnetically detectable species, {FeNO}[7] (S=3/2).[16] The EPR samples were prepared in anaerobic cuvettes (as described in the experimental methods section) and used DEA/NO to provide NO. NO binding to the Fe(II) complexes was confirmed spectroscopically by the absorbance increase at 443 nm (data not shown).[17] The CsiD/Fe(II)/NO EPR sample had an axial feature at 3.97 g at 1722 G, but when αKG was added the shape of the EPR signal in region near $g_\perp$ became more rhombic as indicated by

the shoulder at 1682 G. This provides added evidence for the interaction of the cosubstrate

with the Fe at the active site of the enzyme.
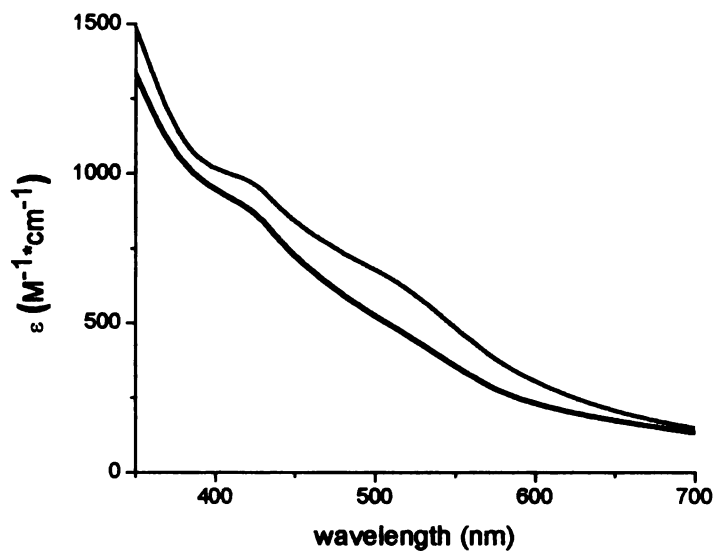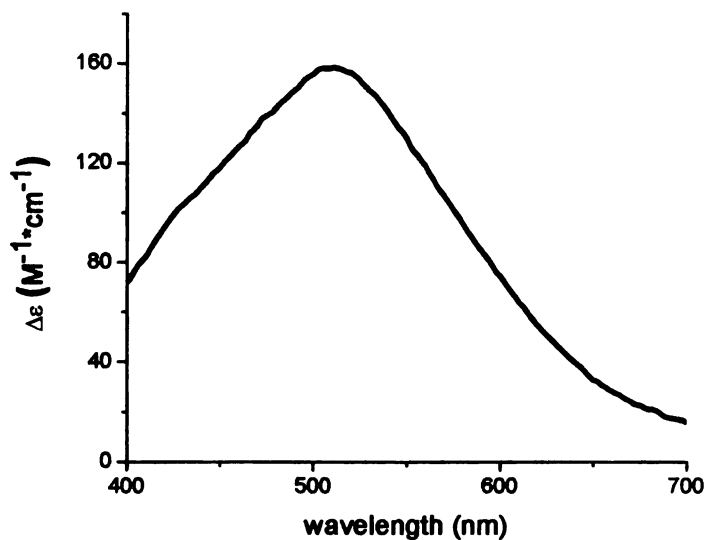
Figure 30. Absorption spectra of CsiD₂. (A) Spectra of anaerobic CsiD/Fe(II)/ascorbate
(black) and CsiD/Fe(II)/ascorbate/αKG (red). CsiD₂ (370 μM of subunit) was mixed with
ferrous ammonium sulfate/ascorbate mixture (740 μM/148 μM) and 1.5 mM αKG in 25

mM Tris buffer, pH 8.0, containing 1 mM DTT. (B) Difference spectra shown for the CsiD/Fe(II)/ascorbate/αKG minus CsiD/Fe(II)/ascorbate.
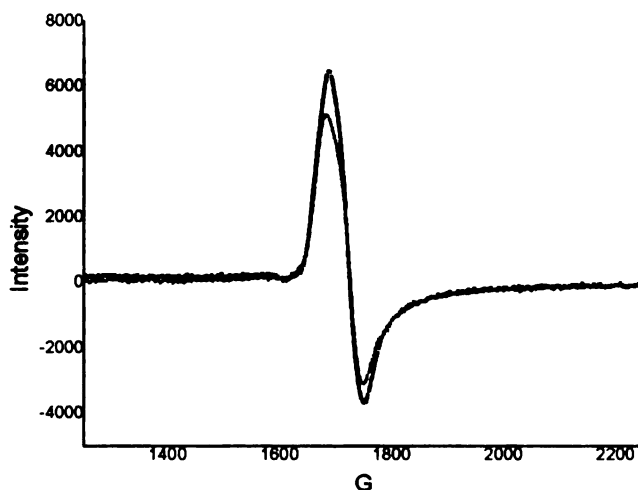
Figure 31. EPR spectra of CsiD₁/Fe(II)/NO (black) and CsiD₁/Fe(II)/αKG/NO (red). Protein 115 μM was adjusted to contain 110 μM ferrous ammonium sulfate and examined in the absence (black) or in the presence (red) of 2 mM αKG. In both samples 550 μM DEA/NO was added ~ 40 min prior to freezing. The buffer was 25 mM Tris, pH 8.

Identification of an uncoupled reaction of CsiD.

Several Fe(II)/αKG dioxygenases are known to catalyze uncoupled reactions *in vitro* in which αKG and O₂ are consumed in the absence of any transformation of the primary substrate. Such aberrant chemistry often is stimulated by the presence of inhibitors or poor substrates.[18] These reactions typically lead to enzyme inactivation and in some cases result in self-modification (e.g. TfdA, AlkB, TauD).[19,20,21] The ability of CsiD to catalyze an uncoupled reaction was examined by oxygen and αKG consumption and succinate production.

$CsiD_1$ and $CsiD_2$ exhibited similar oxygen consumption behavior as assessed by using an oxygen electrode (Figure 32). The initial rate of oxygen consumption by purified CsiD (i.e., that occurred in the first 30 sec) is 700-900 (nmoles/min)/mg protein, depending on the purification batch and on the number of days CsiD was stored at 4 °C. The reduction in rate at longer times was shown to be due to depletion of ascorbate during the experiment.
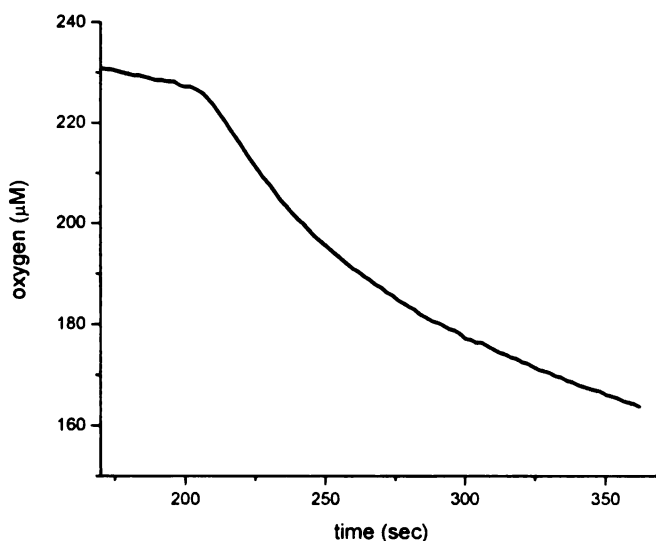
Figure 32. Oxygen consumption of the uncoupled reaction of CsiD. αKG (1 mM) was added to buffer (25 mM imidazole, pH 6.75) containing ascorbate (200 μM) and Fe(II) (100 μM) at 170 sec, and the reaction was initiated with addition of 2 μM CsiD at 208 sec.

To determine whether the oxygen concentration was tied to αKG consumption and succinate production, the concentrations of these compounds were monitored using the organic acids HPLC column. A reaction mixture of $CsiD_1$, Fe(II), ascorbate, and αKG was incubated at 30 °C and aliquots were taken at several time points (Figure 33). The initial rates of αKG consumption (738 nmol/min/mg protein) and succinate production (612

nmol/min/mg protein) agree very well with the rate of O_2 consumption. The αKG consumption and succinate production curves mirror each other, as shown in Figure 33.

The presence of ascorbate was shown to be required for oxygen consumption, αKG consumption, and succinate production (data not shown). The uncoupled oxidation of αKG has been linked to a requirement of ascorbate in several enzymes (e.g. prolyl-4-hydroxylase).[22] This dependence has been attributed to the enzyme reacting with αKG to form the iron-oxo state which decays to the inactive Fe(III) state. Ascorbate is suggested to reduce the metal to restore the active Fe(II) species, capable of further uncouple chemistry. Consistent with this hypothesis, ascorbate is consumed stoichiometrically in these uncoupled reactions.

To further confirm the production of succinate, the reaction products were examined by proton NMR spectroscopy (Figure 34). In a control experiment Fe(II) (50 μM), ascorbate (400 μM) and αKG (1 mM) were mixed in 25 mM imidazole buffer (pH 6.75), without CsiD present, and incubated at 30 °C for 30 min. Formic acid was added and water was evaporated under reduced pressure. The NMR spectrum of this mixture included the resonances expected of αKG at 2.27 and 2.80 ppm, ascorbate at 3.62 and 3.90 ppm, and imidazole at 7.26 and 8.36 ppm in Figure 34. The same mixture in the presence of CsiD$_2$ (2 μM) was subjected to the same conditions. A proton NMR spectrum of the crude reaction mixture in D_2O for the uncoupled reaction showed the presence of features derived from succinate at 2.30 ppm as the only species produced.

90
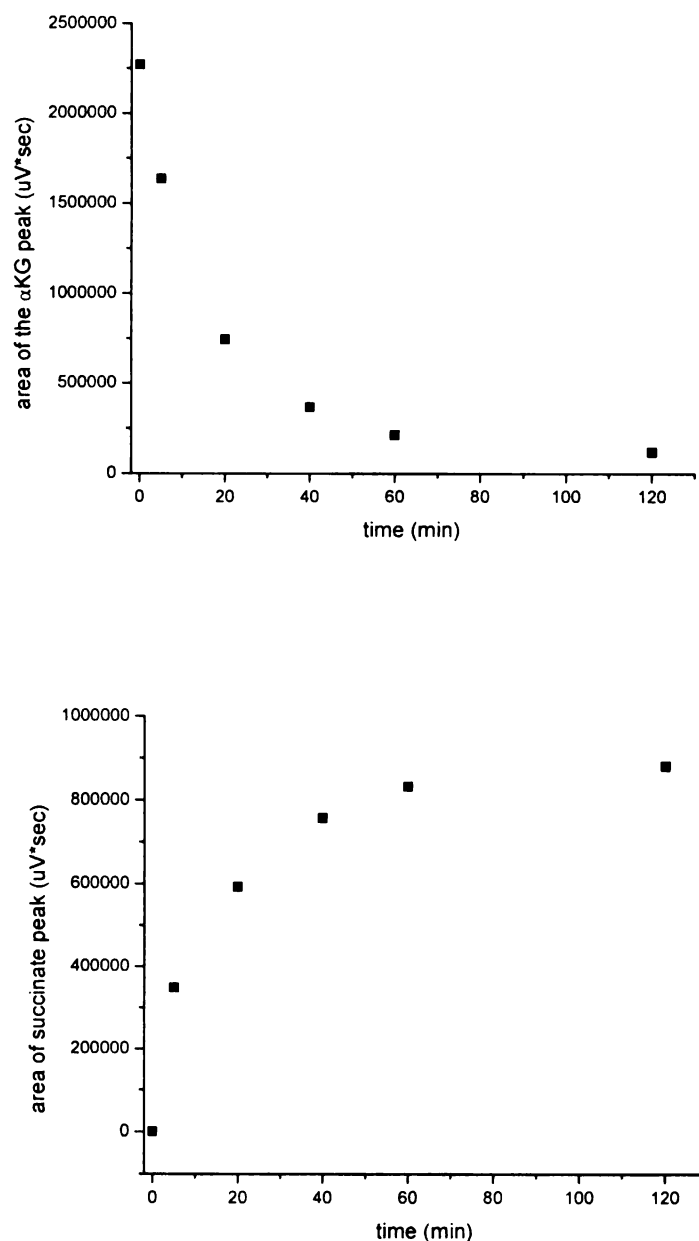
Figure 33. The αKG consumption (A) and succinate production (B) curves for the uncoupled reaction of CsiD as followed by HPLC. CsiD$_1$ (2.5 μM) was mixed with Fe(II) (50 μM), ascorbate (0.4 mM) and αKG (1 mM) in 25 mM imidazole buffer at pH 6.75, and incubated at 30 °C. Aliquots of 300 μl were collected from the reaction mixture at 5, 20, 40, 60 and 120 min. A control experiment lacking CsiD$_1$ was incubated for 120 min, and interpreted as the reaction at 0 min. The separation and detection of αKG and succinate was done by HPLC equipped with a refractive index detector.

91

Figure 34. Proton NMR spectra of the uncoupled reaction and a blank experiment.
A) Blank experiment: ascorbate mixed with αKG in imidazole buffer in the absence of CsiD. B) Reaction: ascorbate mixed with αKG in imidazole buffer in the presence of CsiD. C) Blow up of the interesting area of spectrum B.
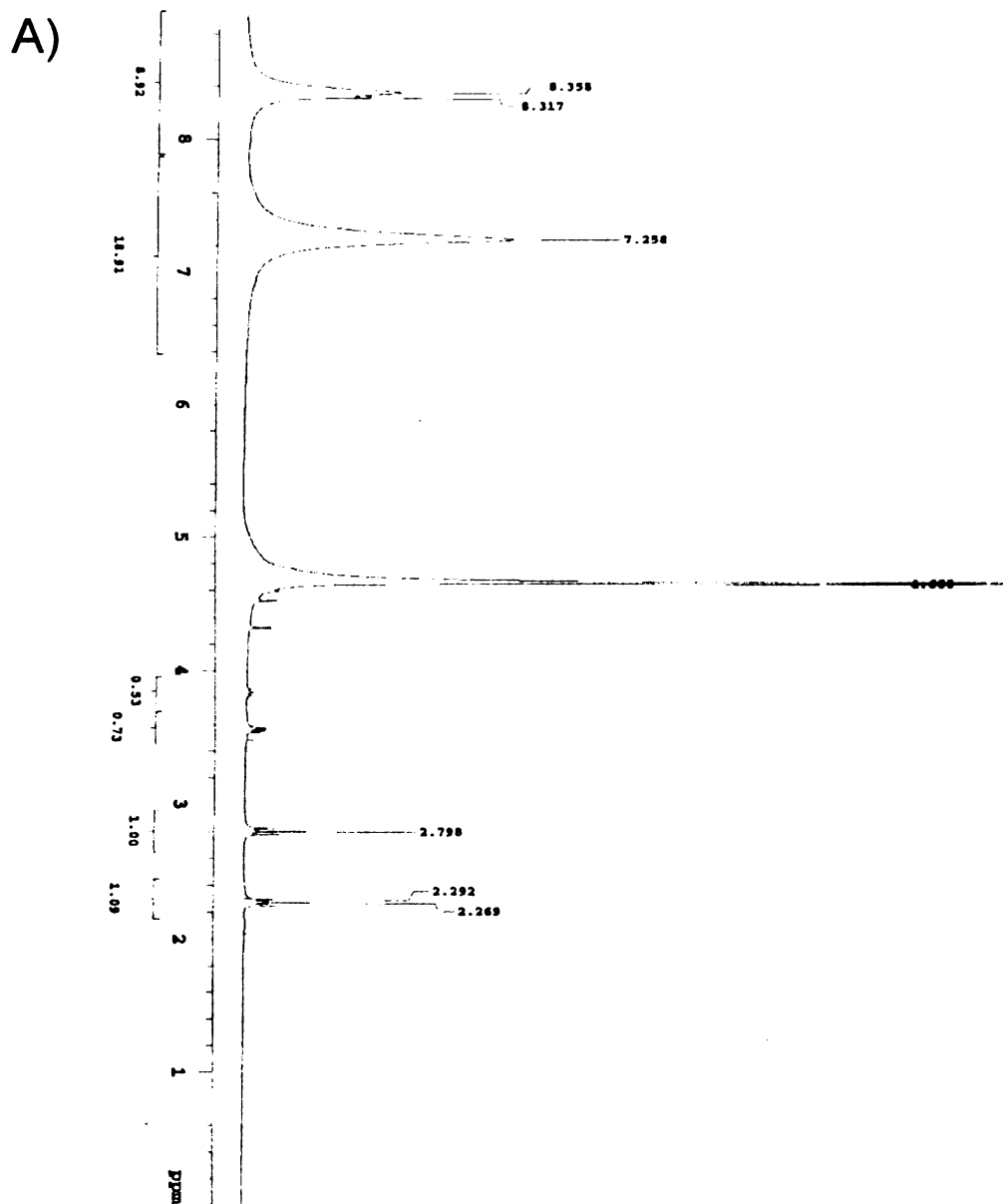
B)

Figure 34 (continued).

C)

Figure 34 (continued).

94
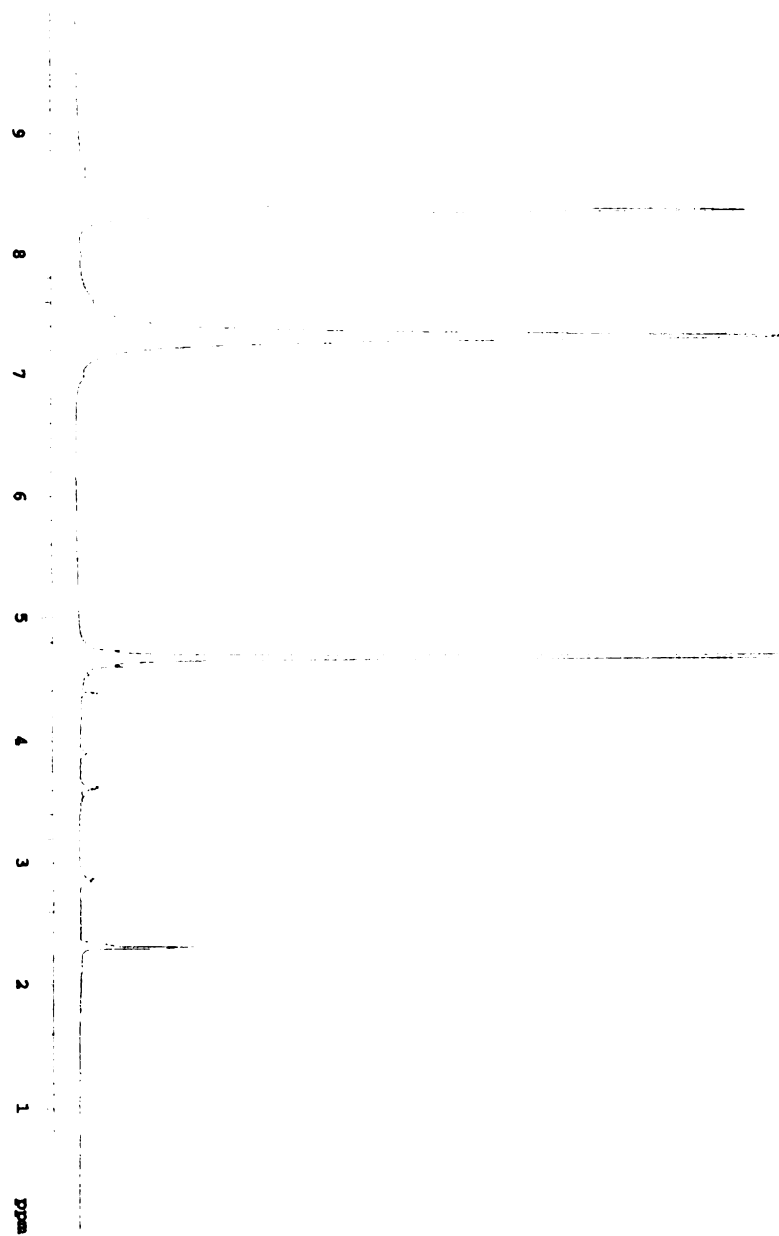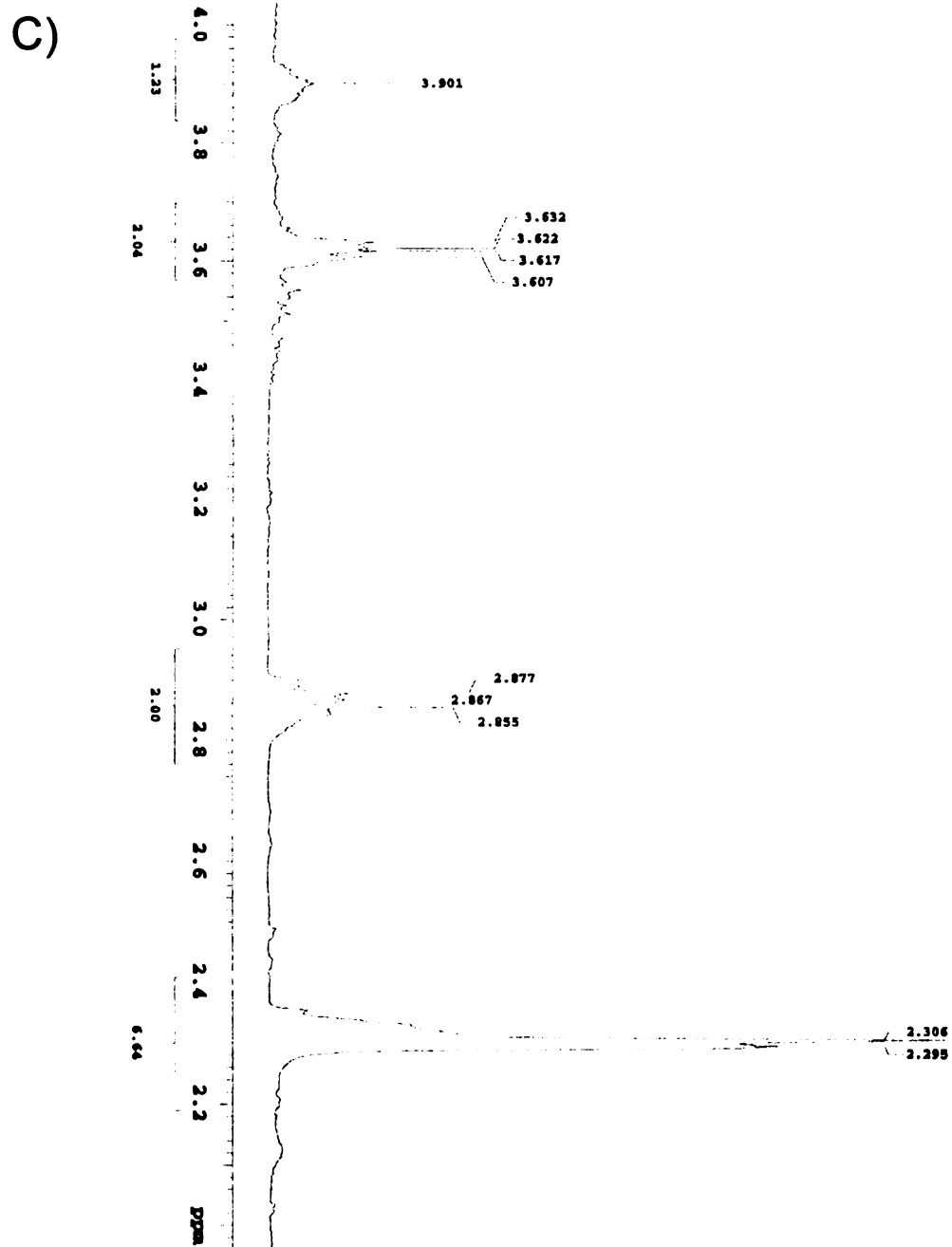
Biolog plates analysis.

A method for studying differences in metabolism between two bacterial strains is Phenotype Microarrays (PM) analysis.[23] Many phenotypes can be tested simultaneously in a very simple, efficient, standardized format. PMs are sets of 96-well microtiter plates. Each well contains a different dried cell culture medium that is designed to test a unique phenotype or cell function. A colorimetric method is used to detect respiring bacteria. If the cells can grow on the specific culture medium they respire normally to give a dark purple color. If the growth is weak, the respiration is slow and only light purple color is observed. If the phenotype and growth are negative, the well remains colorless. The plates provide different carbon (PM-1 and PM-2 plates), nitrogen (PM-3 plate), and phosphorous and sulfur sources (both in PM-4 plate).

The two strains that we compared with this method were BW25113 wild-type cells and the isogenic *csiD*-KO mutant. The knock out mutant was generated by insertion of a kanamycin resistance gene into the reading frames of the *csiD* gene. The PMs were inoculated with each strain and incubated at 37 °C for 30 h (C-sources) and 48 h (all others), respectively. For the first 30 h, pictures of the plates were taken every 6 h and then, for the N, S and P plate a last picture at 48 h. In several cases the CsiD-KO strain grew slower but finally reached the same intensity as BW25113. The most interesting differences between the strains involved the following C-sources: D-alanine, acetic acid, L-glutamine, *m*-tartaric acid, β-methyl-D-glucoside, *N*-acetyl-β-D-mannosamine and glucuronamide (Figure 35A). N-sources of particular interest were: L-arginine, L-aspartic acid, L-tryptophan, D-valine, L-homoserine, agmatine, adenine, D,L-α-amino-N-butyric acid, D,L-α-amino-valeric acid, δ-amino-N-valeric acid and alanine-leucine (Figure 35B).

For the S-sources conclusions couldn't made because growth was observed even in the negative control. All the interesting molecules were tested as substrates of CsiD using oxygen electrode (vide infra).
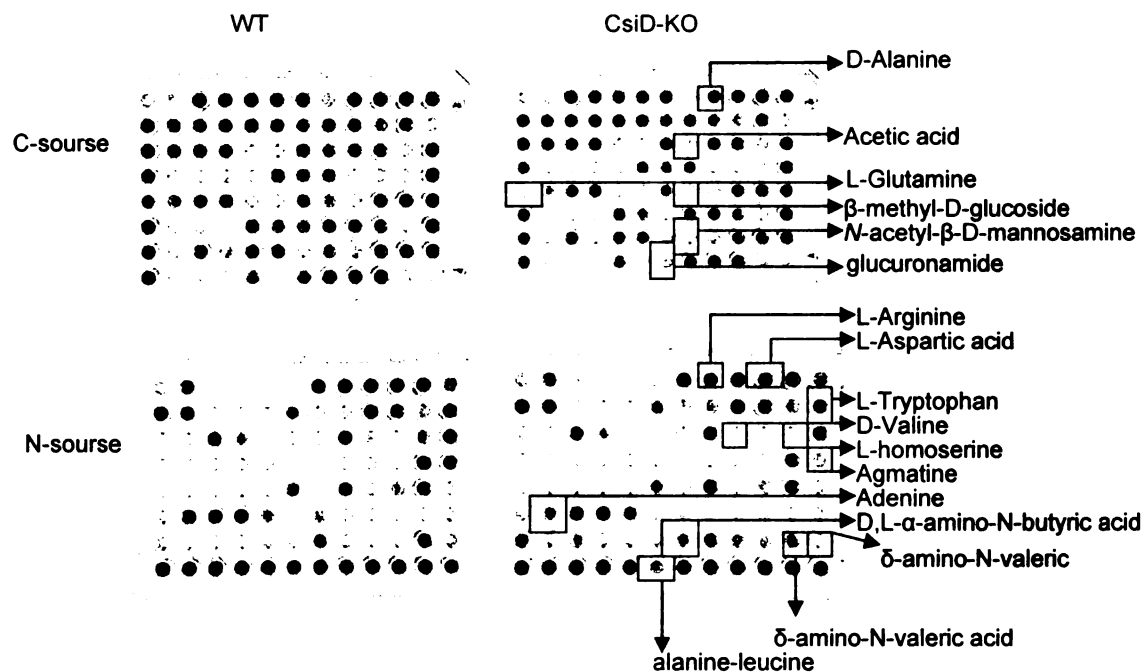
Figure 35. Photos of Biolog plates. Plate with C-sources (PM-1) of BW25113 and CsiD-KO of 30 h of incubation at 37 °C. Plate with N-sources (PM-3) of BW25113 and CsiD-KO of 48 h of incubation at 37 °C.

GC-MS analysis.

A second method comparing the metabolites of two bacterial strains involves GC-MS analysis. BW25113 and *csiD*-KO strains were grown identically up to the stationary phase and then the metabolites were extracted, derivatized and finally measured using a GC-MS instrument. Initially, the growths were centrifuged and both supernatants and cells were saved. The supernatant solutions have all the compounds that were exported from the cells ($A_{BW25311}$ and $A_{csiD-KO}$), whereas the pellets have all the molecules that remain within

96

($B_{BW25311}$ and $B_{csiD\text{-}KO}$). From the analysis having D-Ala as the C-source the samples $B_{BW25311}$ and $B_{csiD\text{-}KO}$ exhibited differences in two unidentified molecules with molecular weights after derivatization of 373 and 290 respectively and almost identical mass spectra; whereas the interesting compounds from the analysis of the $A_{BW25311}$ and $A_{csiD\text{-}KO}$ samples were 3-carboxy-6-ethoxy-4-hydroxy-1,5-naphthyridine, N-methylaminopropionic acid, hexanoic acid, aspartic acid and acetic acid. For the cells that grew in L-Trp as the only N-source the samples $B_{BW25311}$ and $B_{csiD\text{-}KO}$ exhibited differences in (1-ethyl-2-methylpropyl)methylamine and 3,5-dichloro-4-methoxy-2,6-dimethyl-pyridine; whereas $A_{BW25311}$ and $A_{csiD\text{-}KO}$ showed differences in 4,6-dimethyl-1-oxa-4,6-diazacyclooctane-5-thione, benzenebutanoic acid, silanol, pyrroindole, glycine, dihydrocodeine, D-threo-2,5-hexodiulose, malic acid, 3-methylvaleric acid, pentanedioic acid, erythrose and benzenepropanoic acid.

Amino acid analysis.

Another attempt to identify the biological role of CsiD involved comparison of the cellular amino acids produced by the BW25113 and *csiD*-KO strains (Figure 36). Several amino acids were observed to differ in concentration in the two strains, with the biggest difference noted for glutamic acid where the CsiD-KO strain possessed half the level of glutamic acid compared to the BW25113 strain (Figure 36). This result could imply that CsiD is involved in a pathway that enhances the production of this particular amino acid or that it reduces its rate of consumption. The two strains exhibit differences in other amino acids too (e.g. Ala, Gly, α-aminoadipic acid), although those changes were considerably smaller, and within the range of experimental error.
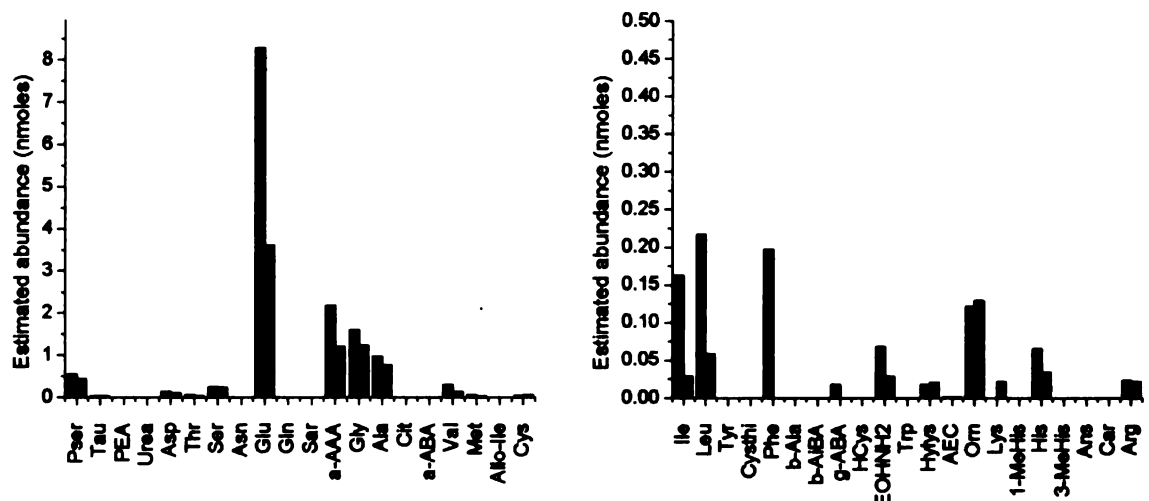
Figure 36. Comparison of the amino acid analysis of the BW25113 (black) and *csiD*-KO (red) strains. Acronyms except of natural amino acids that have been used are: Pser (phosphoserine), Tau (taurine), PEA (phosphoethanolamine), MetSO4 (methione sulfoxide), Sar (sarcosine), a-AAA (α-aminoadipic acid), Cit (citruline), a-ABA (α-amino-η-butyric acid), Allo-Ile (allo-isoleucine), Cysthi (cystathionine), b-Aiba (β-amino-isobutyric acid), Hcys (homocysteine), EOHNH2 (ethanolamine), Hylys (δ-hydroxylysine), AEC (aminoethylcysteine), Orn (ornithine), S-AHCys (S-adenosyl homocysteine), 1-MeHis (1-methyl histidine) and 3-MeHis (3-methyl histidine).

Investigation of potential substrates using an oxygen electrode.

A search for the primary substrate of CsiD was performed by using an oxygen electrode. Compounds tested included those proposed to be involved in GABA metabolism (Figure 26, putrescine, GABA, agmatine, L-arginine, L-glutamate) along with all other native amino acids. All tested substrates consumed the same amount of oxygen as observed for the uncoupled reaction except L-tryptophan, which acted as an inhibitor by diminishing the uncoupled reaction after its addition to the CsiD mixture. Other molecules (chosen on the basis of their reactivity of the Biolog studies, their use as substrates by other distantly related enzymes, or to test specific hypotheses of CsiD function) were tested by using the same assay and included: D-alanine, D-alanine-D-alanine, D-valine, L-

homoserine, L-phenyl propionic acid, thymine, adenine, ribose, sucrose, glucose, 5-aminovaleric acid, γ-butyrobetaine, δ-amino-N-valeric acid, D,L-α-amino-N-butyric acid, glucuronamide, m-tartaric acid, N-acetyl-β-D-mannosamine, D,L-2-aminobutyric acid and kynurenine. None of these substrates stimulated oxygen consumption.

Pull down assays.

In the absence of any evidence to directly identify the primary substrate of CsiD, I tested whether this protein might form a complex with the product of the downstream gene *ygaF*. As discussed in Chapter 4, YgaF, is an FMN-containing L-2-hydroxyglutarate oxidase. To test for interaction between CsiD and YgaF, purified $CsiD_2$ was mixed with cell extracts containing YgaF, incubated overnight at 4 °C, and loaded onto a Ni-NTA column. If the two enzymes interacted strongly, both proteins would bind to the resin because of the His_6-tag on CsiD. In the absence of interaction, YgaF wouldn't bind to the affinity column. The experiment was carried out using three different salt concentrations in the buffer: 20 mM imidazole containing 300, 100 and 0 mM NaCl. In no case did the enzyme co-elute from the column; (Figure 37) rather, YgaF consistently failed to bind to the column (eluting in the flow through fraction). In contrast, CsiD eluted with the 500 mM imidazole buffer in the first experiments, and in the wash buffer in the third experiment. A blank experiment using only the cell extracts of YgaF proved that this protein doesn't bind to the column, as expected.
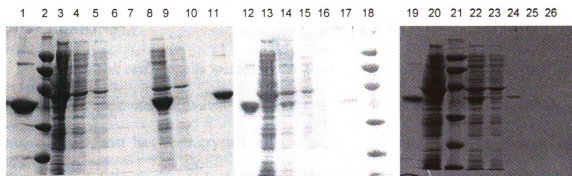
Figure 37. Pull down assays with His$_6$-tagged CsiD$_2$ mixed with cell extracts of non-tagged YgaF. Blank experiment lanes 1-7: purified CsiD$_2$, 1; standard, 2; cell extracts of non-tagged YgaF, 3; cell extracts of YgaF with buffer instead of CsiD, 4; flow through, 5; wash, 6; elution, 7. Pull down assay with 300 mM NaCl: cell extracts of YgaF with CsiD, 8; flow through, 9; wash, 10; elution, 11. Pull down assay with 100 mM NaCl: purified CsiD$_2$, 12; cell extracts of YgaF, 13; cell extracts of YgaF with CsiD, 14; flow through, 15; wash, 16; elution, 17; standard, 18. Pull down assay with 0 mM NaCl: purified CsiD$_2$, 19; cell extracts of YgaF, 20; standard, 21; cell extract of YgaF with CsiD, 22; flow through, 23; wash, 24; elution with buffer that doesn't contain salt, 25; elution with buffer that contains 300 mM NaCl, 26. Wash buffer: 100 mM imidazole with A) 300 mM, B) 100 mM and C) 0 mM NaCl at pH 8. Elution buffer: 500 mM imidazole with A) 300 mM, B) 100 mM and C) 0 mM NaCl at pH 8.

CONCLUSIONS

The *E. coli csiD* gene is located in the *csiD-ygaF-gabDTP-csiR* operon, controlled by the *csiD*$_p$ promoter, activated exclusively under carbon starvation and encodes a protein, CsiD, that has been crystallized and shown to belong to the non-heme Fe(II) dioxygenase family. In this study the purification and general characteristics of CsiD have been described.

Purification and native size. Two forms of CsiD were isolated. The CsiD$_1$ protein is the one that was crystallized and has an N-terminal His$_6$-SUMO-tag, but is missing the first fifteen amino acids. The CsiD$_2$ protein is the full-length protein with an N-terminal His$_6$-tag. Both were purified very effectively in one step by using affinity column chromatography. Their stabilities were enhanced in the presence of the DTT and they were able to be stored at 4 °C for several weeks. Estimation of the native size of the CsiD forms by gel filtration chromatography revealed that both are tetramers, agreeing with the crystallographic result. The presence of the tags didn't affect the quaternary structure of the protein because the N-terminis is not involved in the interactions between the monomers.

CsiD-Fe(II)-αKG complex. The crystals of CsiD were grown under anaerobic conditions in the presence of 20 mM αKG. Nevertheless, diffraction analysis didn't indicate any complexation of the αKG with Fe(II) at the active site. To investigate whether αKG can bind to enzyme-bound Fe(II), two approaches, absorption spectroscopy and EPR spectroscopy, were used. All the αKG-dependent dioxygenases develop a characteristic chromophore in the visible area of the spectrum upon binding Fe(II) and αKG due to metal-to-ligand charge-transfer transitions.[24] The spectrum of anaerobic CsiD/Fe(II)

mixed with αKG developed the characteristic chromophore (λ_{max} = 510 nm, ϵ_{510} = 158 M$^{-1}\cdot$cm^{-1}). The binding of αKG to the CsiD active site was also confirmed by EPR studies, in which superimposition of the EPR spectra of CsiD/Fe(II) with and without αKG indicated that the two spectra are not identical. The EPR spectrum of CsiD/Fe(II)/αKG exhibits a more rhombic signal compared to the one where αKG was absent. Both experiments prove that αKG binds to the active site of CsiD. Concerning the failure of Chance *et al.* to observe such a complex in the crystal structure of CsiD,[7] I hypothesize that the complex was destabilized by the conditions used to grow the crystals.

Uncoupled reaction. Another characteristic property of αKG-dependent dioxygenases is the ability to oxidize the cosubstrate in the absence of the primary substrate, a situation known as an uncoupled reaction. In air-saturated buffer, CsiD consumed oxygen and in the presence of Fe(II), ascorbate and αKG, as expected. The presence of ascorbate seemed to be completely necessary. This phenomenon can be explained as an aberrant short cutting of the normal catalytic cycle of the dioxygenase. In the absence of primary substrate, oxidative decarboxylation of αKG slowly forms an Fe(IV)-oxo intermediate which decays to yield an Fe(III) species. Ascorbate acts as a reductant, returning the iron from the Fe(III) to its active Fe(II) state, making the protein ready for another cycle. The consumption of αKG during the uncoupled reaction was confirmed by using an organic acids column to separate products while monitoring the refractive index. The appearance of succinate (the product of the oxidation of αKG) coincided with the loss of αKG during the course of the reaction. The production of succinate was also demonstrated by NMR.

Searching for the CsiD substrate. Four methods were used to investigate potential substrates for CsiD. First, metabolic analysis used GC-MS methods and revealed several compounds that differed in abundance in BW25113 and *csiD*-KO growths both outside and inside the cells. Further studies on the molecules that looked promising showed that none of them served as a substrate for CsiD. Biolog plate analysis was another method that gave us the opportunity to compare the growths of *E. coli* BW25113 and *CsiD*-KO having many different carbon, nitrogen, phosphorous and sulfur sources. Several subtle changes were noted, but follow up studies failed to identify any primary substrate from this approach. It is possible that *E. coli* possesses more than one pathway to metabolize the specific compound of interest. If this is the case for CsiD, then the *csiD*-KO strain would grow in exactly the same way, or maybe a little bit slower than the WT strain. A third approach to test for the primary substrate of CsiD involved direct assays for oxygen consumption. Again, the approach was fruitless as none of the compounds served as a substrate of CsiD. A forth method examined the role of CsiD by amino acid analysis, where we specifically investigated differences in the amino acids levels of BW25113 and *csiD*-KO cells. The most pronounced difference between the two strains was found in the amount of L-glutamic acid, but it is unclear how this result relates to the presence or absence of CsiD.

A very recent review by Shelley D. Copley discusses reasons to explain why some metabolic enzymes in *E. coli* are essential for growth on glucose as a sole carbon source, whereas others are not.[25] Surprisingly, 80 out of 227 genes encoding enzymes in central metabolic pathways are not essential for growth on glucose. This discrepancy can be explained by the existence of: i) alternative pathways, ii) the availability of isozymes, iii)

enzymes with broad-specificity, or iv) redundant multifunctional enzymes. In some cases, interconnecting metabolic pathways allow the organism to bypass a defective metabolic step, however it is possible the cell will not survive due to the toxicity which can be caused by the accumulation of the substrate of the missing enzyme. With regard to the Krebs cycle, often considered an essential series of reactions for obtaining energy during growth on glucose several steps are in fact nonessential because the intermediates can be produced by alternative pathways. Many nonessential metabolic genes encode enzymes for which isozymes are encoded by other genes and catalyze the same reaction using different reactants. Enzymes with broad substrate specificities often can compensate for a missing enzyme. For example, the transaminase class enzymes convert a wide range of 2-keto acids to amino acids. There are also occurrences where enzymes have redundant catalytic activities. A representative example is the conversion of shikimate to shikimate 3-phosphate from both shikimate kinases AroK and AroL, with differing K_m for shikimate, equal to 200 and 20 µM respectively. The fact that a significant number of genes (~ 35 %) encoding enzymes involved in metabolism of *E. coli* is not essential for the growth of the cell on glucose, raises the possibility that *csiD* might be included in this class.

Pull-down assay. A final effort to investigate the role of CsiD explored whether it formed a complex with the product of *ygaF*, a gene that is adjacent to *csiD* and encodes a protein not previously characterized. The possibility of interaction between CsiD and YgaF was tested by pull-down experiments using His$_6$-tagged CsiD and cell extracts containing overexpressed YgaF. No interactions between these proteins were detected.

In summary, I demonstrated that αKG binds to the active site of CsiD, something that was not obvious in the crystal structure, and conclude that the protein is an αKG-

dependent dioxygenase. Moreover, the uncoupled reaction, an *in vitro* reaction performed by several members from this family, was observed by several methods and provides further evidence for this classification. I tried to identify the biological role of CsiD by several approaches, but was not successful. Finally, I used pull-down assays with cell extracts containing overexpressed YgaF to show that no interactions are formed between these proteins.

REFERENCES

[1] Niegemann, E., Schulz, A., and Bartsch, K. (1993) Molecular organization of the *Escherichia coli gab* cluster: nucleotide sequence of the structural genes *gabD* and *gabP* and expression of the GABA permease gene. *Arch. Microbiol. 160*, 454–460.

[2] Shaibe, E., Metzer, E., and Halpern, Y. S. (1985) Metabolic pathway for the utilization of L-arginine, L-ornithine, agmatine, and putrescine as nitrogen sources in *Escherichia coli* K-12. *J.Bacteriol. 163*, 933-937.

[3] Schneider, B., L., Kiupakis, A., K., Reitzer, L., J. (1998) Arginine catabolism and the arginine succinyltransferase pathway in *Escherichia coli*. *J. Bacteriol. 180*, 4278-4286.

[4] Schneider, B. L., Ruback, S., Kiupakis, A. K., Kasbarian, H., Pybus, C., Reitzer, L. (2002) The *Escherichia coli gabDTPC* operon: specific γ-aminobutyrate catabolism and nonspecific induction. *J. Bacteriol. 184*, 6976-6986.

[5] Metzner, M., Germer, J., and Hengge, R. (2004) Multiple stress signal integration in the regulation of the complex σ^s-dependent *csiD-ygaF-gabDTP* operon in *Escherichia coli*. Molec. Microbiol. *51*, 799-811.

[6] Marschall, C., Labrousse, V., Kreimer, M., Weichart, D., Kolb, A., and Hengge-Aronis, R. (1998) Molecular analysis of the regulation of *csiD*, a carbon starvation-inducible gene in *Escherichia coli* that is exclusively dependent on σ^s and requires activation by cAMP-CRP. *J. Molec. Biol. 276*, 339–353.

[7] Chance, M. R., Bresnick, A. R., Burley, S. K., Jiang, J. S., Lima, C. D., Sali, A., Almo, S. C., Bonanno, J. B., Buglino, J. A., Boulton, S., Chen, H., Eswar, N., He, G., Huang, R., Ilyin, V., McMahan, L., Pieper, U., Ray, S., Vidal, M., and Wang, L. K. (2002) Structural genomics: a pipeline for providing structures for the biologist. *Protein Sci. 11*, 723-738.

[8] Hausinger, R. P. (2004) Fe(II)/α-ketoglutarate-dependent hydroxylases and related enzymes. *Crit. Rev. Biochem. Mol. Biol. 39*, 21-68.

[9] Schofield, C. J., and Zhang, Z. (1999) Structural and mechanistic studies on 2-oxoglutarate-dependent oxygenases and related enzymes. *Curr. Opin. Struct. Biol. 9*, 722-731.

[10] Bradford, M. M. (1976) A rapid and sensitive method for the quantitation of microgram quantities of protein utilizing the principle of protein-dye binding. *Anal.l Biochem. 72*, 248-254.

[11] Laemmli, U. K. (1970) Cleavage of structural proteins during the assembly of the head of bacteriophage T4. *Nature (London)* *227*, 680-685.

[12] Kalliri, E., Grzyska, P. K., and Hausinger, R. P. (2005) Kinetic and spectroscopic investigation of Co^{II}, Ni^{II}, and *N*-oxalylglycine inhibition of the Fe^{II}/*a*-ketoglutarate dioxygenase, TauD. *Biochem. Biophys. Res. Commun.* *338*, 191–197.

[13] Purpero, V., and Moran, G. R. (2007) The diverse and pervasive chemistries of the a-keto acid dependent enzymes. *J. Biol. Inorg. Chem.* *12*, 587-601.

[14] Ryle, M. J., Padmakumar, R., and Hausinger, R. P. (1999) Stopped-flow kinetic analysis of *Escherichia coli* taurine/α-ketoglutarate dioxygenase: interactions with α-ketoglutarate, taurine, and oxygen. *Biochemistry 38*, 15278-15286.

[15] Grzyska, P. K., Müller, T. A., Campbell, M. G., and Hausinger, R. P. (2007) Metal ligand substitution and evidence for quinone formation in taurine/α-ketoglutarate dioxygenase. *J. Inorg. Biochem.* *101*, 797-808.

[16] Hegg, E. L., Whiting, A. K., Saari, R. E., McCracken, J., Hausinger, R. P., and Que, L., Jr. (1999) Herbicide-degrading α-keto acid-dependent enzyme TfdA: metal coordination environment and mechanistic insights. *Biochemistry 38*, 16714-16726.

[17] Enemark, J. H., and Feltham, R. D. (1974) Principles of structure, bonding, and reactivity for metal nitrosyl complexes. *Coord. Chem. Rev. 13*, 339.

[18] Welford, R. W. D., Schlemminger, I., McNeill, L. A., Hewitson, K. S., and Schofield, C. J. (2003) The selectivity and inhibition of AlkB. *J. Biol. Chem. 278*, 10157-10161.

[19] Bradley, F. C., Lindstedt, S., Lipscomb, J. D., Que, L., Jr., Roe, A. L., and Rundgren, M. (1986) 4-Hydroxyphenylpyruvate dioxygenase is an iron-tyrosinate protein. *J. Biol. Chem. 261*, 11693-11696.

[20] Liu, A., Ho, R. Y. N., Que, L., Jr., Ryle, M. J., Phinney, B. S., and Hausinger, R. P. (2001) Alternative reactivity of an α-ketoglutarate-dependent iron(II) oxygenase: enzyme self-hydroxylation. *J. Amer. Chem. Soc. 123*, 5126-5127.

[21] Ryle, M. J., Liu, A., Muthukumaran, R. B., Ho, R. Y. N., Koehntop, K. D., McCracken, J., Que, L., Jr., and Hausinger, R. P. (2003) O_2- and α-ketoglutarate-dependent tyrosyl radical formation in TauD, an α-keto acid-dependent non-heme iron dioxygenase. *Biochemistry 42*, 1854-1862.

[22] Myllylä, R., Majamaa, K., Günzler, V., Hanauske-Abel, H. M., and Kivirikko, K. I. (1984) Ascorbate is consumed stoichiometrically in the uncoupled reactions catalyzed by propyl 4-hydroxylase and lysyl hydroxylase. *J. Biol. Chem. 259*, 5403-5405.

[23] Loh, K. D., Gyaneshwar, P., Papadimitriou, E. M., Fong, R., Kim, K. S., Parales, R., Zhou, Z., Inwood, W., and Kustu, S. (2006) A previously undescribed pathway for pyrimidine catabolism. *Proc. Nalt. Acad. Sci. USA 103*, 5114-5119.

[24] Pavel, E. G., Zhou, J., Busby, R. W., Gunsior, M., Townsend, C. A., and Solomon, E. I. (1998) Circular dichroism and magnetic circular dichroism spectroscopic studies of the non-heme ferrous active site in clavaminate synthase and its interaction with α-ketoglutarate cosubstrate. *J. Amer. Chem. Soc. 120*, 743-753.

[25] Kim, J., and Copley, S. D. (2007) Why metabolic enzymes are essential or nonessential for growth of *Escherichia coli* K12 on glucose. *Biochemistry ASAP*.

CHAPTER 4

Cloning of the *ygaF* gene, and purification of the encoded protein.

ABSTRACT

The *ygaF* gene, encoding a protein of previously unknown function in *Escherichia coli*, was cloned and overexpressed, and the YgaF protein was shown to possess non-covalently bound FMN. Reaction with dithionite and photoreduction both led to the two-electron reduction of the flavin. Reduced reacted rapidly with oxygen and the oxidized protein was bleached by reaction with sulfite; both of these results are consistent with YgaF being an oxidase. The wild-type strain *Escherichia coli* BW25113 was compared with the *ygaF*-KO strain, lacking an effective *ygaF*, in with growth studies, Biolog plate assays, and amino acid analyses, but these experiments did not identify the primary substrate. Numerous potential substrates with various functional groups were tested in several types of assays, and YgaF was shown to exhibit L-2-hydroxyglutarate oxidase activity. The product of the oxidation of L-2-hydroxyglutarate was proven to be α-ketoglutaric acid by HPLC and colorimetric methods. The inability of anaerobic, reduced enzyme to reverse the reaction by reducing the product α-ketoglutaric acid is explained by the very high reduction potential ($+19 \pm 8$ mV) of this enzyme. Also, it was shown that the D isomer of 2-hydroxyglutarate is not a substrate of YgaF.

INTRODUCTION

The *ygaF* gene of *Escherichia coli* is located immediately downstream of *csiD* (see Chapter 3), encoding a crystallographically-characterized protein of unknown function,[1] and just upstream of the *gabDTP-csiR* operon,[2] encoding succinic semialdehyde dehydrogenase, γ-aminobutyric acid (GABA) transaminase, and a GABA-specific permease (Figure 25, Chapter 3). The set of five genes is co-regulated by CsiR, cAMP-CRP, and σ^s acting at *csiD*$_p$ during carbon starvation and at stationary phase.[3] Expression of *gabDTP-csiR* is separately controlled by σ^s binding to *gabD*$_{p1}$, which triggered by multiple stress induction, and by Nac/σ^{70} interaction with *gabD*$_{p2}$ in response to nitrogen starvation.[2] YgaF is not obviously involved in GABA metabolism since it does not affect the catabolism of GABA or any other nitrogen source (agmatine, arginine and ornithine),[4] and its role is unknown.

On the basis of its amino acid sequence, YgaF is likely to be a flavoenzyme. It has been estimated that 1-3 % of identified proteins in prokaryotic and eukaryotic cells contain flavin,[5] and these abundant enzymes catalyze a wide range of reactions with a diverse set of substrates including alcohols, aldehydes, ketones, amines, dithiols, amino acids, and hydroxy acids.[6] Most of these enzymes transition between the fully oxidized and two-electron reduced forms of their cofactor, but in some cases the one-electron reduced semiquinone species is stabilized. Reoxidation of the reduced flavin coenzyme can take place via several processes including by reaction with oxygen, as in the case of flavin oxidases. The flavin generally is tightly bound to these enzymes, and in selected examples the coenzyme is covalently attached to the protein. Sequence comparisons of YgaF reveal this 422-amino acid *E. coli* protein to be homologous to human mitochondrial L-2-

hydroxyglutarate dehydrogenase (41% identity over 398 residues),[7] *Helicobacter pylori* malate:quinone oxidoreductase (24% identity over 421 residues),[8] *Bacillus creatinase* sarcosine oxidase (23% identity over 255 residues),[9] human mitochondrial dimethylglycine dehydrogenase (24% identity over 227 residues),[10] *Bacillus subtilis* glycine oxidase (25% identity over 146 residues),[11] human peroxisomal L-pipecolic acid oxidase (21% identity over 219 residues),[12] and many other flavoenzymes. This list includes both dehydrogenases and oxidases, with some representatives having covalently bound flavin,[12,13,14] while others do not. In this chapter I describe the cloning and overexpression of *ygaF*, the purification and characterization of YgaF, and the demonstration that it is an oxidase that possesses non-covalently bound FMN. In an effort to define the function of YgaF, I compare wild-type and *ygaF* mutant (BW25113 and *ygaF*-KO) strains using growth studies, Biolog plate assays and amino acid analysis. Finally, I show that YgaF is an L-2-hydroxyglutarate oxidase and discuss on the potential relevance of this activity to *E. coli*.

EXPERIMENTAL PROCEDURES

Materials

D-3-phosphoglycerate disodium salt, O-phospho-L-serine, O-phospho-L-threonine, D-2-hydroxygluratate disodium salt, butyraldehyde, (±)-citramalic acid, L-mandelic acid, D-mandelic acid, L-malic acid, DL-malic acid, L-glutamic acid, D-glutamic acid, L-glutamine, L-ornithine-hydroxide, D-ornithine-hydroxide, and L-threonine were obtained from Sigma. Sarcosine, 2-hydroxycaproic acid, and γ-aminovaleric acid were obtained from Aldrich. DL-lactic, α-ketoglutaric acid disodium salt, agmatine and D-valine were obtained from Fluka. γ-aminobutyric acid was purchased from General Mills Inc. L-2-hydroxyglutarate zinc salt was obtained from City Chemicals LLC.

Cloning and expression of ygaF

The gene encoding YgaF was amplified by PCR using *E. coli* MG1655 DNA as template, Pfu polymerase, and primers (5'-CAA AGG AAT TGA GCA TAT GTA TGA TTT TG-3' and 5'-GCT ACA TCC TGT TTT CAA AAG CTT TTG ATT AAA TGC GGC GTG-3') that introduce NdeI and HindIII sites into the 5' and the 3' ends of the gene, respectively. Ligation of the 1,269-bp PCR product into pET42b (Novagen) provided in an in-frame region encoding a C-terminus His₆ tag. The ligated pET42b-ygaF plasmid was transformed into *E. coli* Max Efficiency DH5α competent cells (Invitrogen), and the amplified plasmid was transformed into *E. coli* C41(DE3)[15] and BL21(DE3) cells.

The transformants were plated onto Luria Broth (LB) agar containing 50 μg/ml of kanamycin. Optimized expression conditions were chosen after experimentations with

113

various growth IPTG concentrations (0, 0.1 and 1 mM), and transformation-competent cell types (C41(DE3) and BL21(DE3)). In detail, a single colony was used to inoculate 3 ml of LB medium with 50 μg/ml kanamycin, and the culture was grown overnight at 37 °C. A portion (1.2 ml) from the overnight growth was used to inoculate 12 ml of Terrific Broth (Fisher Biotech) containing 50 μg/ml kanamycin, and this was incubated at 30 °C to an optical density of 0.7 at 600 nm. IPTG was added (0, 0.1 and 1 mM final concentration) and the growth continued at 30 °C overnight. The cells were harvested by centrifugation at 10,000 × g for 10 min and resuspended in 1 ml of lysis buffer (30 mM imidazole, 300 mM NaCl, 50 mM Na_2HPO_4, 20 % glycerol, 50 μM FAD, 0.5 mM PMSF, pH 7.2). Cells were broken by sonication (Branson sonifier, 5 reputations of 1 min each at 30 W output power, and 50 % duration) and centrifuged at 10,000 × g for 20 min at 4 °C and the expression was examined by SDS-PAGE.[16] The chosen optimized growth conditions were followed to express YgaF in large scale. A single colony of C41(DE3) cells was used to inoculate 50 ml of LB medium with 50 μg/ml kanamycin, and the culture was grown overnight at 37 °C. A portion (15 ml) from the overnight growth was used to inoculate 1 L of Terrific Broth (Fisher Biotech) containing 50 μg/ml kanamycin, and this was incubated at 30 °C to an optical density of 0.7 at 600 nm. IPTG was added (1 mM final concentration) and the growth continued at 30 °C overnight. The cells were harvested by centrifugation at 7,500 × g for 10 min and resuspended in 30 ml of lysis buffer (30 mM imidazole, 300 mM NaCl, 50 mM Na_2HPO_4, 20 % glycerol, 50 μM FAD, 0.5 mM PMSF, pH 7.2). Cells were broken by sonication and centrifuged at 100,000 × g for 1 h at 4 °C.

Purification of His-tagged YgaF

The cell extracts were loaded onto a Ni-NTA-Sepharose 6-Fast Flow column (2.5 cm diameter by 2 cm, GE Healthcare), which had been equilibrated with buffer A (30 mM imidazole, 300 mM NaCl, 50 mM Na_2HPO_4, 20 % glycerol, pH 7.2). The column was washed with buffer B (100 mM imidazole, 300 mM NaCl, 50 mM Na_2HPO_4, 20 % glycerol, pH 7.2) in order to remove any weakly bound protein from the resin, and YgaF was eluted with buffer C (500 mM imidazole, 300 mM NaCl, 50 mM Na_2HPO_4, 20 % glycerol, pH 7.2). The YgaF was immediately exchanged into buffer D (25 mM HEPES, 100 mM NaCl, 5 mM EDTA, 1 mM dithiothreitol (DTT), 20 % glycerol, pH 8.2) by using a Superdex G-25 column that had been equilibrated with this buffer. The fractions were analyzed by (SDS)-PAGE 12% polyacrylamide gel. Molecular weight markers included phosphorylase b (M_r 97,400), bovine serum albumin (M_r 66,200), ovalbumin (M_r 45,000), carbonic anhydrase (M_r 31,000), trypsin inhibitor (M_r 21,500) and lysozyme (M_r 14,400) (Bio-Rad Laboratories).

Native size of YgaF

The native size of purified YgaF was investigated by gel filtration chromatography using a Superdex 75 (1.5 cm diameter by 66 cm GE Healthcare) and a Sephacryl 300 (1.5 cm diameter by 66 cm, GE Healthcare) column. The first column was equilibrated with 25 mM HEPES buffer containing 100 mM NaCl, at pH 8.2. The second column was equilibrated with 25 mM HEPES buffer containing 100 mM or 300 mM NaCl, at pH 8.2. In all cases the flow rate was 1 ml/min. The calibration protein mixture contained

thyroglobulin (M_r 670,000), γ-globulin (M_r 158,000), ovalbumin (M_r 44,000), myoglobin (M_r 17,000) and vitamin B$_{12}$ (M_r 1,350) (Bio-Rad).

Spectroscopic studies

Absorption spectra were obtained at room temperature using a Shimadzu UV-2401 UV/visible spectrophotometer. For analyses requiring the absence of oxygen, anaerobic cuvettes (1 ml or a 200 µl, Helma) were used. YgaF was made anaerobic by 10 cycles of vacuum-argon while keeping the protein on ice to avoid precipitation and evaporation. In some cases, trace amounts of oxygen were eliminated from the buffers by including 0.04 units/ml protocatechuic 3,4-dioxygenase (PCD) and its substrate 80 µM protocatechuic acid (PCA) (both obtained from Sigma-Aldrich). Additives were prepared in sealed serum vials and similarly treated by alternate cycles of vacuum and argon flushing. Solutions were added using gas-tight syringes.

To assess whether the flavin chromophore was covalently attached to the enzyme, YgaF (600 µl of 23 µM enzyme) was treated for 1 h on ice in the dark with 10 % trichloroacetic acid.[17] After centrifugation at 10,000 *g* for 10 min to separate the protein pellet from the solution, the spectrum of the protein free sample was compared to that of the original enzyme solution. Exactly the same procedure was followed for detaching the flavin from YgaF for the cofactor identification experiment. The TCA-treated supernatant after centrifugation was filtrated (5 kDa cut off, Amicon ultra filters) and the MALDI spectra were obtained by the MS facility at MSU.

The effect of dithionite on the YgaF spectrum was examined. Anaerobic YgaF (10 µM) in 25 mM HEPES buffer with 100 mM NaCl, 1 mM DTT, 20 % glycerol at pH 8.2

was incubated with PCD and PCA in a 200 μl cuvette for 10 min at 4 °C to ensure removal of all oxygen, and titrated with an anaerobic solution of sodium dithionite (2 mM). The reaction was monitored spectroscopically, and the fully reduced sample was mixed with an equal volume of buffer equilibrated with 100 % oxygen. The concentration of dithionite was calibrated by titration of a solution of authentic FAD (Sigma).

Photoreduction of YgaF was analyzed. Anaerobic enzyme (40 μM) was incubated with PCD, PCA, and 5-deazaflavin (4 μM) on ice for 10 min, adjusted to contain 30 mM EDTA, and exposed to light (using a 50 W halogen spotlight at a distance of 6 inches) at 4 °C. Spectra were monitored over time.

The effect of sulfite addition on the spectrum of YgaF was investigated. YgaF was exchanged into 25 mM HEPES, 100 mM NaCl, 5 mM EDTA, 1 mM DTT, 20 % glycerol, pH 7.0. Sodium sulfite (Baker Analyzed Reagents) was dissolved in the same buffer and used to titrate the enzyme (15 μM), allowing the mixtures to equilibrate for 2 min before monitoring their spectra. The dissociation constant K_d of sulfite was calculated by using equation 3.

$$\Delta A = (\Delta A_{max} \bullet [L]) / (K_d + [L]) \qquad (eq. 3)$$

In this equation, ΔA is the observed change in absorbance at 450 nm, ΔA_{max} is the maximum change in absorbance, and [sulfite] is the concentration of free ligand (in this case sulfite).

Potential substrates were examined spectroscopically for their capacity to reduce or oxidize the flavin of YgaF. Putative substrates were prepared as stock solutions (5-20 mM) in 25 mM HEPES, 100 mM NaCl, 5 mM EDTA, 1 mM DTT, 20 % glycerol, pH 8.2, and made anaerobic by vacuum/argon cycling. To test whether these chemicals were

capable of reducing the enzyme flavin, anaerobic YgaF in the same buffer was titrated with the test chemicals while monitoring the spectral changes. To test whether the compounds would oxidize the bound FMN, the anaerobic enzyme was first treated with sufficient dithionite to reduce the flavin and then titrated with the potential oxidants.

Determination of the YgaF FMN redox potential

The reduction potential of the FMN cofactor of YgaF was determined spectroscopically by reductive titration of a mixture of the protein and each of several redox dyes. The most useful indicators were methylene blue (MB) and phenazine methosulfate (PMS) with reduction potentials of -5 mV and +65 mV, respectively, at pH 7.5.[18,19] YgaF (10 µM) and the selected redox dye (10 µM) were placed into an anaerobic cuvette along with PCD in (25 mM HEPES buffer with 100 mM NaCl, 1 mM DTT, 20 % glycerol at pH 7.5). The mixture was degassed and PCA was added to eliminate any traces of oxygen. The sample was titrated with freshly prepared dithionite (calibrated by titration of free FMN) while monitoring the changes in the spectrum after allowing time to achieve redox equilibration. The reduction potential of the system (E) was calculated by using the Nernst equation (Eq. 4) where E_m is the midpoint potential of the redox dye, R is the gas constant (8.314 J mol^{-1} K^{-1}), T is the temperature in K, n is the number of electrons transferred and F is the Faraday constant (96.5 J (mV)$^{-1}$ mol^{-1}). By plotting log([YgaF$_{ox}$] / [YgaF$_{red}$]) versus E, the E_m of the YgaF flavin was calculated.

$$E = E_m + \frac{2.3\,RT}{nF} \log \frac{[dye_{ox}]}{[dye_{red}]}$$

(Eq. 4)

Growth studies

E. coli BW25113 and *ygaF*-KO are wild-type and *ygaF* deletion strains obtained

from the Keio collection.[20] The cells were plated on LB agar containing 50 μg/ml

kanamycin and incubated overnight at 37 °C. Colonies from the plates were transferred

(using autoclaved cotton-tip applicators) into 15 ml Corning tubes that contained 4 ml of

M9 minimal medium that was missing the C-source. The specific C-sources of interest

were added to the cells (0.4%), and a portion (1 ml) was used to monitor the initial O.D. at

600 nm. The remaining samples (3 ml) were incubated at 37 °C for several days and the

final O.D. at 600 nm was monitored. The same procedure was followed for investigating

various N-sources (0.4%) using M9 minimal medium lacking ammonium chloride, but

containing succinate (as the C-source).

Biolog plates growth assays

Growths of the BW25113 and *ygaF*-KO strains were compared for different

carbon, nitrogen, phosphorous and sulfur sources by using Biolog plate assays. The

procedure followed that of Chapter 3.

Amino acid analysis

The abundance of amino acids and cellular amines was estimated for *E. coli*

BW25113 and *ygaF*-KO strains by amino acid analysis carried out by the Macromolecular

Structure Facility of MSU. The preparation of these samples is the same as that described

in Chapter 3.

Ortho-Phenylenediamine (OPDA) assay

A series of 2-hydroxyacid compounds were tested as substrates of YgaF by using OPDA. This reagent is known to react with many α-ketoacids,[21,22] the potential products of the reaction. In addition, this reagent was used to determine the kinetic parameters of L-2-hydroxyglutarate oxidation in comparison with authentic α-ketoglutarate. For the latter experiments, a freshly prepared stock solution containing 10 mg OPDA in 10 ml of 1 M phosphoric acid was adjusted to pH 2 and 25 μl β-mercaptoethanol was added. Samples (7.76 ml) of 1 μM YgaF (in 25 mM HEPES, pH 7.0, buffer containing 100 mM NaCl, 5 mM EDTA, 1 mM DTT, and 20 % glycerol) were mixed with L-2-hydroxyglutarate (0-400 μM) and incubated at room temperature. At selected time points, aliquots (0.97 ml) were transferred to glass tubes containing OPDA (280 μl of 8.9 mM) which quenched the reactions. To monitor the amount of product generated, samples were boiled 3 min, cooled, and the absorbance at 340 nm determined.

Oxygen electrode assay

To assay any potential oxidase activity of YgaF, the enzyme was mixed with various compounds while monitoring O_2 consumption with a Clark-type oxygen electrode (YSI Incorporated). The experiments were carried out at room temperature using air-saturated buffer (25 mM HEPES, 100 mM NaCl, 5 mM EDTA, 1 mM DTT, 20 % glycerol, pH 8.2), 2 μM YgaF, and 1 mM of the potential substrate in a 5 ml solution.

Organic acids HPLC analysis

Reaction mixtures (1 ml) containing 1 μM enzyme and 500 μM L-2-hydroxyglutarate in 25 mM HEPES buffer (pH 8.2), 100 mM NaCl, 5 mM EDTA, 20 % glycerol, and 2 mM DTT were incubated at room temperature for 4.5 h. Aliquots (300 μl) were quenched with 5 μl of 6 M sulfuric acid, centrifuged at 10,000 *g* for 5 min, and 250 μl portions of each supernatant was filtered (Amicon ultrafree-MC from Millipore) at 10,000 *g* for 1 min. Samples (200 μl) was analyzed by using Waters Breeze HPLC system equipped with an organic acids column (7.8 mm diameter by 300 mm, Bio-Rad) that had been equilibrated with 13 mM sulfuric acid with detection by reductive index. The concentrations of L-2-hydroxyglutarate (eluting at 23.0 min) and α-ketoglutarate (20.1 min) were determined by comparison to standards.

Synthesis of R and S-5-aminovalerate

For the synthesis of S-5-amino-2-hydroxy valerate, L-ornithine was the starting material (Scheme 7).[23] L-ornithine · HCl (1 g, 6 mmol) was dissolved in 3 ml water, loaded onto an Amberlite IRA-120 (H⁺) column (8 ml of resin), washed with 30 ml of water, and eluted with 40 ml of 3% ammonium hydroxide. The solution was lyophilized and the powder was dissolved in 5 ml water. After cooling in ice (~ 0 °C), the solution was mixed with 1.75 ml concentrated sulfuric acid, followed by dropwise addition of sodium nitrite (1.35 g dissolved in 5 ml water) over a period of 1 h. The solution was allowed to stand as the temperature was raised from 0 °C to 25 °C and incubated at room temperature for 50 h. The unreacted nitrite was quenched with urea, which was added until the solution gave a negative KI-starch test. The ^{1}H NMR of sample dissolved in D$_2$O

revealed two multiplets at 1.5-1.8 ppm, a feature at 2.76 ppm, and a triplet at 3.85 ppm similar to the previously reported NMR spectrum.[23] For synthesis of R-5-amino-2-hydroxyvalerate, the same procedure was followed, but using D-ornithine as the starting material.
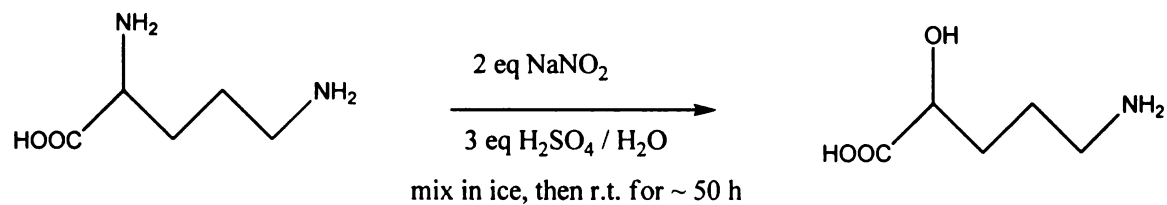
Scheme 7. Synthesis of S-5-aminovalerate from L-ornithine.

RESULTS

Cloning and expression of ygaF

The *E. coli* gene *ygaF* was successfully ligated into pET-42b plasmid and transformed into BL21(DE3) and C41(DE3) competent cells, as described in the experimental methods. The optimized expression conditions of the *ygaF* gene were chosen after comparison among growths in both cell types treated with several IPTG concentrations (0, 0.1 and 1 mM final concentration). The gene of interest was expressed in most of the conditions tested and appeared in both soluble and insoluble fractions (Figure 38). The conditions that were chosen as the best were use of C41(DE3) cells and 1 mM IPTG, where the expressed level of soluble YgaF was satisfactory.
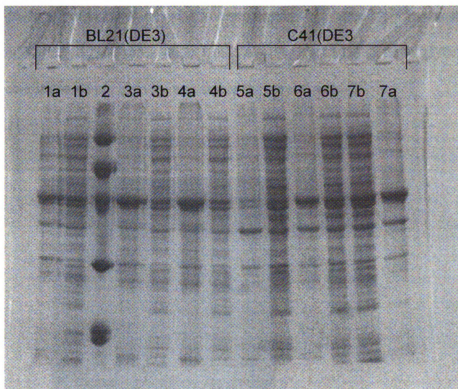
Figure 38. SDS-PAGE analysis of the expression conditions tested for *ygaF*.
Denatured samples were analyzed on a 12% acrylamide gel. Expression of *ygaF* in
BL21(DE3) cells: lanes 1a and 1b, 0 mM IPTG; lanes 3a and 3b, 0.1 mM IPTG; and lanes
4a and 4b, 1 mM IPTG. Expression of *ygaF* in C41(DE3) cells: lanes 5a and 5b, 0 mM
IPTG; lanes 6a and 6b, 0.1 mM IPTG; and lanes 7a and 7b, 1 mM IPTG. Standard: lane 2.
The pellets are symbolized with 'a' and the cell extracts with 'b'.

Purification of YgaF

YgaF containing a C-terminal His$_6$-tag was purified by Ni-NTA-Sepharose 6-Fast

Flow chromatography from soluble extracts of *E. coli* C41 (DE3) containing pET42b-

ygaF. Immediately after elution, the protein was exchanged into imidazole-free buffer to

enhance its stability. Glycerol, EDTA, and DTT further stabilized the protein (data not

shown). SDS-PAGE revealed the protein to be ~95 % homogeneous with a molecular

mass in agreement with that predicted from the sequence (47.64 kDa), as shown in Figure

39. A 1 L culture typically provided 55-65 mg of YgaF after the Ni-Sepharose column or

30-40 mg after Sephadex G-25 chromatography. Purified YgaF was stored in buffer D (25 mM HEPES, 100 mM NaCl, 5 mM EDTA, 1 mM DTT, 20 % glycerol, pH 8.2) at 4 °C, conditions where activity was stable for several weeks.
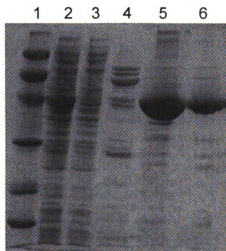

Figure 39. . Purification of YgaF as monitored by SDS-PAGE analysis. Denatured samples were analyzed on a 12% acrylamide gel. Lane 1, standards; lane 2, cell extracts; lane 3, flow through of the Ni-NTA-Sepharose 6-fast flow column; lane 4, wash of the Ni resin with buffer containing 100 mM imidazole; lane 5, YgaF elution from Ni resin with buffer containing 500 mM imidazole; lane 6, YgaF elution from Superdex G-25. (Molecular weight markers: phosphorylase b (M_r 97.4 kDa), bovine serum albumin (M_r 66.2 kDa), ovalbumin (M_r 45.0 kDa), carbonic anhydrase (M_r 31.0 kDa), trypsin inhibitor (M_r 21.5 kDa) and lysozyme (M_r 14.4 kDa)).

Native size of His$_6$-tagged YgaF

Two gel filtration columns were used for testing the polymerization state of YgaF. The protein eluted from a Superdex 75 column and a Sephacryl 300 column primarily as an aggregate. The results for the latter column are illustrated (Figure 40A and B). SDS-PAGE revealed that YgaF eluted both at 44.16 min (the point where the protein absorbance is greater at 280 nm) and in all subsequent fractions (Figure 40C). The same results were noted when the salt concentration was increased from 100 mM to 300 mM

NaCl. In conclusion, most YgaF appeares to be highly aggregated and a portion of YgaF appears to interact with the gel exclusion resins.
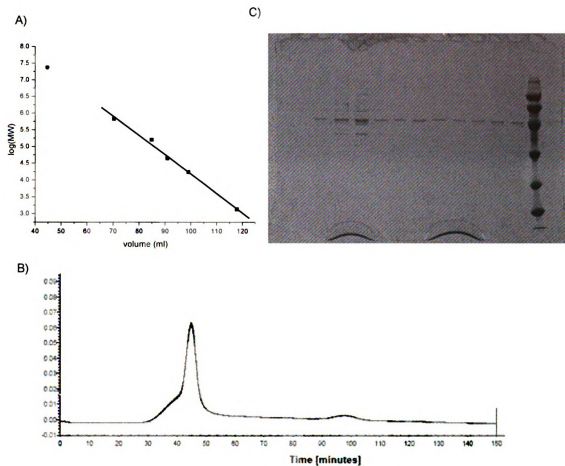

Figure 40. Determination of the native size of YgaF by sephacryl 300 chromatography. A) A standard curve that correlates the elution time with the log(MW) of the standard proteins (■)and the estimated position of YgaF (●). B) Elution of YgaF. Time in minutes is equal to elution volume in ml. C) 12 % SDS-PAGE: lane 1, fraction 12; lane 2, fraction 13; lane 3, fraction 14; lane 4, fraction 15; lane 5, fraction 16; lane 6, fraction 22; lane 7, fraction 24; lane 8, fraction 26; lane 9, fraction 28; lane 10, fraction 31; lane 11, fraction 32; lane 12, fraction 33; lane 13, fraction 34; lane 14, standard; lane 15, and fraction 35.

Testing whether the flavin binds covalently to YgaF and identification of the flavin cofactor by MALDI analysis.

Purified YgaF is yellow in color, and its spectrum (maxima at 378 and 450 nm, with a shoulder at 476 nm) is consistent with that of a flavoprotein. To distinguish whether the flavin is covalently attached to YgaF, as is reported for several sequence-related enzymes,[12,13,14] the protein was precipitated with trichloroacetic acid (TCA). The resulting pellet was white whereas the supernatant remained yellow. The spectrum of the supernatant was similar with that of the as-purified YgaF (Figure 41), demonstrating that the cofactor is not covalently attached to YgaF. Direct confirmation of the presence of FMN and not FAD, was obtained by MALDI-MS analysis, which revealed a feature at m/z of 458.1 (data not shown) (the calculated values for FMN and FAD are 456.1 and 785.1 respectivelly).
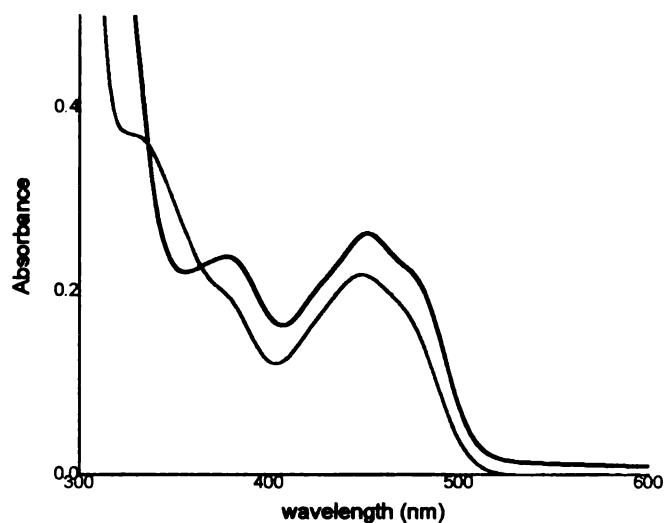
Figure 41. FMN is not covalently bound to YgaF. Black line: 23 μM untreated YgaF with TCA, red lane: supernatant after the centrifugation of YgaF that had been treated with TCA. Baseline is the protein buffer.

Reduction and oxidation of YgaF

It is known that EDTA can be used as a source of reductant in the presence of small amounts of free flavins (like 5-deazaflavin) and light to catalyze the photoreduction of flavoenzymes.[24,25] Photoreduction of YgaF for 72 min in the presence EDTA and 5-deazaflavin converted the protein to its reduced form, pointing out that YgaF undergoes a two-electron reduction leading directly to the fully reduced cofactor, with no semiquinone intermediate observable (Figure 42).
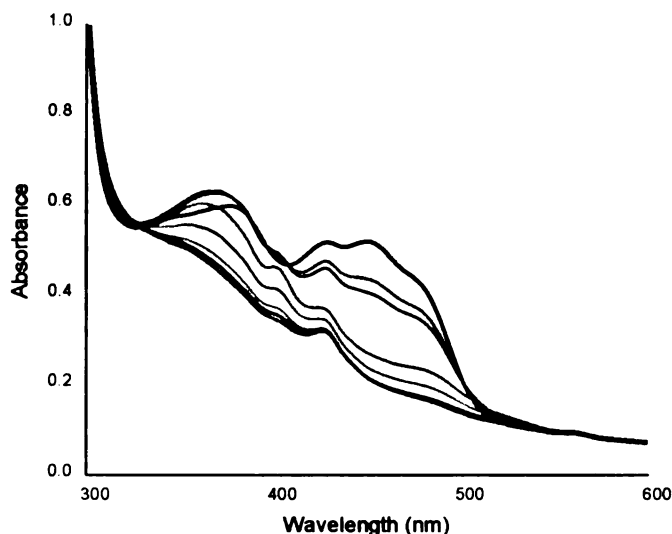
128

Figure 42. Photoreduction of YgaF. Anaerobic YgaF (40 µM) in the presence of EDTA and 5-deazaflavin (upper scan) was photoreduced at 4 °C and spectra were obtained after 7, 14, 36, 54, 72, 92 and 120 min.

Similarly, chemical reduction of YgaF with dithionite led to a smooth transition to the two-electron reduced species (Figure 43). No anionic or neutral semiquinone species was observed during the titration. Approximately 1.6 equivalents of dithionite were required to reduce YgaF (Figure 43), consistent with the presence of some remaining oxygen in the sample. The addition of an equal volume of buffer equilibrated with 100 % oxygen to dithionite-reduced enzyme led to the immediate reoxidation of the FMN to half (due to dilution) the starting spectral intensity. The rapid reoxidation of the flavin with oxygenated buffer is evidence that YgaF is an oxidase.
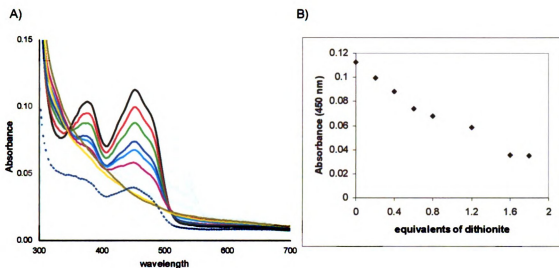
Figure 43. Reductive titration of YgaF by dithionite. A) Anaerobic YgaF (10 μM) (upper scan) was treated with sequential additions of dithionite until the flavin was completely reduced. The fully reduced sample was mixed with an equal volume of oxygenated buffer, resulting in immediate reoxidation of the flavin (dashed line). B) Absorbance of the flavin at 450 nm versus the equivalents of dithionite added.

Flavin-sulfite adduct

Many flavin-containing oxidases (but not other flavoproteins) are bleached by formation of a complex between sulfite and FMN.[26] If a similar reaction takes place with YgaF that would provide additional evidence that it is an oxidase. The addition of sulfite to YgaF resulted in loss of the flavin absorbance (Figure 44), providing a sulfite dissociation constant (K_d) of 102 ± 7 μM at pH 7. A correlation has been noted between the measured K_d of sulfite and the redox potentials of several flavoenzymes;[27] extrapolation of those data allowed us to roughly estimate the redox potential of the YgaF flavin as approximately –25 mV at pH 7.
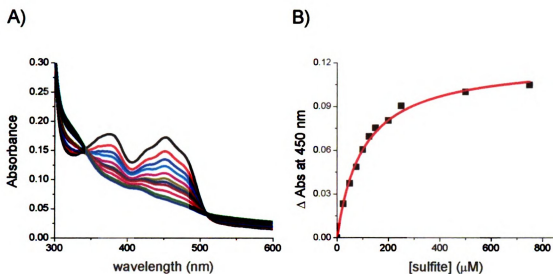
A)

B)

Figure 44. A) Titration of YgaF with sulfite. YgaF (15 µM) was titrated with 25, 50, 75, 100, 125, 150, 200, 250, 500 and 700 µM sulfite in 25 mM HEPES buffer, pH 7.0, containing 100 mM NaCl, 5 mM EDTA, 1 mM DTT, and 20 % glycerol. B) Absorbance change at 450 nm versus the concentration of free sulfite.

Determination of the redox potential of the flavin

To more directly determine the reduction potential of the YgaF-bound FMN, reductive titrations were carried out in the presence of redox dyes. To illustrate, YgaF was mixed with MB (E_m= -5 mV at pH 7.5), made anaerobic, and titrated with increasing levels of dithionite (Figure 45A). YgaF was preferentially reduced over MB, leading to the conclusion that the redox potential of the flavin should be higher than the MB potential. By monitoring the concentration of oxidized MB (λ_{max} = 666 nm with ε_{666} = 35,440 M^{-1} cm^{-1}, while its reduced form has essentially no absorbance at this wavelength),[28] the system reduction potential (E) after each addition could be determined by using the Nernst equation. A comparison of E versus the log of the ratio of the oxidized to reduced YgaF was used to determine the E_m of +26.5 ± 5 mV for YgaF (Figure 45B).
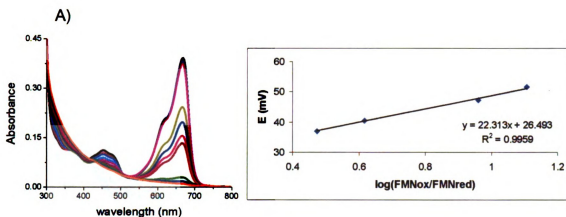
Figure 45. Analysis of the YgaF flavin reduction potential using MB as the redox dye.
A) An anaerobic mixture of YgaF and MB (10 μM each) was titrated with sodium dithionite while monitoring the absorption spectrum. The changes in the relative concentrations of the reduced and oxidized forms of MB were used to deduce the system reduction potential (E) for each condition. B) Correlation of the measured E with the log(FMN$_{ox}$/FMN$_{red}$) of YgaF.

A second redox dye used to determine the redox potential of the YgaF-bound FMN was phenazine methosulfonate (PMS), which has a midpoint potential at pH 7.5 of +65 mV. Upon reduction, PMS exhibits a sharp absorption feature at 388 nm ($\varepsilon_{388} = 21,390$ M^{-1} cm^{-1}). The PMS absorbancies at 388 nm and 450 nm overlap with the YgaF absorbancies, so it was necessary to calculate the fractions of PMS and YgaF that were oxidized and reduced by taking into account the observed changes for PMS and YgaF reduced separately. PMS was preferentially reduced over YgaF when treated together with dithionite, indicating that the redox potential of the YgaF flavin was smaller than +65 mV (Figure 46A). The estimated E_m value for YgaF was +11 ± 5 mV by comparison of E of the system versus the log of the ratio of the oxidized to reduced YgaF (Figure 46B). Thus, by taking into account both experiments (MB and PMS), we can conclude that the redox potential of the flavin bound to YgaF is 19 ± 8 mV.
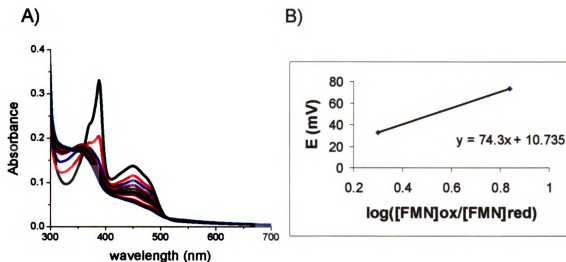
Figure 46. Analysis of the YgaF flavin reduction potential using PMS as the redox dye. A) An anaerobic mixture of YgaF and PMS (10 μM each) was titrated with sodium dithionite while monitoring the absorption spectrum. The changes in the relative concentrations of the reduced and oxidized forms of PMS were used to deduce the system reduction potential (E) for each condition. B) Correlation of the measured E with the log(FMN$_{ox}$/FMN$_{red}$) of YgaF.

Growth studies

An attempt to identify the biological role of YgaF involved comparison of the growths of the BW25113 and *ygaF*-KO strains while they grew on particular carbon and nitrogen sources. The sources that were investigated included several L- and D-amino acids, and molecules that could potentially be involved in GABA metabolism. The cells were grown to stationary phase and their absorbances at 600 nm were compared. As shown in Figure 47 A, both strains grew with succinate (positive control) and with L-Pro, but none of the other C-sources led to growth, under these conditions. On the other hand, when the same molecules were tested as N-sources (with NH$_4$Cl as the positive control), growth was observed in both strains for several conditions (Figure 47B). The most interesting difference observed between the BW25113 and knock-out strains was using L-

133

Glu as an N-source, where there was less growth after 67 h of incubation for the mutant strain, which disappeared after 90 h. L-Glu along with other interesting molecules were tested as substrates of purified YgaF, as shown below.

Biolog plates analysis

The Biolog plate analysis (described in Chapter 3) was used to compare the metabolism of BW25113 and *ygaF*-KO strains. The *ygaF*-KO mutant, like the *csiD*-KO mutant, was generated by insertion of a kanamycin resistance gene into the reading frame of the *ygaF* gene. Many carbon (PM1 and PM2), nitrogen (PM3), phosphorous and sulfur sources (PM4) were tested. C-sources that resulted in less extensive growth for the knock out mutant compared to the BW25113 strain included: L-Asn, L-Glu, M-tartaric, pyruvic acid, L-sorbose, 5-keto-D-gluconic acid. The most interesting differences between the strains involved the following N-sources: L-Glu, L-Thr, D-Asn, L-homoserine, agmatine, N-acetyl-D-mannosamine, guanosine, and D,L-α-aminocaprylic acid. Moreover, several N-sources that caused a slower growth in the *ygaF*-KO cells, which finally reached similar growth level with the BW25113 cells were: L-Cys, L-Lys, L-Pro, L-Ser, L-ornithine and δ-amino-valeric acid. The P-sources that should some differences were: D-3-phosphoglyceric acid, O-phospho-L-serine, and O-phospho-L-threonine. For S-sources, conclusions could not be made because the negative control of both strains grew.

Figure 47. Comparison of the growth of BW25113 (WT) and *ygaF*-KO strains with different C- and N-sources. A and B) Absorbance of strains grown on several C-sources at 600 nm at 0 h (blue) and after 116 h (red). C and D) Absorbance of strains grown on several N-sources at 600 nm at 67 h (blue) and after 90 h (red).

135

C)

D)
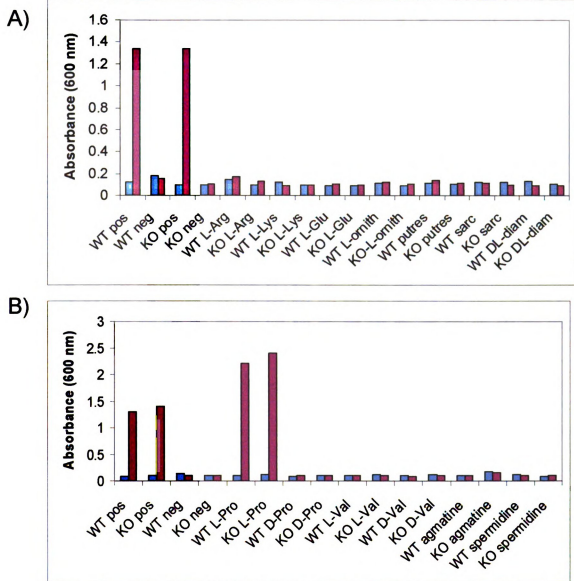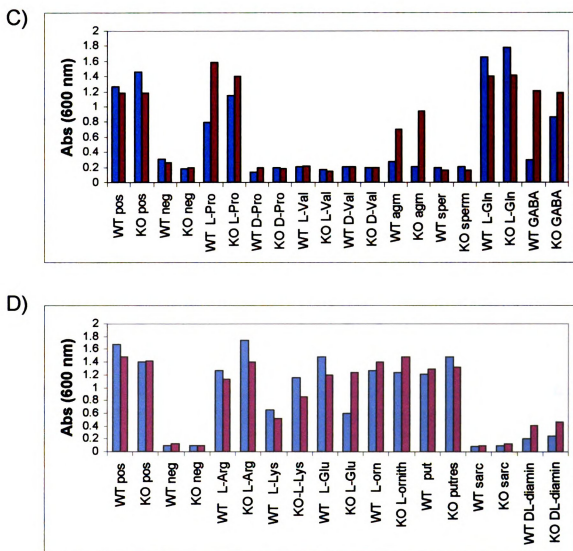
Figure 47 (continued).

Amino acid analysis

As described in detail in Chapter 3, amino acid analysis enables the comparison of the cellular levels of free amino acids among different strains. This experiment was the third attempt for identification of the physiological substrate of YgaF. The most pronounced differences in abundance between the two strains are present in glutamic acid and α-aminoadipic acid, as shown in Figure 48. Both amino acids were found to be in

136

smaller abundance in the *ygaF*-KO mutant compared to BW25113 cells. The fact that similar behavior was reported for the *csiD*-KO mutant (see Chapter 3), can be interpreted as indicating that the encoded proteins CsiD and YgaF might be closely correlated in a yet unknown pathway.
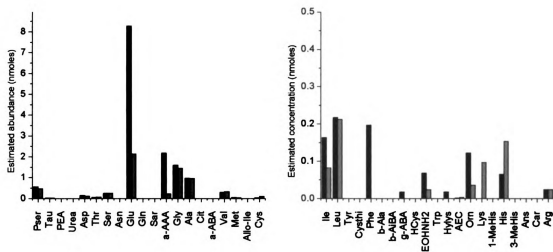
Figure 48. Comparison of the amino acid analysis of the BW25113 (black) and *ygaF*-KO (red) strains. Acronyms other than the of natural amino acids are: Pser (phosphoserine), Tau (taurine), PEA (phosphoethanolamine), MetSO4 (methione sulfoxide), Sar (sarcosine), a-AAA (α-aminoadipic acid), Cit (citruline), a-ABA (α-amino-η-butyric acid), Allo-Ile (allo-isoleucine), Cysthi (cystathionine), b-Aiba (β-amino-isobutyric acid), Hcys (homocysteine), Hylys (δ-hydroxylysine), AEC (aminoethylcysteine), Orn (ornithine), S-AHCys (S-adenosyl homocysteine), 1-MeHis (1-methyl histidine) and 3-MeHis (3-methyl histidine).

Investigations of potential substrates of YgaF

Several compounds were tested as potential substrates of YgaF by assaying for their ability to (a) reduce FMN or oxidize FMNH₂ in the anaerobic enzyme, (b) stimulate oxygen consumption, or (c) react with OPDA, a reagent for detecting α-ketoacids (Table 3). Significantly, neither the reduced nor the oxidized forms of NAD⁺ or NADP⁺ affected

the flavin spectrum; thus, YgaF is not a nicotinamide-dependent enzyme. No spectroscopic changes or O_2 consumption activity was detected when YgaF was incubated with GABA or several compounds that could plausibly be used in GABA production (agmatine, putrescine, glutamic acid, glutamine, and the R- and S- isomers of 5-amino-2-hydroxyvaleric acid). Similarly, no activity was detected for selected methylated compounds (dimethylglycine, sarcosine), representative aldehyde (butyraldehyde) and 3-hydroxyacid (3-hydroxybutyric acid) compounds. Furthermore most 2-hydroxyacids were ineffective as substrates, including L- or DL-malic acid, DL-lactic acid, L- or D-mandelic acid, and 2-hydroxycaproic acid. In contrast, as described below, robust activity was detected in the case of L-2-hydroxyglutaric acid.

Table 3. List of the compounds tested as potential substrates of YgaF and the methods that were used. The four experimental methods included oxygen consumption, UV-vis absorption spectra of potential substrate added to the oxidized and to the reduced form of YgaF, and the OPDA assay. The method(s) used for each hypothetical substrate is indicated by "✓".

Substrate	O_2-consumption	Anaerobic YgaF + substrate	Anaerobic YgaF + dithionite + substrate	OPDA assay
NADH		✓		
NADPH		✓		
D-Ala	✓	✓		
Putrescine	✓	✓		
DL-diaminopimelic acid	✓			
Malic acid		✓		
Butyraldehyde		✓		
Sarcosine		✓		
n-butyl-CoA		✓		

DL-2-OH-Glu	✓	✓		
L-2-OH-Glu	✓	✓		✓
D-2-OH-Glu		✓		✓
2-OH-caproic acid	✓	✓		✓
(+/-) citramalic acid	✓	✓		
L-mandelic		✓		✓
D-mandelic		✓		✓
DL-lactic	✓			✓
DL-malic				✓
L-malic		✓		✓
Dimethylglycine		✓		
3-OH-butyric acid		✓		
S-5-amino-2-OH-valeric acid	✓	✓		✓
R-5-amino-2-OH-valeric acid		✓		✓
R/S-5-amino-2-OH-valeric acid		✓		
2-propanol	✓			
αKG		✓	✓	
L-Glu		✓		✓
D-Glu		✓		✓
L-Arg		✓		
L-Gln				✓
Agmatine		✓		
D(-)-3-phosphoglycerate		✓		
O-phospho-L-Ser		✓		
O-phospho-L-Thr		✓		
GABA			✓	
4-amino benzoic acid			✓	
Butyric acid			✓	
3-chloropropionic acid			✓	

Table 3 (continued).

139

L-2-hydroxyglutarate is a substrate for YgaF:

The behavior of L-2-hydroxyglutarate as a substrate of YgaF was examined in greater detail. As illustrated in Figure 49, the addition of increasing concentrations of L-2-hydroxyglutarate to an anaerobic solution of YgaF resulted in successive reduction of the FMN (the feature at 410 nm was a contaminant in this particular preparation), with fully reduced sample requiring about 1.5 equivalents of substrate. Analysis of the concentration dependent changes in the difference spectra by use of equation 3 yielded an L-2-hydroxy-glutarate K_d of 20 ± 4 μM. Furthermore L-2-hydroxyglutarate was shown to be a substrate of YgaF according to both the oxygen electrode, and OPDA assays. The latter method was used at several substrate concentrations to produce an initial velocity (v_i) versus L-2-hydroxyglutarate concentration graph, providing a K_m of 95 ± 26 μM, V_{max} of 113 ± 14 nmoles min^{-1} (mg of protein)$^{-1}$, and a turnover number, k_{cat}, of 0.08 s^{-1} (Figure 50).
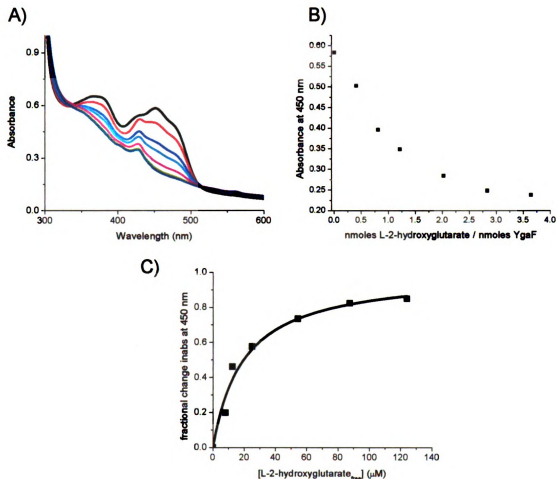
Figure 49. Titration of anaerobic YgaF with L-2-hydroxyglutarate. A) Anaerobic YgaF (47 μM in 25 mM HEPES, pH 8.2, containing 100 mM NaCl, 5 mM EDTA, 1 mM DTT, and 20 % glycerol) was adjusted to contain 19, 38, 57, 95, 133 and 171 μM L-2-hydroxyglutarate. B) Change in absorbance at 450 nm as a function of the concentration of free substrate in the solution. C) Fractional change in absorbance at 450 nm as a function of the concentration of free L-2-hydroxyglutarate.

Figure 50. Determination of the K_m and V_{max} of the L-2-hydroxyglutarate oxidation from a graph of the initial velocity (v_i) versus its concentration.

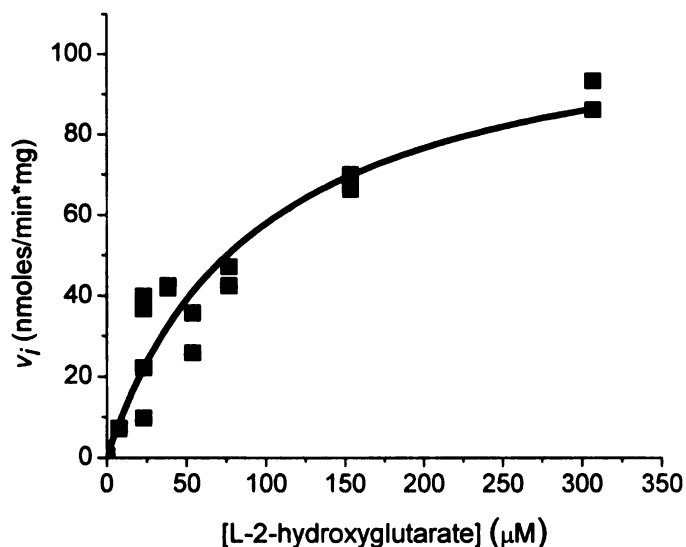The product of the reaction of YgaF with L-2-hydroxyglutarate was expected to be α-ketoglutarate on the basis of the OPDA reactivity and the oxidase activity with this substrate. The production of 330 μM α-ketoglutarate from 380 μM substrate was confirmed by HPLC (details in the experimental methods). As shown in Figure 51A, in the first control experiment (where YgaF is absent) L-2-hydroxy glutarate elutes after 23 min, and there is no observable peak at an elution time of 20.1 min, where αKG elutes. On the other hand, when the enzyme is present and incubated at room temperature for the same amount of time as the control experiment (4.5 h), the peak that corresponded to the substrate disappeared and a new peak appeared where αKG elutes (Figure 51C). The amount of αKG produced from the enzymatic reaction (330 μM) was calculated from its standard curve. Although α-ketoglutarate is the product of the enzymatic reaction, the addition of this oxoacid to anaerobic YgaF (with its FMN reduced by dithionite) did not

result in flavin oxidation; these results indicate the reaction is essentially irreversible (data not shown), in agreement with the high reduction potential of the flavin.

In order to make sure that the His_6-tag did not have a major interference with the activity of YgaF, cell extracts containing the over-expressed His_6-tagged protein were compared on the basis of activity to extracts containing overexpressed un-tagged YgaF. The amounts of αKG produced in both cell extracts in a period of 20 min at room temperature, were very similar. This experiment demonstrates the His_6-tag has little effect on the activity of YgaF, though it is an estimation taking into account that the cell extracts don't contain exactly the same amount of YgaF.

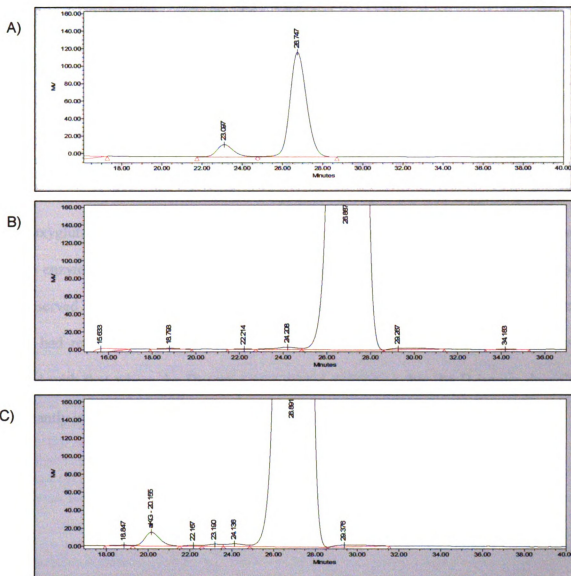**Figure 51. Identification of the product of the enzymatic reaction of L-2-hydroxyglutarate.** Organic acid HPLC analysis for A) 380 μM L-2-hydroxyglutarate, B) 1 μM YgaF and C) reaction of 1 μM YgaF with 380 μM L-2-hydroxyglutarate at room temperature for 4.5 h. The buffer for all three HPLC samples was : 25 mM HEPES, 100 mM NaCl, 5 mM EDTA, 20 % glycerol, 2 mM DTT, pH 8.2. The peak at ~26.8 min elution time is glycerol.

The D-2-hydroxyglutarate isomer is not a substrate of YgaF:

In contrast to the results with L-2-hydroxyglutarate, no flavin reduction was detected using D-2-hydroxyglutarate. Furthermore, only very low levels of activity were detected using the OPDA procedure. As illustrated in Figure 52, the low level reactivity of D-2-hydroxyglutarate was transient and was repeated when another aliquot of the substrate was added, consistent with the enzyme remaining active and suggesting that D-2-hydroxyglutarate contains a low concentration of the L isomer. As further confirmation that the enzyme retains activity after incubation with the D isomer, high level of activity was observed when L-2-hydroxyglutarate was added to the reaction mixture (after the system had reached the first platue). The αKG production under these conditions was identical with that where the D-isomer was absent, indicating that the D-isomer doesn't significantly inhibit YgaF.
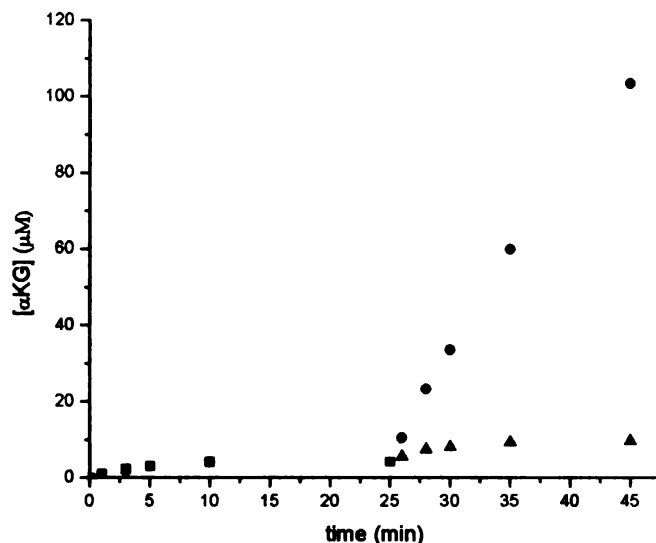
Figure 52. Timecourse of the αKG production for the reaction of YgaF with the isomers of 2-hydroxyglutarate. YgaF (1 μM) was incubated with D-2-hydroxyglutarate (300 μM) in 25 mM HEPES buffer containing 100 mM NaCl, 1 mM DTT, and 20 % glycerol at pH 8.2 at 25 °C. Aliquots of 970 μl were collected from the reaction mixture at 1, 3, 5, 10 and 25 min and treated with OPDA (black squares). The remaining reaction mixture was separated into two equal portions (7.76 ml). D-2-hydroxyglutarate (300 μM) was added to one (blue triangles); and L-2-hydroxyglutarate (300 μM) was added to the other (red cycles). Aliquots of 970 μl were collected from both reactions at 1, 3, 5, 10, 20 and 40 min and treated with OPDA.

D-3-phosphoglycerate is a poor substrate of YgaF:

As discussed above, the *ygaF*-KO mutant grew slower but finally reached the same growth point with the BW25113 strain on D-3-phosphoglycerate as a P-source. 3-Phosphoglycerate is a close structural mimic of 2-hydroxyglutarate (Scheme 8); thus, we tested this common cellular intermediate as a substrate of YgaF. As shown in Figure 53A, 90, 270 and 540 μM of 3-phosphoglycerate led to only sligh reduction of 18 μM YgaF, whereas 900 μM of this particular substrate was able to reduce the enzyme at a slow rate. Therefore, D-3-phospho-D-glycerate, acts as a poor substrate of the enzyme. By contrast,

146

two other phosphorylated compounds, O-phospho-L-serine and O-phospho-L-threonine exhibited no activity.
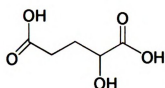
2-hydroxyglutarate
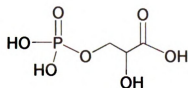
3-phosphoglycerate

Scheme 8. Structural similarity of 2-hydroxyglutarate and 3-phosphoglycerate.
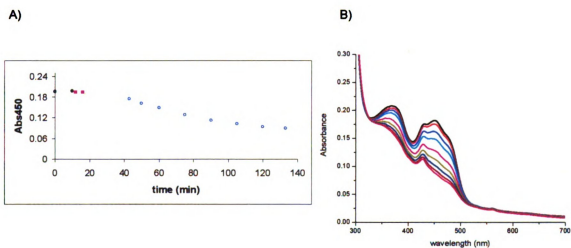
Figure 53. Titration of anaerobic YgaF with D-3-phosphoglycerate. A) Change in absorbance at 450 nm as a function of time. Anaerobic YgaF (18 µM in 25 mM HEPES, pH 8.2, containing 100 mM NaCl, 5 mM EDTA, 1 mM DTT, and 20 % glycerol) was adjusted to contain 90 (blue squares), 270 (pink squares), 540 (yellow triangles) and 900 µM (cyan cycles) D-3-phosphoglycerate. B) Anaerobic YgaF incubated with 900 µM of D-3-phosphoglycerate for 10, 20, 35, 50, 65, 80 and 93 min.

CONCLUSIONS

The *E. coli ygaF* gene is located in the *csiD-ygaF-gabDTP-csiR* operon, controlled by the *csiD*$_p$ promoter and activated exclusively under carbon starvation together with the *csiD* gene. It encodes a protein, YgaF, which has been considered a putative dehydrogenase with unknown function. In this study I cloned, expressed, purified and characterized the general properties of YgaF.

Cloning, expression and purification. In this work, the *E. coli ygaF* gene was cloned and expressed with success for the first time. The encoded protein, C-terminus-His$_6$-tagged YgaF, was easily purified in one step by using a Ni-NTA affinity column. The color of the purified protein was yellow, as it was expected for a flavin-containing protein. The protein was more than 95 % homogeneous, according to the SDS-PAGE, and obtained with an overall yield of 30-40 mg per L growth. YgaF was stable in 25 mM HEPES buffer that contained 100 mM NaCl, 20 % glycerol, 5 mM EDTA and 1 mM DTT at pH 8 for several weeks at 4 °C. The attempt to estimate the native size of the YgaF by gel filtration chromatography was inconclusive, due to unidentified interactions between the protein and the resin, but the major portion of the protein was a large aggregate.

YgaF is a FMN bound oxidase. The absorbance spectrum of the purified enzyme has the characteristic shape of a bound flavin, with dual maxima at 378 nm and 450 nm. The flavin of YgaF was proven to be non-covalently bound FMN. Photoreduction of YgaF occurred in the presence of EDTA and 5-deazaflavin with no intermediated semiquinone observed. This experiment indicates that the YgaF goes through two-electron reduction in a single step. Similar results were noted when the flavin was reduced chemically by dithionite. Immediate reoxidation of chemically-reduced YgaF by addition of an equal
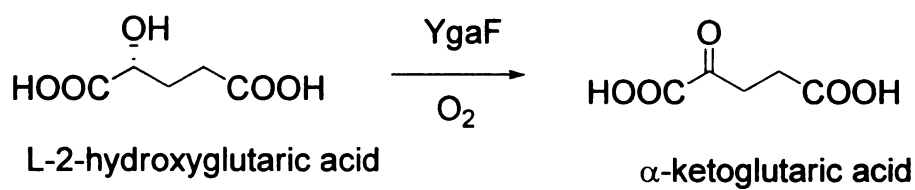
volume of oxygenated buffer implies that YgaF is an oxidase. Support for this assignment was obtained by a characteristic reaction catalyzed only by oxidases involving the formation of a flavin-sulfite adduct through a covalent bond at the N(5) position of the isoalloxazine ring of the flavin. The dissociation constant (K_d = 102 µM) of the FMN-sulfite complex is in the micromolar range, as commonly observed for flavin-containing oxidases,[29] and was used to approximate the reduction potential of the protein (-24 mV at pH 7). This value is close to the reduction potential measured spectroscopically when using the MB and the PMS as redox dyes (+19 mV at pH 7.5), and suggests that E_m increases with increasing pH.

Searching for the YgaF substrate. Several methods were used to identify the primary substrate of YgaF. Growths of *E. coli* BW25113 and *ygaF*-KO strains revealed that the mutant grows more slowly than the wild type cells using L-Glu as the N-source. Further studies indicated that L-Glu is not a substrate of YgaF. Biolog plate analysis, enabled the comparison of growths of *E. coli* BW25113 and *ygaF*-KO for a large variety of different carbon, nitrogen, phosphorous and sulfur sources. This study identified several potentially interesting compounds, but none were subsequently shown to be substrates of YgaF. As mentioned in the discussion part of Chapter 3 for the *csiD* gene, it cannot be excluded that *E. coli* possesses more than one pathway to metabolize the specific compound of interest, so that the analyses of the growth of the *ygaF*-KO and BW25113 strains may not be definitive.[30] A third approach to compare the BW25113 and the *ygaF*-KO strains was by amino acid analysis. This method specifically detects the level of amino acids and specific other compounds in the cells. The mutant cells contained less L-Glu, a result that might be connected with the slower growth rates on this N-source for the

knock-out mutant compared to the WT. Other experiments attempted to directly identify the substrates of YgaF using purified YgaF and four detection methods. These were assaying for the ability to reduce FMN or to oxidize $FMNH_2$ under anaerobic conditions, to consume oxygen, or to react with OPDA, which is a reagent that can react with α-ketoacids. The molecules investigated included compounds involved in GABA catabolism, along with alcohols, aldehydes, primary and secondary amines, acids, amino acids, and α and β-hydroxy acids. Most molecules failed to react with YgaF when examined by any method. The only compounds that showed activity were L-2-hydroxyglutarate and the D-3-phosphoglycerate, with the latter one showing that it was poor substrate for YgaF.

L-2-hydroxyglutarate is a substrate of YgaF. YgaF exhibits robust activity toward L-2-hydroxyglutarate (Scheme 9), while negligible activity was detected with the D isomer. The use of L-2-hydroxyglutarate as a substrate was not surprising given the close sequence similarity (41 % identity) between this *E. coli* protein and human FAD-dependent L-2-hydroxyglutarate dehydrogenase. Furthermore, the finding that YgaF is an oxidase rather than a dehydrogenase is consistent with the ability of the protein to generate a complex with sulfite, as discussed above. It is instructive to compare YgaF to the mammalian enzyme L-2-hydroxyglutarate dehydrogenase to which it is related. The K_m of YgaF for L-2-hydroxyglutarate (95 μM) is lower than those reported for L-2-hydroxyglutarate dehydrogenases from human or rat (800 μM and 150 μM, respectively).[7,31] The dissociation constant K_d of the YgaF-L-2-hydroxyglutarate was found to be 20 ± 4 μM. The expected product of this enzymatic reaction (αKG) was shown to be produced by using both the OPDA assay (because OPDA reacts with 2-keto

acids) and by the organic acids HPLC column, where the product of the reaction had the same elution time with αKG. Importantly, the reaction seems to be irreversible. The relatively high reduction potential of this flavoprotein explains the apparent irreversibility of the reaction (i.e., the reduction of α-ketoglutarate by anaerobic, reduced YgaF) when monitored spectroscopically. Also, the His_6-tag seems not to affect the activity of YgaF.

$$\text{HOOC} \overset{\overset{\text{OH}}{|}}{\diagup\diagdown} \text{COOH} \quad \xrightarrow[\text{O}_2]{\text{YgaF}} \quad \text{HOOC} \overset{\overset{\text{O}}{||}}{\diagup\diagdown} \text{COOH}$$

L-2-hydroxyglutaric acid   α-ketoglutaric acid

Scheme 9. The catalytic YgaF reaction with L-2-hydroxyglutarate.

The potential relevance of the L-2-hydroxyglutarate activity of YgaF to E. coli. In mammalian cells, L-2-hydroxyglutarate has been suggested to arise from the non-specific reduction of α-ketoglutarate by L-malate dehydrogenase. Thus, the physiological role of the human enzyme is proposed to be a metabolite repair enzyme to prevent accumulation of this compound in tissues.[32] Mutation of the gene encoding human L-2-hydroxyglutarate dehydrogenase (in particular, mutations associated with K81E and E176D variants or deletion of exon 9) leads to such accumulation,[31] a disease state known as L-2-hydroxyglutarate aciduria and characterized by ataxia, mental deficiency with subcortical leukoencephathology, and cerebellar atrophy.[7] L-malate dehydrogenase may play a similar role in *E. coli*, but in addition SerA is known to reduce α-ketoglutarate to form both D- and L-2-hydroxyglutarate.[33] The normal reaction catalyzed by SerA is the oxidation of 3-phospho-D-glycerate (a poor substrate of YgaF) to form 3-phospho-hydroxypyruvate, using NAD^+ as cofactor. We propose that *E. coli* uses YgaF to oxidize L-2-

151

hydroxyglutarate (and 3-phospho-L-glycerate), where these compounds arise by such aberrant side reactions.

REFERENCES

[1] Chance, M. R., Bresnick, A. R., Burley, S. K., Jiang, J. S., Lima, C. D., Sali, A., Almo, S. C., Bonanno, J. B., Buglino, J. A., Boulton, S., Chen, H., Eswar, N., He, G., Huang, R., Ilyin, V., McMahan, L., Pieper, U., Ray, S., Vidal, M., and Wang, L. K. (2002) Structural genomics: a pipeline for providing structures for the biologist. *Protein Sci. 11*, 723-738.

[2] Metzner, M., Germer, J., and Hengge, R. (2004) Multiple stress signal integration in the regulation of the complex σ^s-dependent *csiD-ygaF-gabDTP* operon in *Escherichia coli*. *Molec. Microbiol. 51*, 799-811.

[3] Marshchall, C., Labrousse, V., Kreimer, M., Weichart, D., Kolb, A., and Hengge-Aronis R. (1998) Molecular analysis of the regulation of *csiD*, a carbon starvation-inducible gene in *Escherichia coli* that is exclusively dependent on sigma^s and requires activation by cAMP-CRP. *J. Mol. Biol. 276*, 339-353.

[4] Schneider, B. L., Ruback, S., Kiupakis, A. K., Kasbarian, H., Pybus, C., Reitzer, L. (2002) The *Escherichia coli gabDTPC* operon: specific γ-aminobutyrate catabolism and nonspecific induction. *J. Bacteriol. 184*, 6976-6986.

[5] De Colibus, L., and Mattevi, A. (2006) New frontiers in structural flavoenzymology. *Curr. Opin. Struct. Biol. 16*, 722-728.

[6] Walsh, C. T. (1979) Enzymatic reaction mechanisms. W. H. Freeman and Company, San Francisco.

[7] Rzem, R., Veiga-da-Cunha, M., Noël, G., Goffette, S., Nassogne, M.-C., Tabarki, B., Schöller, C., Marquardt, T., Vikkula, M., and Van Schaftingen, E. (2004) A gene encoding a putative FAD-dependent L-2-hydroxyglutarate dehydrogenase is mutated in L-2-hydroxyglutaric aciduria. *Proc. Natl. Acad. Sci. USA 101*, 16849-16854.

[8] Tomb, J. F., White, O., Kerlavage, A. R., Clayton, R. A., Sutton, G. G., Fleischmann, R. D., Ketchum, K. A., Klenk, H. P., Gill, S., Dougherty, B. A., Nelson, K., Quackenbush, J., Zhou, L., Kirkness, E. F., Peterson, S., Loftus, B., Richardson, D., Dodson, R., Khalak, H. G., Glodek, A., McKenney, K., Fitzergerald, L. M., Lee, N., Adams, M. D., Hickey, E. K., Berg, D. E., Gocayne, J. D., Utterback, T. R., Peterson, J. D., Kelley, J. M., Cotton, M. D., Weidman, J. M., Fujii, C., Bowman, C., Watthey, L., Wallin, E., Hayes, W. S., Borodovsky, M., Karp, P. D., Smith, H. O., Fraser, C. M., and Venter, J. C. (1997) The complete genome of the gastric pathogen *Helicobacter pylori*. *Nature 388*, 539-547.

[9] Suzuki, K., Sagai, H., Imamura, S., and Sugiyama M. (1994) Cloning, sequencing, overexpression in *Escherichia coli* of a sarcosine oxidase-encoding gene linked to the *Bacillus creatinase* gene. *J. Ferm. Bioeng.* 77, 231-234.

[10] Binzak, B. A., Vockley, J. G., Jenkins, R. B., and Vockley, J. (2000) Structure and analysis of the human dimethylglycine dehydrogenase gene. Molec. Genet. Metab. 69, 181-187.

[11] Kunst, F., Ogasawara, N., Moszer, I., Albertini, A. M., Alloni, G., Azevedo, V., Bertero, M. G., Bessières, P., Bolotin, A., Borchert, S., Borriss, R., Boursier, L., Brans, A., Braun, M., Brignell, S. C., Bron, S., Brouillet, S., Bruschi, C. V., Caldwell, B., Capuano, V., Carter, N. M., Choi, S.-K., Codani, J.-J., Connerton, I. F., Cummings, N. J., Daniel, R. A., Denizot, F., Devine, K. M., Düsterhöft, A., Ehrlich, S. D., Emmerson, P. T., Entian, K. D., Errington, J., Fabret, C., Ferrari, E., Foulger, D., Fritz, C., Fujita, M., Fujita, Y., Fuma, S., Galizzi, A., Galleron, N., Ghim, S.-Y., Glaser, P., Goffeau, A., Golightly, E. J., Grandi, G., Guiseppi, G., Guy, B. J., Haga, K., Haiech, J., Harwood, C. R., Hènaut, A., Hilbert, H., Holsappel, S., Hosono, S., Hullo, M.-F., Itaya, M., Jones, L., Joris, B., Karamata, D., Kasahara, Y., Klaerr-Blanchard, M., Klein, C., Kobayashi, Y., Koetter, P., Koningstein, G., Krogh, S., Kumano, M., Kurita, K., Lapidus, A., Lardinois, S., Lauber, J., Lazarevic, V., Lee, S.-M., Levine, A., Liu, H., Masuda, S., Mauël, C., Mèdigue, C., Medina, N., Mellado, R. P., Mizuno, M., Moesti, D., Nakai, S., Noback, M., Noone, D., O'Reilly, M., Ogawa, K., Ogiwara, A., Oudega, B., Park, S.-H., Parro, V., Pohl, T. M., Portetelle, D., Porwollik, S., Prescott, A. M., Presecan, E., Pujic, P., and Purnelle, B. (1997) The complete genome sequence of the Gram-positive bacterium *Bacillus subtilis*. *Nature 390*, 249-256.

[12] Dodt, G., Kim, D. G., Reimann, S. A., Reuber, B. E., McCabe, K., Gould, S. J., and Mihalik S. J. (2000) L-Pipecolic acid oxidase, a human enzyme essential for the degradation of L-pipecolic acid, is most similar to the monomeric sarcosine oxidases. *Biochem. J. 345*, 487-494.

[13] Hassan-Abdallah, A., Zhao, G., and Jorns M. S. (2006) Role of the covalent flavin linkage in monomeric sarcosine oxidase. *Biochemistry 45*, 9454-9462.

[14] Leys, D., Basran, J., and Scutton, N. S. (2003) Channeling and formation of 'active' formaldehyde in dimethylglycine oxidase. *EMBO J.* 22, 4038-4048.

[15] Miroux, B., and Walker J. E. (1996) Over-production of proteins in Escherichia coli: mutant hosts that allow synthesis of some membrane protein and globular proteins at high levels. *J. Mol. Biol. 260*, 289-298.

[16] Laemmli, U. K. (1970) Cleavage of structural proteins during the assembly of the head of bacteriophage T4. *Nature (London)* **227**, 680-685.

[17] Mihalik, S. J., McGuinness, M., and Watkins, P. A. (1991) Purification and characterization of peroxisomal L-pipecolic acid oxidase from monkey liver. *J. Biol. Chem.* **266**, 4822-4830.

[18] Pollegioni, L., Porrini, D., Molla, G., and Pilone, M. S. (2000) Redox potentials and their pH dependence of D-amino acid oxidase of *Rhodotorula gracilis* and *Trigonopsis variabilis*. *Eur. J. Biochem.* **267**, 6624-6632.

[19] Prince, R. C., Linkletter, S. J. G., and Dutton, L. (1981) The thermodynamic properties of some commonly used oxidation-reduction mediators, inhibitors and dyes, as determined by polarography. *Biochim. Biophys. Acta* **635**, 132-148.

[20] http://ecoli.naist.jp/gb6/Resources/deletion/deletion.html.

[21] Hayashi, T., Tsuchiya, H., Todoriki, H., and Naruse, H. (1982) High-performance liquid chromatographic determination of alpha-keto acids in human urine and plasma. *Anal. Biochem.* **122**, 173-179.

[22] Romanov, V., Merski, M. T., and Hausinger, R. P. (1999) Assays for allantoinase. *Anal. Biochem.* **268**, 49-53.

[23] Sefler, A. M., Kozlowski, M. C., Guo, T., and Bartlett, P. A. (1997) Design, Synthesis, and Evolution of a Depsipeptide Mimic of Tendamistat. *J. Org. Chem.* **62**, 93-102.

[24] Massey, V., Stankovich, M., and Hemmerich, P. (1978) Light-mediated reduction of flavoproteins with flavins as catalysts. *Biochemistry* **17**, 1-8.

[25] Massey, V., and Hemmerich, P. (1978) Photoreduction of flavoproteins and other biological compounds catalyzed by deazaflavins. *Biochemistry* **17**, 9-17.

[26] Massey, V., Müller, F., Feldberg, R., Schuman, M., Sullivan, P. A., Howell, L. G., Mayhew, S. G., Matthews, R. G., and Foust, G. P. (1969) The reactivity of flavoproteins with sulfite. Possible relevance to the problem of oxygen reactivity. *J. Biol. Chem.* **244**, 3999-4006.

[27] Müller, F., and Massey, V. (1969) Flavin-sulfite complexes and their structures. *J. Biol. Chem.* **244**, 4007-4016.

[28] Pande, S., Ghosh, S. K., Nath, S., Praharaj, S., Jana, S., Panigrahi, S., Basu, S., and Pal, T. (2006) Reduction of methylene blue by thiocyanate: kinetic and thermodynamic aspects. *J. Colloid Interface Sci.* *299*, 421-427.

[29] Job, V., Marcone, G. L., Pilone, M. S., and Pollegioni, L. (2002) Glycine oxidase from *Bacillus subtilis*. *J. Biol. Chem.* *277*, 6985-6993.

[30] Kim, J., and Copley, S. D. (2007) Why metabolic enzymes are essential or nonessential for growth of *Escherichia coli* K12 on glucose. *Biochemistry ASAP*.

[31] Rzem, R., Van Schaftingen, E., and Veiga-da-Cunha, M. (2006) The gene mutated in L-2-hydroxyglutaric aciduria encodes L-2-hydroxyglutarate dehydrogenase. *Biochimie 88*, 113-116.

[32] Rzem, R., Vincent, M.-F., Van Schaftingen, E., and Veiga-da-Cunha M. (2007) L-2-Hydroxyglutaric aciduria, a defect of metabolite repair. *J. Inherit. Metab. Dis.*,in press.

[33] Zhao, G., and Winkler, M. E. (1996) A novel α-ketoglutarate reductase activity of the *serA*-encoded 3-phosphoglycerate dehydrogenase of *Escherichia coli* K-12 and its possible implications for human 2-hydroxylglutaric aciduria. *J. Bacteriol. 178*, 232-239.